LLNL-TR-417498

LAWRENCE
LIVERMORE
NATIONAL
LABORATORY

Cross Sections for Neutron-induced Reactions on Actinide Targets Extracted from Surrogate Experiments: A Status Report

J. E. Escher, J. T. Burke, F. S. Dietrich, S. R. Lesher, N. D. Scielzo, I. J. Thompson, W. Younes

October 2, 2009

Disclaimer

This document was prepared as an account of work sponsored by an agency of the United States government. Neither the United States government nor Lawrence Livermore National Security, LLC, nor any of their employees makes any warranty, expressed or implied, or assumes any legal liability or responsibility for the accuracy, completeness, or usefulness of any information, apparatus, product, or process disclosed, or represents that its use would not infringe privately owned rights. Reference herein to any specific commercial product, process, or service by trade name, trademark, manufacturer, or otherwise does not necessarily constitute or imply its endorsement, recommendation, or favoring by the United States government or Lawrence Livermore National Security, LLC. The views and opinions of authors expressed herein do not necessarily state or reflect those of the United States government or Lawrence Livermore National Security, LLC, and shall not be used for advertising or product endorsement purposes.

This work performed under the auspices of the U.S. Department of Energy by Lawrence Livermore National Laboratory under Contract DE-AC52-07NA27344.

Cross sections for neutron-induced reactions on actinide targets extracted from Surrogate experiments:

A status report

Draft

Jutta E. Escher, Jason T. Burke, Frank S. Dietrich, Shelley R. Lesher,
Nicholas D. Scielzo, Ian J. Thompson, and Walid Younes

Lawrence Livermore National Laboratory, Livermore, CA 94550

October 1, 2009

Abstract

The Surrogate nuclear reactions method, an indirect approach for determining cross sections for compound-nuclear reactions involving difficult-to-measure targets, is reviewed. Focusing on cross sections for neutron-induced reactions on actinides, we review the successes of past and present applications of the method and assess its uncertainties and limitations. The approximations used in the analyses of most experiments work reasonably well for (n,f) cross sections for neutron energies above 1-2 MeV, but lead to discrepancies for low-energy (n,f) reactions, as well as for (n,γ) applications. Correcting for some of the effects neglected in the approximate analyses leads to improved (n,f) results. We outline steps that will further improve the accuracy and reliability of the Surrogate method and extend its applicability to reactions that cannot be approached with the present implementation of the method.

Contents

1 Introduction and overview of the report 6

2 The Surrogate idea 8

3 Surrogate analyses using the Weisskopf-Ewing approximation 11

3.1 The Weisskopf-Ewing limit of the Hauser-Feshbach description: formalism . 11
3.2 Early Surrogate work using the Weisskopf-Ewing approximation 13
3.3 CENBG Surrogate experiments using the Weisskopf-Ewing approximation . 19
  3.3.1 Experimental apparatus 19
  3.3.2 Data reduction and analysis 19
  3.3.3 Cross sections for neutron-induced fission 22
3.4 Surrogate experiments at STARS/LiBerACE 28
  3.4.1 The STARS charged particle detector system 28
  3.4.2 The LIBERACE γ-ray detector system 36
  3.4.3 Results using the Weisskopf-Ewing approximation 39
3.5 Validity of the Weisskopf-Ewing Approximation 44
  3.5.1 Fission probabilities and the WE approximation. 44
  3.5.2 Impact on extracted fission cross sections 46
  3.5.3 Experimental evidence for spin mismatch effects in (n,f) cross sections 47

4 Surrogate analyses using ratios 49

4.1 The Ratio approach 49
4.2 Energy matching in the Ratio approach 51
4.3 Surrogate ratio experiments at STARS/LiBerACE 53
  4.3.1 Determination of the ^{237}U(n,f) cross section 53
  4.3.2 Determination of the ^{239}U(n,f) cross section 53
4.4 Other variants of the Surrogate Ratio method 56
4.5 Validity of the Ratio approach 58
  4.5.1 Uncertainty assessment for (n,f) cross sections 58
  4.5.2 Experimental benchmark for the Ratio Approach 60
  4.5.3 Testing the limits of the Ratio approach 61

5 Modeling approach 64

5.1 Modeling approach for low-energy (n,f) reactions 65
5.2 Extension of the method to higher neutron energy 66

5.3 Comments on the modeling approach 68

6 Surrogate reactions for (n,γ) 74

6.1 Challenges for Surrogate measurements of (n,γ) cross sections 74
6.2 Validity of the Weisskopf-Ewing approximation for (n,γ) 78
6.3 Validity of the Ratio approximations for (n,γ) 80
6.4 Experimental efforts for (n,γ) 82
6.5 Comments on (n,γ) cross sections 86

7 Moving beyond current approximations 88

7.1 Spin-parity mismatch and related challenges 88
7.2 Addressing the theory challenges: present status 89
  7.2.1 Direct reaction to the continuum 89
  7.2.2 Damping into the compound nucleus 90
  7.2.3 Width fluctuation corrections 91
7.3 Addressing the challenges for each Surrogate reaction mechanism 92
  7.3.1 Reaction theory requirements 92
  7.3.2 Pickup reactions 93
  7.3.3 Inelastic reactions 94
  7.3.4 Stripping (transfer) reactions 95
  7.3.5 Charge-exchange reactions 96
  7.3.6 Two-nucleon transfer reactions 97

8 Summary and recommendations 98

Acknowledgments 101

A Appendix 102

A.1 Hauser-Feshbach formalism 102
A.2 Dependence of fission probabilities on spin cutoff parameters 104
A.3 Optical-model parameterization 107
A.4 The role of preequilibrium neutron emission 112
A.5 Fission-fragment anisotropies 114

Bibliography 117

List of Figures

1 Schematic representation of the “desired” and “Surrogate” reaction mechanisms 8
2 Determination of fission coincidence probabilities in early Surrogate experiments 14
3 Various (n,f) cross sections from early Surrogate (t, pf) measurements 16
4 Various (n,f) cross sections from early Surrogate $(^3\mathrm{He}, tf)$ measurements . . . 17
5 Comparison of older and modern compound-nucleus formation cross sections 18
6 Experimental setup used by the CENBG group at IPN Orsay 20
7 Singles spectra from a representative CENBG experiment 21
8 Fission-fragment angular distribution from a representative CENBG experiment 22
9 Fission coincidence probabilities from a representative CENBG experiment . 23
10 ^{230}Th(n,f) cross section from CENBG experiments 24
11 ^{231}Pa(n,f) cross section from CENBG experiments 25
12 ^{233}Pa(n,f) cross section from CENBG experiments 26
13 ^{241}Am(n,f), ^{243}Cm(n,f) and ^{244}Cm(n,f) cross sections from CENBG group . . 27
14 Top view of the STARS/LiBerACE detector system 29
15 Photo of the STARS chamber 30
16 Schematic of the 8-position target holder of the STARS detector system . . . 31
17 A typical ^{226}Ra calibration spectrum observed in a STARS detector 32
18 Particle identification plots 33
19 Representative range energy plot 34
20 Proton-gated fission spectra from ^{235}U(d,pf) STARS/LiBerACE experiment . 34
21 Efficiency of the LiBerACE HPGe array 37
22 STARS/LiBerACE particle singles and coincidence spectra 40
23 Fission probability for the ^{238}Np nucleus 41
24 ^{237}Np(n,f) cross section determined from a STARS/LiBerACE experiment . . 42
25 ^{236}U(n,f) cross section from a STARS/LiBerACE experiment 43
26 Calculated branching ratios $G^{CN}_{fission}(E, J, \pi)$ for fission of ^{236}U* 45
27 Distributions of total angular momentum for ^{236}U* 46
28 Weisskopf-Ewing estimates of the ^{235}U(n,f) cross section 47
29 ^{236}U(n,f) cross section obtained from a Weisskopf-Ewing analysis of Surrogate ^{238}U(^{3}He,α) measurements 48
30 ^{237}U(n,f) cross section from a ^{238}U(α,α’f) surrogate experiment 54
31 ^{239}U(n,f) cross sections from different Surrogate experiments 55
32 ^{233}Pa(n,f) cross section determined using a hybrid Surrogate approach 57
33 ^{235}U(n,f) cross section from a Ratio analysis of simulated Surrogate experiments 59

34 Experimental test of the External Surrogate Ratio method for fission 60
35 Comparison of measured fission probability ratios to simulated ratios 62
36 ^{236}U(n,f) cross section from a Ratio analysis of Surrogate (^{3}He,αf) experiments 63
37 Surrogate fission probabilities and (n,f) cross sections for ^{235}U and ^{239}U . . . 67
38 Surrogate fission probabilities and (n,f) cross sections for ^{236}U, ^{234}U, and ^{240}Pu 69
39 Surrogate fission probabilities and (n,f) cross sections for ^{241}Am 70
40 Summary of low-energy (n,f) cross section averages 71
41 ^{235}U(n,f) cross section 72
42 ^{237}U(n,f) and ^{239}U(n,f) cross sections 73
43 Calculated γ-decay probabilities $G_{\gamma}^{CN}(E, J, \pi)$, for ^{236}U 75
44 Calculated yields of γ rays for transitions in the ground-state band of ^{236}U . 76
45 Schematic spin-parity distribution ABB 78
46 Weisskopf-Ewing estimates for the ^{235}U(n,γ) and ^{233}U(n,γ) cross sections from simulated Surrogate experiments 79
47 External Surrogate Ratio estimates for ^{235}U(n,γ) 80
48 Internal Surrogate Ratio estimates for ^{233}U(n,γ) 81
49 ^{233}Pa(n,γ) cross section from two Surrogate experiments 82
50 ^{237}U(n,γ) cross section from a Surrogate experiment 84
51 ^{235}U(n,γ) cross section from a Surrogate experiment 85
52 Gamma yields in ^{236}U for different $J\pi$ distributions 87
53 Fission probabilities for ^{239}Pu extracted from (d,p) experiments 96
54 Spin cutoff parameters in the neutron and fission decays of ^{236}U. 104
55 Spin dependence of the fission probability 106
56 Comparison of optical-model total and compound cross sections with experiment for n + ^{238}U 110
57 Compound-nuclear reaction cross section for n+^{234}U 111
58 Hauser-Feshbach calculation illustrating the effect of preequilibrium emission 112

List of Tables

1 Parameters for Flap 1.5 n+U optical potential 108
2 Parameters for Flap 2.2 n+U optical potential 109

1 Introduction and overview of the report

The Surrogate nuclear reactions method plays a crucial role for the determination of compound-nuclear reaction cross sections. It is the only indirect method available for compound-nuclear reactions that cannot be measured directly since the reaction of interest involves a very short-lived or highly-radioactive target. The Surrogate technique aims at determining the cross section for a two-step ("desired") reaction that proceeds through a compound nuclear state by using a combination of experiment and theory. The compound nucleus is produced by means of an alternative ("Surrogate") reaction, and the desired cross section is obtained by combining a calculation of the compound-nucleus formation in the desired reaction with a measurement of the compound-nucleus decay in the Surrogate reaction.

Originally introduced in the 1970s, the method has recently attracted renewed attention by research groups in the United States and in Europe. Both the early and the more recent applications of the method have focused on cross section estimates for neutron-induced fission for actinide targets, although a few experiments have been designed to obtain (n,γ) cross sections for some rare earth and actinide nuclei. The method has generated a host of valuable cross section information, in particular for (n,f) reactions. Comparisons with directly-measured cross sections show reasonable agreement for neutron energies above 1-2 MeV, but sizable discrepancies can occur for lower energies. These results, as well as (n,γ) cross sections extracted from Surrogate measurements and theoretical studies of the method, illustrate the limitations of the approach in its present implementation. Almost all applications to date employ significant approximations which reduce the accuracy of the cross sections extracted from Surrogate measurements and limit the reach of the Surrogate approach. As applications to new areas of interest (lower energies, additional types of compound nucleus reactions, new regions of the isotopic chart) are being explored, a more comprehensive treatment of the Surrogate approach becomes necessary in order to obtain accurate cross sections and assign reliable uncertainties. Some steps that improve the accuracy and reliability of the method have already been taken, and the tasks for developing a more comprehensive approach to the method have been identified.

In this report, we review the present status of the Surrogate method for applications involving neutron-induced reaction on actinide targets. We review the success of past and present applications of the method and assess its uncertainties and limitations, and we identify possibilities for further improvements. We pay particular attention to the approximations employed in the analyses of the Surrogate experiments discussed. The organization of the present report reflects this emphasis.

In Section 2, we introduce the Surrogate idea. We give a brief summary of the formalism and outline how an unknown cross section can be obtained from a Surrogate measurement.

The early Surrogate experiments relied on the *Weisskopf-Ewing* approximation in their analysis. In Section 3, we focus on this approximation scheme. We explain the concept, discuss calculations that test the validity of the approach, and show applications. In particular, we summarize the work carried out in the 1970s, as well as the more recent experiments by researchers in France and by the STARS/LiBerACE collaboration, which is led by LLNL and LBNL scientists. The focus is on (n,f) reactions, although the formalism is more general.

The *Surrogate Ratio approach* is an approximation that makes use of the Surrogate idea and requires the (approximate) validity of the Weisskopf-Ewing limit. In Section 4 we discuss several variants of the Ratio approach. We summarize the formalism of the Ratio approach, show applications of the method, and discuss calculations as well as experiments that test its validity. The focus is again on (n,f) cross sections.

The *modeling approach*, discussed in Section 5, represents an important step towards improving the accuracy of the Surrogate approach and moving beyond the present limitations. Initial steps towards developing the Surrogate modeling approach were taken by Back *et al.* in the 1970s and recently improved upon by Younes and Britt. Their approach is explained, representative results are shown, and suggestions are made for further developments.

While most of the Surrogate efforts so far have focused on fission, some experiments have been carried out to determine (n,γ) cross sections, which are important for a variety of applications. In Section 6, we describe the challenges that particularly affect the determination of (n,γ) reaction cross sections from Surrogate measurements. We test the validity of the various approximate methods with calculations and discuss the available experimental results for (n,γ) reactions on actinide targets.

In Section 7 we outline steps for moving beyond the currently-used approximations. The present understanding of the reaction mechanisms that produce the compound nucleus in a Surrogate reaction is incomplete. We specify the developments at are needed to remedy this situation, both in general and for the specific Surrogate reaction mechanisms that are presently being used or discussed.

The appendix contains a more detailed description of the Hauser-Feshbach formalism underlying the Surrogate approach (Section A.1), remarks on the effects of preequilibrium neutron emission (Section A.4), a study of the dependence of fission probabilities on the spin cutoff parameters, which is relevant for understanding the Weisskopf-Ewing limit for fission (Section A.2), and a description of the optical model potential employed in many of the applications carried out by the STARS/LiBerACE collaboration (Section A.3). We also include some comments on the role of fission-fragment anisotropies and pre-equilbrium in Surrogate applications (Section A.5). Concluding remarks are given in Section 8.

2 The Surrogate idea

This section introduces the Surrogate idea. It gives a brief summary of the formalism and outlines how an unknown cross section can be obtained from a Surrogate measurement.

The Surrogate nuclear reaction technique is an indirect method for determining the cross section for a particular type of "desired" reaction, namely a two-step reaction, $a + A \to B^* \to c + C$, that proceeds through a compound nuclear state B^*, a highly excited state in statistical equilibrium (see Figure 1, left panel).

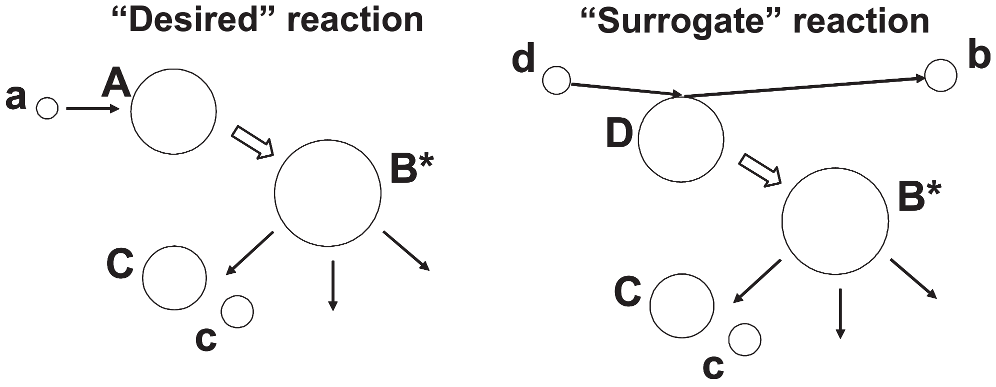

Figure 1: Schematic representation of the "desired" (left) and "Surrogate" (right) reaction mechanisms. The basic idea of the Surrogate approach is to replace the first step of the desired reaction, $a + A$, by an alternative (Surrogate) reaction, $d + D \to b + B^*$, that populates the same compound nucleus. The subsequent decay of the compound nucleus into the relevant channel, $c + C$, can then be measured and used to extract the desired cross section.

In the Hauser-Feshbach formalism [60], the cross section for this "desired" reaction takes the form:

$$\sigma_{\alpha\chi}(E_a) \ = \ \sum_{J,\pi} \sigma_{\alpha}^{CN}(E_{ex}, J, \pi) \ \ G_{\chi}^{CN}(E_{ex}, J, \pi) \ , \tag{1}$$

with α and χ denoting the relevant entrance and exit channels, $a+A$ and $c+C$, respectively. The excitation energy E_{ex} of the compound nucleus, B^*, is related to the center-of-mass energy E_a in the entrance channel via the energy needed for separating a from B: $E_a = E - S_a(B)$. In many cases the formation cross section $\sigma_{\alpha}^{CN} = \sigma(a + A \to B^*)$ can be calculated to a reasonable accuracy by using optical potentials, while the theoretical decay probabilities G_{χ}^{CN} for the different decay channels χ are often quite uncertain. The latter are difficult to calculate accurately since they require knowledge of optical models, level densities, and strength functions for the various possible exit channels. The objective of the Surrogate method is to determine or constrain these decay probabilities experimentally.

In a Surrogate experiment, the compound nucleus B^* is produced via an alternative ("Surrogate"), direct reaction $d+D \to b+B^*$ and the decay of B^* is observed in coincidence with the outgoing particle b (see Figure 1, right panel). The direct-reaction particle is typically stopped in a detector which provides particle identification, as well as information on the kinetic energy and direction of b, which makes it possible to determine the excitation energy, E_{ex}, of the compound nucleus B^* formed in the Surrogate reaction. The desired exit channel χ can be identified, *e.g.*, by detecting fission fragments from B^* or γ rays from the desired residual nucleus C. The probability for forming B^* in the Surrogate reaction (with specific values for the excitation energy E_{ex}, angular momentum J, and parity π) is $F_\delta^{CN}(E_{ex}, J, \pi)$, where δ refers to the entrance channel $d + D$. The quantity

$$P_{\delta\chi}(E_{ex}) = \sum_{J,\pi} F_\delta^{CN}(E_{ex}, J, \pi) \;\; G_\chi^{CN}(E_{ex}, J, \pi) \; , \tag{2}$$

which gives the probability that the compound nucleus B^* was formed with energy E_{ex} and decayed into channel χ, can thus be obtained experimentally, by measuring N_δ, the total number of Surrogate events, and $N_{\delta\chi}$, the number of coincidences between the direct-reaction particle and the observable that identifies the relevant exit channel:

$$P_{\delta\chi}^{exp}(E_{ex}) = \frac{N_{\delta\chi}}{N_\delta} \; . \tag{3}$$

In practical applications, efficiencies for detecting the outgoing direct-reaction particle b, as well as the relevant exit channel χ need to be taken into account. These efficiencies are not shown in Eq. 3, but will be explicitly displayed in this report where appropriate. For simplicity, we have omitted the angular dependence of both the desired and the Surrogate reactions in the above discussion. The extension of the Hauser-Feshbach formulae is straightforward [52].

To determine the desired cross section, Eq. 1, from a Surrogate measurement, one can pursue the following strategies:

I. Ideal Approach. Ideally, one calculates the spin-parity distribution, $F_\delta^{CN}(E_{ex}, J, \pi)$ in Eq. 2, which may be very different from the compound-nuclear spin-parity populations following the absorption of the projectile a in the desired reaction, from a suitable theory that describes the formation of the compound nucleus following the direct reaction $d + D \rightarrow b + B^*$. Given a reliable prediction of the quantities $F_\delta^{CN}(E_{ex}, J, \pi)$, and a sufficient range of experimental coincidence data $P_{\delta\chi}(E_{ex})$ (for a range of energies and angles of the outgoing particle b, and possibly for various exit channels), it might be possible to extract the $G_\chi^{CN}(E_{ex}, J, \pi)$. The latter can then be inserted in Eq. 1 and thus used to calculate the desired cross section. At this time, this idealized approach has not been implemented since a combination of possible reaction mechanisms, predicted F_δ^{CN}, and experimental data has not been available to unambiguously extract useful branching ratios.

II. Modeling Approach. More realistically, the decay of the compound nucleus is modeled in a Hauser-Feshbach-type calculation that makes use of independently available (but typically incomplete) nuclear structure information, including, e.g. neutron resonance spacings and average radiative widths, that allow one to constrain level densities and γ-ray strength functions, respectively. The $G_{\chi}^{CN}(E, J, \pi)$ obtained from such modeling can then be combined with theoretically predicted $F_{\delta}^{CN}(E_{ex}, J, \pi)$ to yield a prediction for $P_{\delta\chi}(E_{ex})$. By fitting the latter to the Surrogate data, the Hauser-Feshbach parameters entering the calculation of the branching ratios $G_{\chi}^{CN}(E, J, \pi)$ can be determined. The so improved model branching ratios can then be employed in the calculation of the desired cross section, Eq. (1).

Steps towards developing this modeling approach were taken by Andersen *et al.* [4], Back *et al.* [7], and, more recently, by Younes and Britt [99, 100]. A major challenge for this approach (and even more so for the "ideal approach" outlined above) is achieving a reliable (and tested) prediction of the $F_{\delta}^{CN}(E_{ex}, J, \pi)$ for the Surrogate reaction under consideration. This issue will be discussed in more detail in Section 7.

III. Approximations. An alternative to employing the full Surrogate formalism outlined above is to make use of approximations. A large majority of the Surrogate applications to data has relied on invoking approximations, such as the Weisskopf-Ewing limit of the Hauser-Feshbach theory (which treats the $G_{\chi}^{CN}(E, J, \pi)$ as independent of $J\pi$), or the Surrogate Ratio method. In the Ratio approach, the measurements are carried out on two similar targets, for one of which the desired reaction has been accurately determined in an independent measurement or evaluation. The Ratio method assumes the validity of the Weisskopf-Ewing approximation, but may reduce the effects of modest violations of this approximation on the extracted cross sections. In Sections 3 and 4, respectively, we discuss the Weisskopf-Ewing and the Ratio approximations in more detail.

IV. "Serendipitous" Approach. From the above descriptions, it becomes evident that a primary challenge to extracting a desired reaction cross section from a Surrogate measurement lies in accounting for the spin-parity mismatch between the desired and Surrogate reactions. Should it be possible to identify a Surrogate reaction (*i.e.* a reaction mechanism, projectile-target combination, beam energy, outgoing-particle angle) that reproduces the spin-parity distribution of the desired reaction,

$$F_{\delta}^{CN}(E_{ex}, J, \pi) \quad \approx \quad F_{\alpha}^{CN}(E_{ex}, J, \pi) \equiv \frac{\sigma_{\alpha}^{CN}(E_{ex}, J, \pi)}{\sum_{J', \pi'} \sigma_{\alpha}^{CN}(E_{ex}, J', \pi')}, \tag{4}$$

where F_{α}^{CN} is the compound-nuclear $J\pi$ population in the desired reaction, the situation would simplify greatly, as in this limit, we find:

$$\sigma_{\alpha\chi}(E_a) \quad \approx \quad \left(\sum_{J', \pi'} \sigma_{\alpha}^{CN}(E_{ex}, J', \pi') \right) \times P_{\delta\chi}^{exp}(E_{ex}), \tag{5}$$

with $P_{\delta\chi}^{exp}(E_{ex})$ determined from the experiment. While it is sometimes argued that a given Surrogate experiment approximately satisfies Eq. 4, there has not been sufficient evidence to support such claims. In order to identify candidate reactions that might satisfy this condition approximately, it is important to have reliable theoretical predictions of $F_{\delta}^{CN}(E_{ex}, J, \pi)$, as well as experimental signatures that can test the underlying theory.

3 Surrogate analyses using the Weisskopf-Ewing approximation

Most Surrogate experiments carried out so far have been analyzed using the Weisskopf-Ewing approximation (or the related Ratio approach, which will be discussed in Section 4). Here we discuss the Weisskopf-Ewing approximation to the full Surrogate formalism. We explain the concept in Section 3.1, discuss calculations that test the validity of the approximation (Section 3.5), and show applications. In particular, we briefly summarize the early Surrogate work, carried out in the 1970s (Section 3.2), and more recent experiments undertaken by the group at the CENBG (see Section 3.3) and by the STARS/LiBerACE collaboration (Section 3.4). The focus here is on neutron-induced fission of actinide targets. The use of the Weisskopf-Ewing approximation in analyses of Surrogate experiments aimed at determining (n,γ) cross sections is discussed in Section 6.

3.1 The Weisskopf-Ewing limit of the Hauser-Feshbach description: formalism

The Hauser-Feshbach theory used in the previous section rigorously conserves total angular momentum J and parity π. Under certain conditions the branching ratios $G_{\chi}^{CN}(E_{ex}, J, \pi)$ can be treated as independent of J and π and the form of the cross section (for the desired reaction) simplifies to

$$\sigma_{\alpha\chi}^{WE}(E_a) \;=\; \sigma_{\alpha}^{CN}(E_{ex})\, \mathcal{G}_{\chi}^{CN}(E_{ex}) \tag{6}$$

where

$$\sigma_{\alpha}^{CN}(E_{ex}) \;=\; \sum_{J\Pi} \sigma_{\alpha}^{CN}(E_{ex}, J, \pi) \tag{7}$$

is the reaction cross section describing the formation of the compound nucleus at energy E_{ex} and $\mathcal{G}_{\chi}^{CN}(E_{ex})$ denotes the $J\pi$-independent branching ratio for the exit channel χ. This is the Weisskopf-Ewing limit of the Hauser-Feshbach theory. It can be formally shown that the Hauser-Feshbach theory reduces to the Weisskopf-Ewing limit when a series of conditions are satisfied [53, 36]. In particular, width-fluctuation correlations have to be negligible, the decay of the compound nucleus to discrete states of nuclei in the various exit channels has to be small, and the level densities in the decay channels have to possess a particular dependence on the spins of the residual nuclei. Since these conditions tend to be satisfied at higher compound-nucleus energies, it is often assumed that the Weisskopf-Ewing approximation can be employed above a certain bombarding energy, e.g. above 1-2 MeV in neutron-induced reactions. In Section 3.5, we will demonstrate that the situation is more complex and that it is not *a priori* clear whether the Weisskopf-Ewing approximation is valid in a particular energy regime.

When applicable, the Weiskopf-Ewing limit provides a simple and powerful approximate way of calculating cross sections for two-step reactions proceeding through a compound nucleus. In the context of Surrogate reactions, it greatly simplifies the application of the method: It becomes straightforward to obtain the $J\pi$-independent branching ratios $\mathcal{G}_{\chi}^{CN}(E_{ex})$ from measurements of the coincidence probability $P_{\delta\chi}(E_{ex})$, since $\sum_{J\Pi} F_{\delta}^{CN}(E_{ex}, J, \pi)$ $= 1$ and

$$P_{\delta\chi}(E_{ex}) \quad = \quad \mathcal{G}_{\chi}^{CN}(E_{ex}) \tag{8}$$

holds in that limit. Calculating the direct-reaction probabilities $F_{\delta}^{CN}(E_{ex}, J, \pi)$ and modeling the decay of the compound nucleus are no longer required; the desired cross section then takes the simple form:

$$\sigma_{\alpha}^{CN}(E_{ex}) \quad = \quad \sigma_{\alpha}^{CN}(E_{ex}) P_{\delta\chi}(E_{ex}) \tag{9}$$

Most applications of the Surrogate method so far have been based on the assumption that the Weisskopf-Ewing approximation is valid for the cases of interest.

3.2 Early Surrogate work using the Weisskopf-Ewing approximation

The Surrogate approach was first used in the 1970s to extract (n, f) cross sections for various actinides from transfer reactions with t and ^{3}He projectiles on neighboring (long-lived) nuclei, followed by fission [33, 25]. Measured fission probabilities, P_f (or $P_{\delta f}$ in the notation of Eq 2), were simply multiplied by an estimated cross section for the formation of the compound nucleus in the neutron-induced reaction of interest. The results of this approach typically agreeed with direct measurements (where available) to within 10–20% at energies $\gtrsim$1 MeV but showed larger deviations at lower energies. Below, we summarize the results of the early experiments from which the surrogate approach has evolved.

The first time fission probabilities, P_f, were measured using a direct reaction instead of a neutron-induced reaction was in 1959 [75]. The absolute fission probabilities were determined for ^{239}Pu and ^{233,235,238}U from the relative number of particle-fission coincidence counts, $N_{\delta f}$, and particle singles counts, N_δ, from the relation

$$P_f = \frac{N_{\delta f}}{N_\delta \epsilon_f}. \tag{10}$$

after accounting for the fission-fragment detection efficiency, ϵ_f. It was pointed out that light-ion reactions, like (d, p), have the advantage that P_f can be determined both above and below the neutron separation energy. The excitation energy of the nucleus was determined by measuring the outgoing proton energy using a ΔE-E telescope consisting of an thin transmission ion chamber backed by a NaI(Tl) detector. Fission fragments were detected using a single proportional counter. The targets were 2 mg/cm^2 of actinide oxide vacuum evaporated on a 200μm/cm^2 gold backing. Backgrounds from carbon, oxygen, and the gold backing were accounted for and subtracted by measuring (d, p) on other targets. The authors even noted that the probability for fission from the (d, p) reaction at 2 MeV for the different nuclei have the same ratios as the neutron-induced reaction. These early results were believed to be accurate to 10-20%.

In the following years, similar techniques were routinely used to study fission properties induced by direct reactions. Measurements were performed using (d, pf), $(\alpha,\alpha' f)$, (t, pf), and (t, df) reactions to determine fission thresholds, the excitation-energy dependence of the fission probabilities, and/or the fission-fragment angular anisotropies for many different actinides [97, 21, 22, 84, 23, 98, 19, 34, 20, 7, 6, 54]. These experiments used semiconductor detectors for both light-ion and fission-fragment detection. For example, in Ref. [23], light ions were identified using a ΔE-E telescope consisting of a 310-μm surface-barrier silicon detector backed by either a 2- or 3-mm thick lithium-drifted silicon detector while fission fragments were observed in coincidence using an array of eight phosphorus-diffused silicon detectors. In this particular measurement, protons from (d, pf) and (t, pf) reactions were detected with a FWHM energy resolution of 120 keV. Typical targets consisted of 150–2000 μg/cm^2 of actinide oxides deposited on a thin carbon or gold backing. Reactions off of ^{12}C and ^{16}O nuclei in the target were often used to calibrate the ΔE-E telescope response. In some cases, additional targets were run to measure the backgrounds from these light contaminants and in other cases the impact of the contamination was estimated by

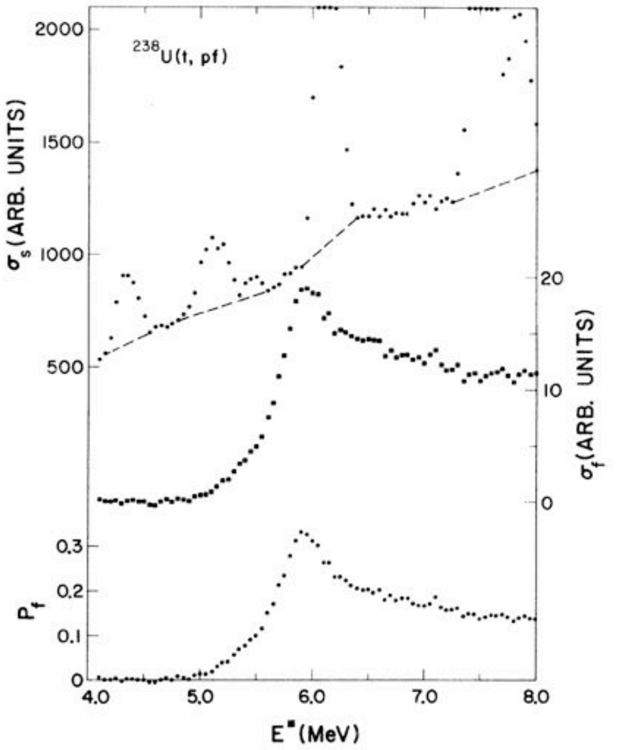

Figure 2: Determination of fission coincidence probabilities in early Surrogate experiments. The proton-singles spectra, N_δ, for ^{238}U(t,p) is shown at the top of the graph with interpolated dashed lines to determine the spectrum under the clear peaks from (t,p) reactions on ^{12}C and ^{16}O. The ratio of this spectrum to the $N_{\delta f}$ spectrum shown below it results in P_f shown at the bottom. Figure reproduced from Ref. [34] Fig. 3.

interpolating values under the obvious light-ion contaminant peaks as is shown in Figure 2 (taken from Ref. [34]). The typical energy resolution that was obtained was 100–200 keV for 10–20 MeV protons, deuterons, and tritons and 300–500 keV for 30–40 MeV ^{3}He and ^{4}He ions and was limited by the intrinsic resolution of the detectors, the kinematic spread due to finite detector solid angles, and other effects like incident beam properties. This resolution was adequate to observe the desired energy-dependent features of P_f and evolution of the fission-fragment anisotropy. In these studies, the fission probabilities obtained from (t,pf) and (d,pf) reactions were found to be qualitatively similar to the fission probabilities deduced from (n,f) measurements [20]. The first application of these probabilities from light-ion reactions to infer (n,f) cross sections was in Ref. [33] where (t,pf) reactions were used to determine cross sections for short-lived actinides. The light-ion telescope detected scattered protons at back angles to minimize the effect of target backgrounds. The use of a 18-MeV t beam limited the accessible energy range to just a few MeV above the neutron separation energy. The (n,f) cross sections, $\sigma_{(n,f)}$ for the short-lived isotopes ^{231,233}Th, ^{237,239}U, and ^{243}Pu over an energy range of 0.5–2.25 MeV were determined from the product of the measured P_f values and an estimated compound-nuclear formation cross section, $\sigma_{(n,f)}$, as

$$\sigma_{(n,f)} \approx \sigma_n^{CN} \times P_f. \tag{11}$$

For these isotopes, only direct measurement of the ^{237}U(n,f) cross section has been attempted in a heroic measurement described in Ref. [72]. The reliability of the method was investigated by also determining ^{235}U and ^{241}Pu cross sections using the method and comparing the results to direct measurement. As can be seen in Fig. 3, the resulting (n,f) cross section estimates agreed with these direct measurements to about 10-20% for incident neutron energies above about 1 MeV, but resulted in 20–40% discrepancies below 1 MeV. These discrepancies were attributed to large uncertainties in the low-energy optical-model calculations employed and the neglect of the difference in the angular-momentum populations of the compound nucleus in the Surrogate (direct) and "desired" (neutron-induced) reactions. The uncertainty in the fission probabilities was estimated at ±10%, the optical-model calculation was estimated to have uncertainties of ±20% at 0.5 MeV, decreasing to ±5% at 2 MeV, and the angular momentum differences were estimated to introduce uncertainties of 5–20%.

This method was subsequently used with (^{3}He,df) and (^{3}He,tf) reactions on a variety of actinide targets to infer (n,f) cross sections for 34 actinide nuclei at energies up to 6 MeV [25]. The highest energy that could be reached was limited by the rapid decrease in cross section caused by the Coulomb barrier for outgoing charged particles and the increase in background from carbon and oxygen in the target. Several of the results are shown in Fig. 4 and compared to the direct measurements and ENDF/B-IV cross-section evaluations that were available at the time. The fission probabilities were thought to be reliable to 10%. For these measurements, the compound nuclear formation cross section was crudely estimated by using a constant 3.1 barns — this value was found to reproduce the available direct measurements. This value is compared to modern optical model calculations in Figure 5 (taken from [100]). In addition to fission measurements, some early experiments were carried out to assess the feasibility of using the Surrogate technique to determine cross sections for (n,α) and (n,p) reactions on nuclei in the mass-90 region [24]. These experiments highlighted further issues that needed to be addressed in order to extract reliable cross sections from Surrogate measurements. In particular, the effects of projectile break-up in the Surrogate reaction needed to be estimated and ambiguities in identifying the reaction sequence in some reactions needed to be resolved. These issues will be discussed further in Section 7.

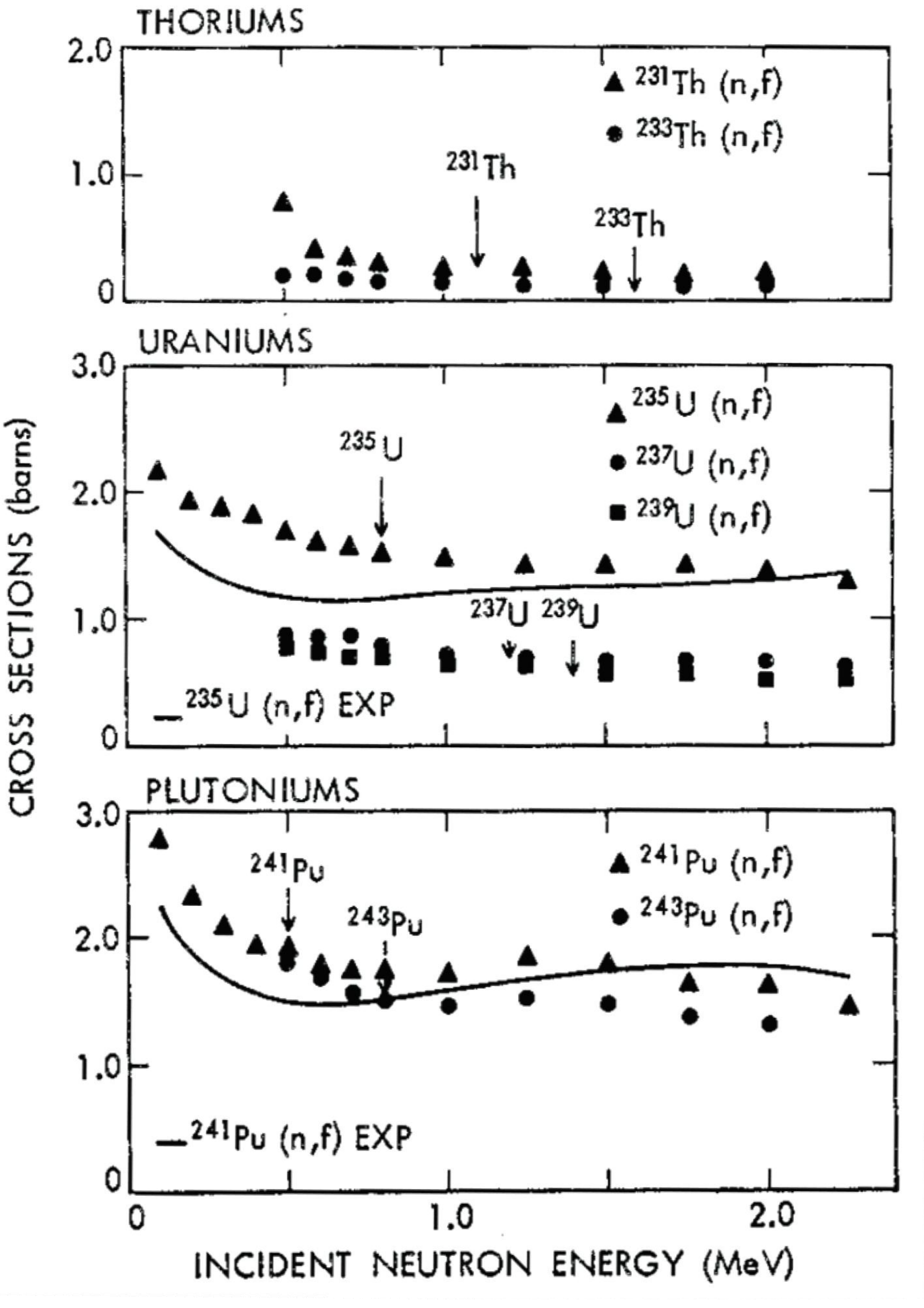

Figure 3: The (n, f) cross sections determined using the Weisskopf-Ewing approximation to analyze (t, pf) data. The solid lines show the results of the direct measurements that existed at the time. The agreement above 1 MeV is quite good. Figure reproduced from Ref. [33] Fig. 5.

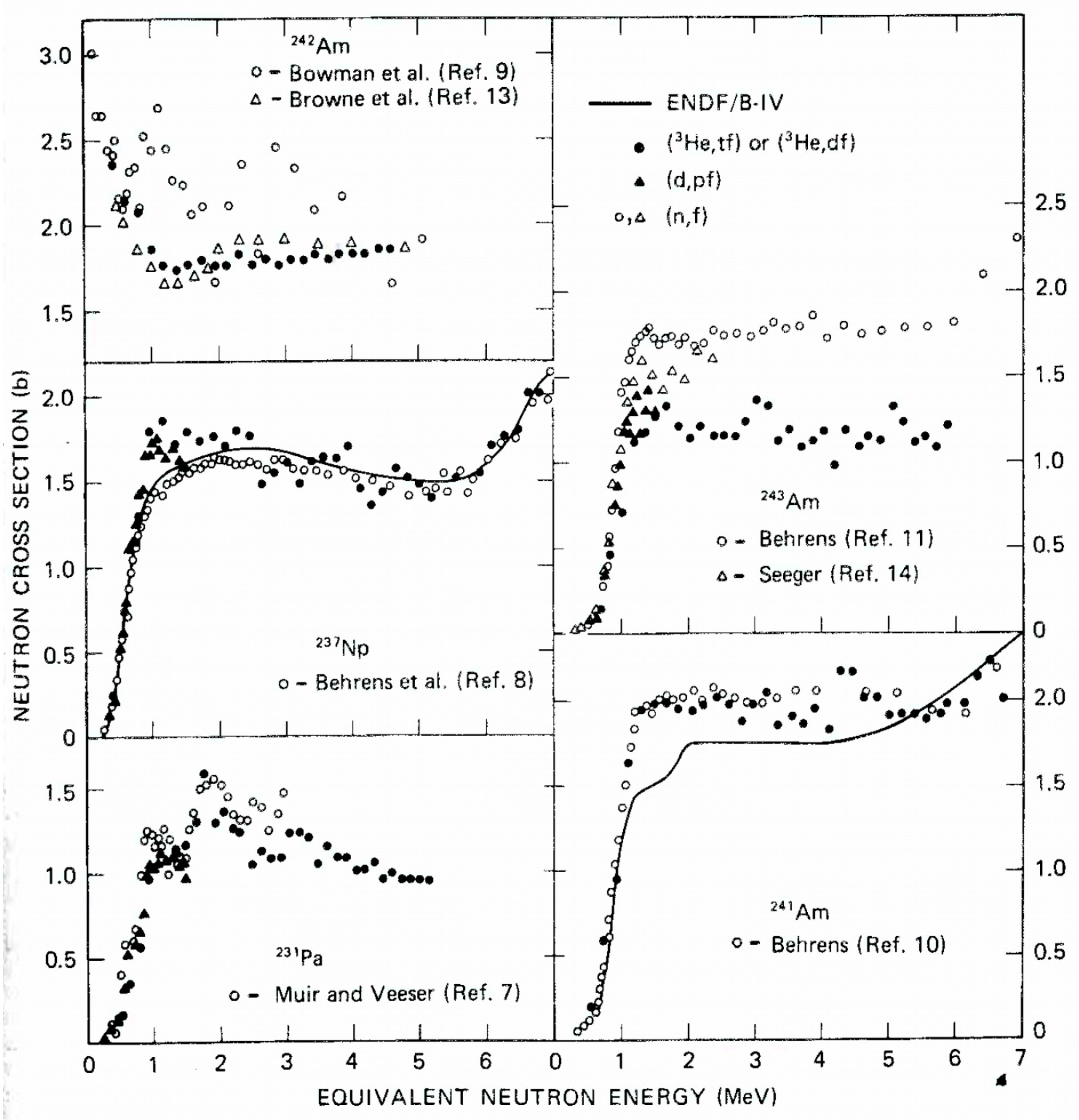

Figure 4: The (n, f) cross sections for ^{241,242,243}Am, ^{237}Np, and ^{231}Pa determined using the Weisskopf-Ewing approximation to analyze (^{3}He,tf) data. The results were compared to direct (n, f) cross sections and ENDF/B-IV evaluations. Figure reproduced from Ref. [25] Fig. 2.

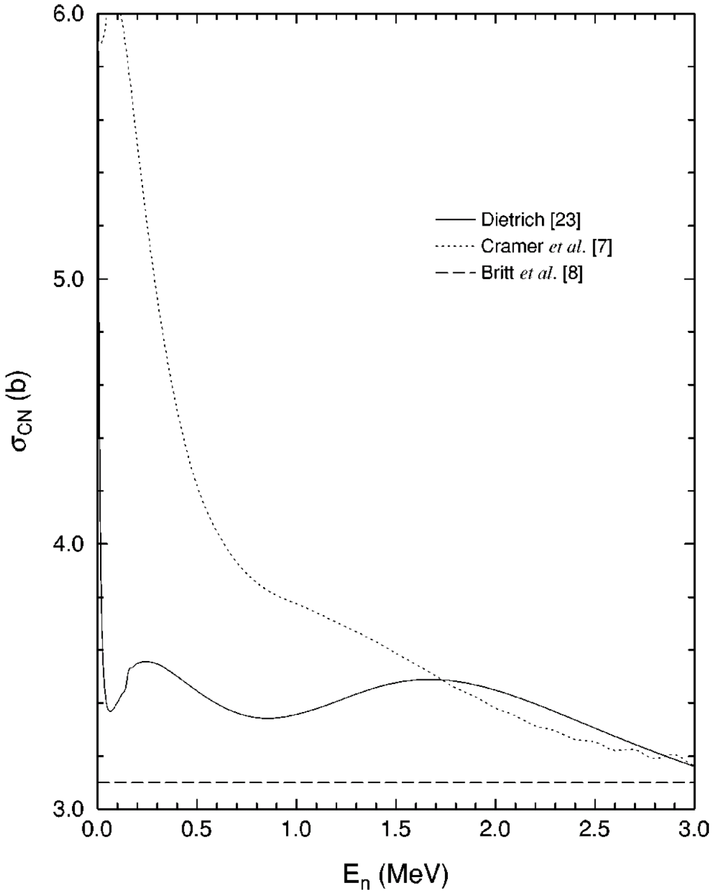

Figure 5: The cross section for the formation of the compound nucleus used in the analyses of Refs. [33, 25, 99]. Figure reproduced from Ref. [99], Fig. 7.

3.3 CENBG Surrogate experiments using the Weisskopf-Ewing approximation

In recent years the nuclear physics group at the Centre d'Études de Bordeaux Gradignan (CENBG) has begun doing absolute surrogate cross section measurements [65]. The research group performs their experiments at the Tandem accelerator at the Institute de Physique Nucléaire d'Orsay (IPN Orsay). In the following sections, the experimental apparatus are described and then specific experiments are discussed.

3.3.1 Experimental apparatus

The CENBG setup consists of four silicon telescopes located at 90° and 130° with respect to the beam axis. The δE-E telescope consisted of a δE with a 150 μm or 300 μm fully depleted silicon detector and a 5 mm thick lithium drifted silicon E detector. This telescope allowed for the isotopic separation of the hydrogen species while providing an energy resolution of approximately 100 keV. A schematic of the apparatus is shown in Figure 6. The solid angle coverage of the detector at 90° was 0.026 steradians and 0.0113 steradians at 130°. The detectors sampled ± 10 degrees at the 90° location and ±7 degrees at the 130° location in the reaction plane. The fission detectors used were photovoltaic cells which measured 20 mm X 40 mm. There were five units with 3 photovoltaic cells each, for a total of 15 fission detectors, arranged in the reaction plane defined by the beam and silicon telescope. The photovoltaic cells were oriented vertically so that one cell was in the reaction plane and there was a cell on either side out of the reaction plane. The four forward angle detectors covered a total angular range from 14° to 125°. The fission detectors were located at a radius of 5 cm from the target and correspondingly covered an out of plane angle range of $\pm 51^o$. A final fission detector was placed at backward angles 180° with respect to the most forward fission detector. The total solid angle coverage of the fission detector array was 48.4%. The energies from the silicon telescopes were recorded using 13 bit analog to digital converters (ADCs).

3.3.2 Data reduction and analysis

The CENBG results are based on measuring absolute surrogate cross sections which require the exact knowledge of how many particle singles and particle coincidence events there were during the experiment. This procedure allows the group to determine the fission probability as a function of energy over the energy range of interest. A primary concern when designing this experiment is how to minimize the systematic effects that be introduced into the single and coincident spectra from background contaminants. Therefore there are two reasons the backward angles for the telescopes were chosen i) the light contaminants are kinematically shifted out of the energy region of interest ii) the elastic peak cross section at backwards angles is greatly reduced. The fission probability as a function of excitation energy is given as

$$P_f(E^*) = \frac{1}{\epsilon_{ff}(E^*)} \frac{N_{coinc}(E^*)}{N_{single}(E^*)} \tag{12}$$

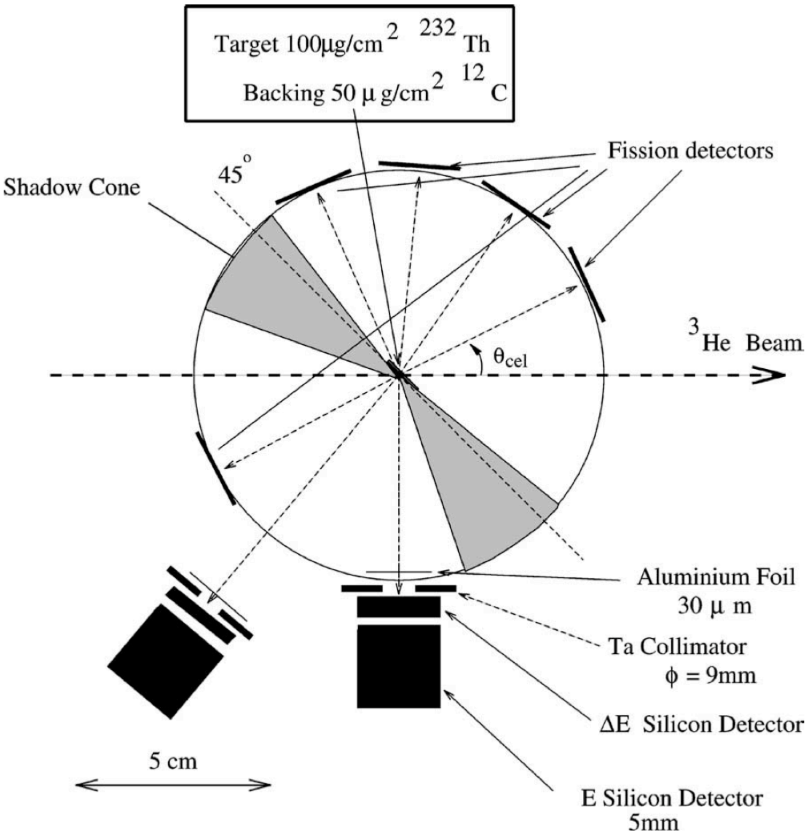

Figure 6: Experimental setup used by the CENBG group at IPN Orsay for fission probability measurements. The beam from the Tandem enters from the left and strikes the target at the center of the chamber. The four silicon telescopes are located at 90° and 130° with respect to the beam and multiple photovoltaic cells are used to detect fission fragments.

where ϵ_{ff} is the fission fragment detection efficiency, $N_{coinc}(E^*)$ is the number of particle-fission coincident events at excitation energy E^* and $N_{single}(E^*)$ is the number of singles events at excitation energy E^*. The proton singles spectra obtained from the ^{232}Th(^{3}He,x)^{23x}Pa experiments in [78] are shown in Figure 7. The particle fission coincident events are accepted if they are prompt in the particle-fission time to amplitude (TAC) spectrum and the energy of the fission fragment is greater than 10 MeV. The particle-fission TAC is also used to background subtract the random fission events from underneath the prompt particle-fission TAC peak as a function of energy. With the particle singles and particle fission events correctly identified the fission detector efficiency must be determined accurately. The fission detector efficiency does not simply correspond to the geometrical solid angle of the fission detector with respect to the target location. Fission fragments have anisotropic distributions that change as a function of energy. The fission fragment angular distributions change the efficiency of the fission fragment detector. The anisotropy of the distribution is also excitation energy dependent. Therefore the fission fragment detector efficiency needs to be determined as a function of excitation energy for each reaction studied. As representative example, the fission fragment anisotropy for the ^{232}Th(^{3}He,d)^{233}Pa reaction at $E^{*} = 11.3$ MeV is shown in Figure 8. The distribution is fit with a Legendre polynomial sum given by

$$W(\theta, E^{*}) \approx \Big(1 + \sum_{L=0,2,...} g_L(E^{*}) P_L(cos(\theta))\Big). \tag{13}$$

The constants from the fit are used to determine the anisotropy and correct then detector efficiency. The fission fragment anisotropy and the information that can be obtained from it are discussed in detail in section **??**. Once the detector efficiency has been determined then the fission probabilities can be determined from the data as a function of excitation energy.

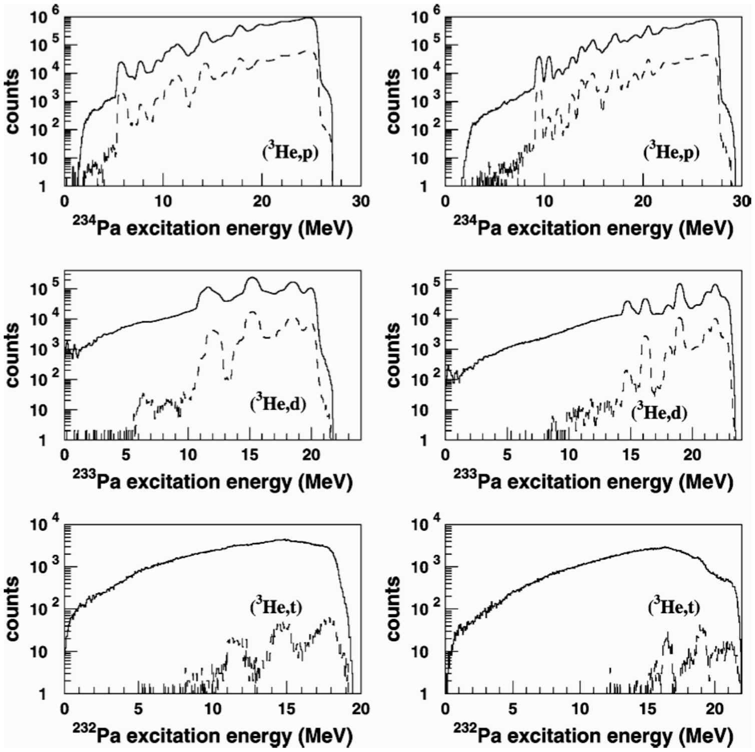

Figure 7: Singles spectra from a representative CENBG experiment. Shown are spectra resulting from ^{232}Th + ^{3}He reactions at 30 MeV incident ^{3}He energy. The histograms on the left (right) correspond to the singles spectra on the target from the telescope at 90° (130°). The solid lines represent the ^{3}He induced reactions on the target and the dashed lines represent singles events from a 50 $\frac{\mu g}{cm^2}$ carbon target.

The fission probability as a function of energy determined from the particle-fission, particle singles and fission detector efficiency is shown in Figure 9 for the ^{232}Pa, ^{233}Pa and ^{234}Pa isotopes. In order to calculate the neutron induced fission cross section one needs to now calculate the compound nucleus formation cross section for neutrons on the desired nucleus.

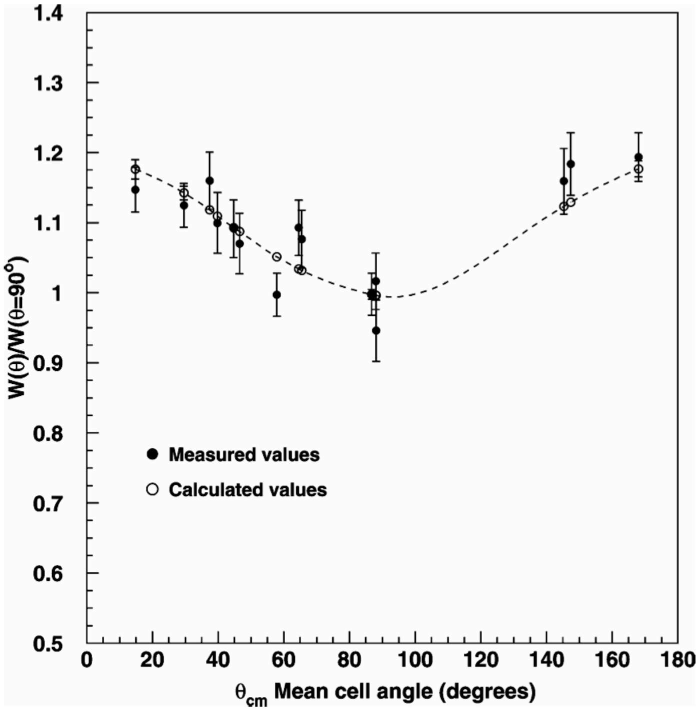

Figure 8: Fission-fragment angular distribution from a representative CENBG experiment, shown for $E^* = 11.7$ MeV for the ^{232}Th(^{3}He,d) as a function of the center of mass angle. The closed circles represent data with statistical errors bars while the open circles and dashed line are the fit to the data from Petit [78].

3.3.3 Cross sections for neutron-induced fission

In the Weisskopf-Ewing limit, the fission cross section can be determined by multiplying the fission probability by the compound nucleus formation cross section, see Eq. 9. One also needs to relate the excitation energy of the nucleus in the calculation to the equivalent incident neutron energy as shown by

$$\sigma_{(n,f)}(E_n) \approx \sigma_{CN}(E_n) P_f\Big(E_{ex} = S_n + \Big(\frac{A-1}{A}\Big)E_n\Big) \tag{14}$$

where σ_f is the neutron induced fission cross section, $P_f(E^*)$ is the energy dependent fission probability and $\sigma_{CN}(E_n)$ is the compound nucleus formation cross section. The excitation energy of the nucleus is translated to the incident neutron energy scale by taking into account the neutron separation energy (S_n) and the reduced mass energy of the neutron incident on the nucleus given by $((A-1)/A)E_n$. Determination of the fission probability has been described in the previous section.

The compound nucleus formation cross section for this work has been calculated using a modern semi-microscopic neutron-nucleus optical model potential [9] [11] [10]. The model

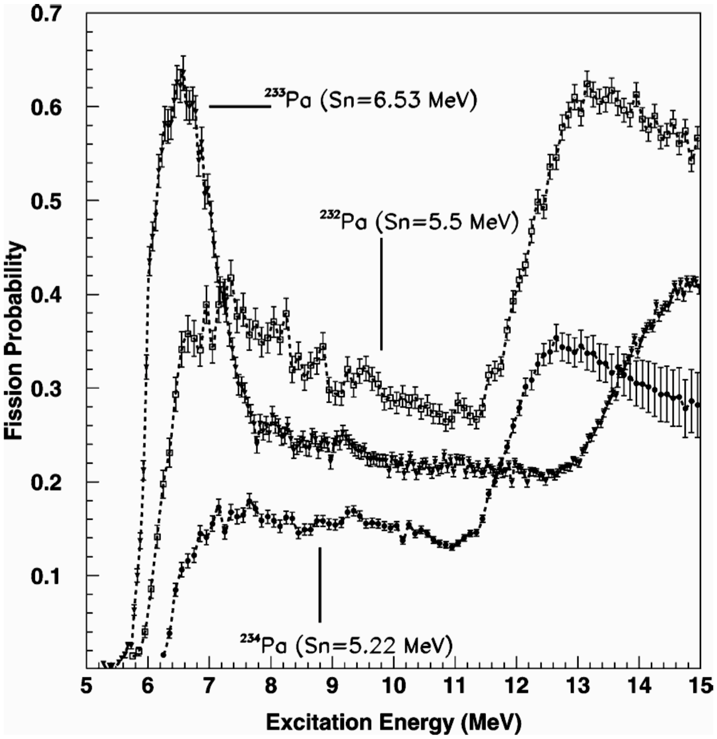

Figure 9: Fission coincidence probabilities from a representative CENBG experiment. Probabilities for detecting fission fragments in coincidence with various direct-reaction particles are shown as a function of excitation energy of the nucleus for ^{231}Pa(n,f),^{232}Pa(n,f) and ^{233}Pa(n,f). The neutron separation energies (S_n) indicate zero incident neutron energy. Figure taken from Petit [78].

incorporates the fact that the target nuclei are deformed and have rotational spectra. The overall approach of the CENBG work has been validated by testing the results against a few known directly measured neutron induced fission cross sections.

Cross sections and results for ^{230}Th(n,f), ^{231}Pa(n,f) and ^{233}Pa(n,f). The method described above has been validated by comparing cross sections for ^{230}Th(n,f) and ^{231}Pa(n,f) reactions deduced from ^{232}Th(^{3}He,^{4}He)^{231}Th and ^{232}Th(^{3}He,t)^{232}Pa Surrogate experiments, using the method described above, to directly-measured (n,f) cross sections. The results for the ^{230}Th(n,f) reaction are shown in Figure 10. Good agreement is seen in the neutron energy region from 0.5 MeV to 7 MeV over the first chance fission region with the results of Meadows citeMeadows:83. The results diverge at the onset of second chance fission from the results of Meadows, but follow the ENDF/B-VI and JENDL-3 evaluations. The ^{231}Pa(n,f) cross section is shown in Figure 11 and compared to the results of Plattard [48]. Again good agreement is seen over the first chance fission region from 0.5 MeV to 6 MeV.

The ^{233}Pa(n,f) cross section has been determined by Petit *et al.* [78] over a neutron energy range from 1 to 10 MeV using the ^{232}Th(^{3}He,p)^{234}Pa transfer reaction. It is compared to a direct measurement by Tovesson *et al.* [45] and to evaluated cross sections in Figure 12. The direct measurements of Tovesson agree within 3σ of the results from Petit. The ENDF/B-IV results disagree with both Tovesson and Petit over the entire range except at the fission barrier near 1 MeV. The JENDL-3 evaluated cross section is in reasonable agreement with the measured cross sections over the energy range from 1 to 6 MeV.

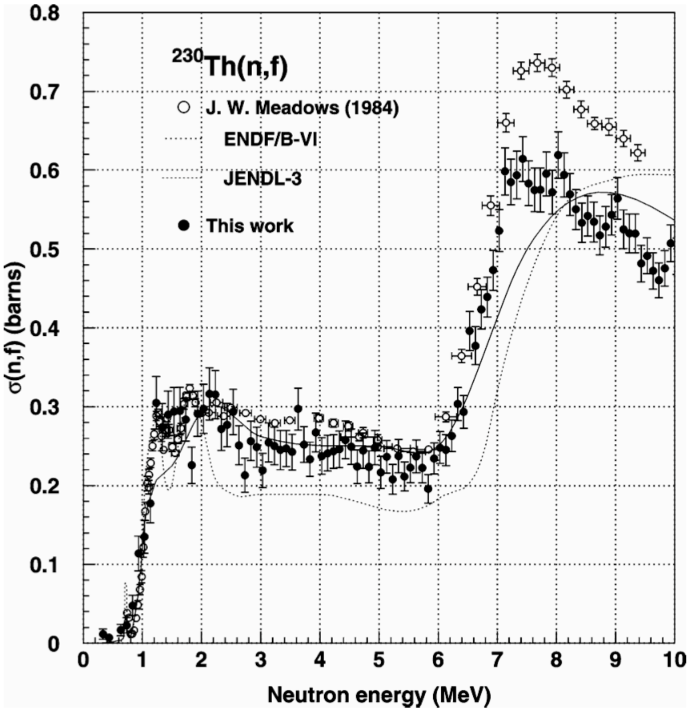

Figure 10: The ^{230}Th(n,f) cross section from Meadows, ENDF/B-VI, JENDL-3 and the CENBG results. The Meadows result is a directly measured neutron induced cross section while the CENBG work is deduced from the ^{232}Th(^{3}He,^{4}He)^{231}Th reaction.

In this body of work lead by the CENBG group they have demonstrated that (^{3}He,^{4}He), (^{3}He,t) and (^{3}He,p) reactions can be used to determine fission cross sections in the actinide region. In general the results are in good agreement with known data in the energy region that covers first-chance fission.

Cross sections and results for ^{241}Am(n,f), ^{243}Cm(n,f) and ^{244}Cm(n,f). Preliminary results for the neutron induced fission cross sections of ^{241}Am(n,f), ^{243}Cm(n,f) and ^{244}Cm(n,f) were presented at the Compound Nuclear Reactions and Related Topics Workshop in 2007. The method used to obtain the cross sections is identical to that used by Petit [78] and described above. The surrogate reactions in this case were ^{243}Am(^{3}He,^{4}He)^{242}Am, ^{243}Am(^{3}He,d)^{244}Cm and ^{243}Am(^{3}He,p)^{245}Cm allowing for a determination of ^{241}Am(n,f), ^{243}Cm(n,f) and ^{244}Cm(n,f) cross sections. The ^{243}Am target was a 106 μg/cm^2 on a 75

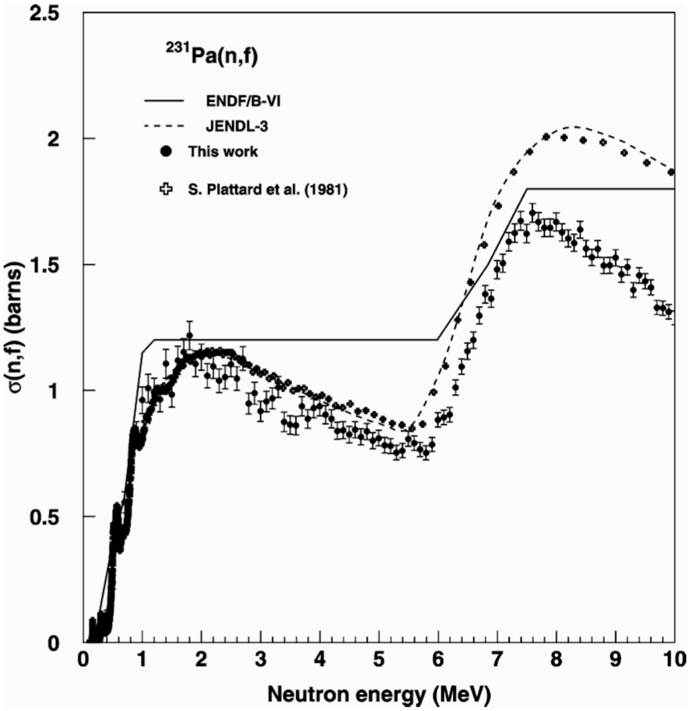

Figure 11: The ^{231}Pa(n,f) cross section is shown for the directly measured neutron induced cross section from Plattard [48] and the Petit results [78]. Good agreement is seen over the first chance fission region.

μg/cm^2 carbon backing. The singles spectra in this experiment were corrected for the reactions on carbon and oxygen present in the target. Only the geometrical fission detector efficiency was taken into account in the results presented here. The anisotropy correction to the fission detector efficiency was estimated to be small, on the order of 2-3 %.

The fission probabilities of ^{242}Am, ^{243}Cm and ^{244}Cm were determined and then multiplied by the compound nucleus formation cross section for each reaction. The resulting cross sections are shown in Figure 13.

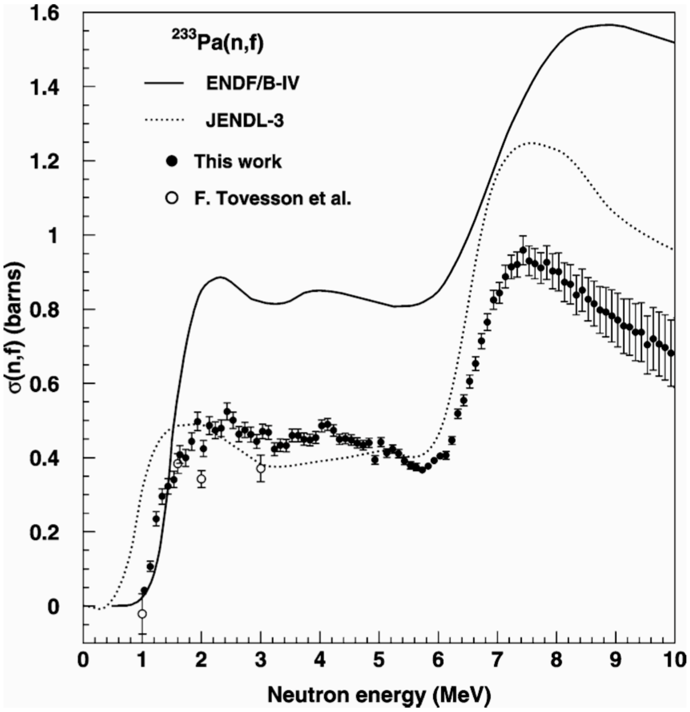

Figure 12: The ^{233}Pa(n,f) cross section has been determined using the ^{232}Th(^{3}He,p)^{234}Pa reaction by Petit [78].

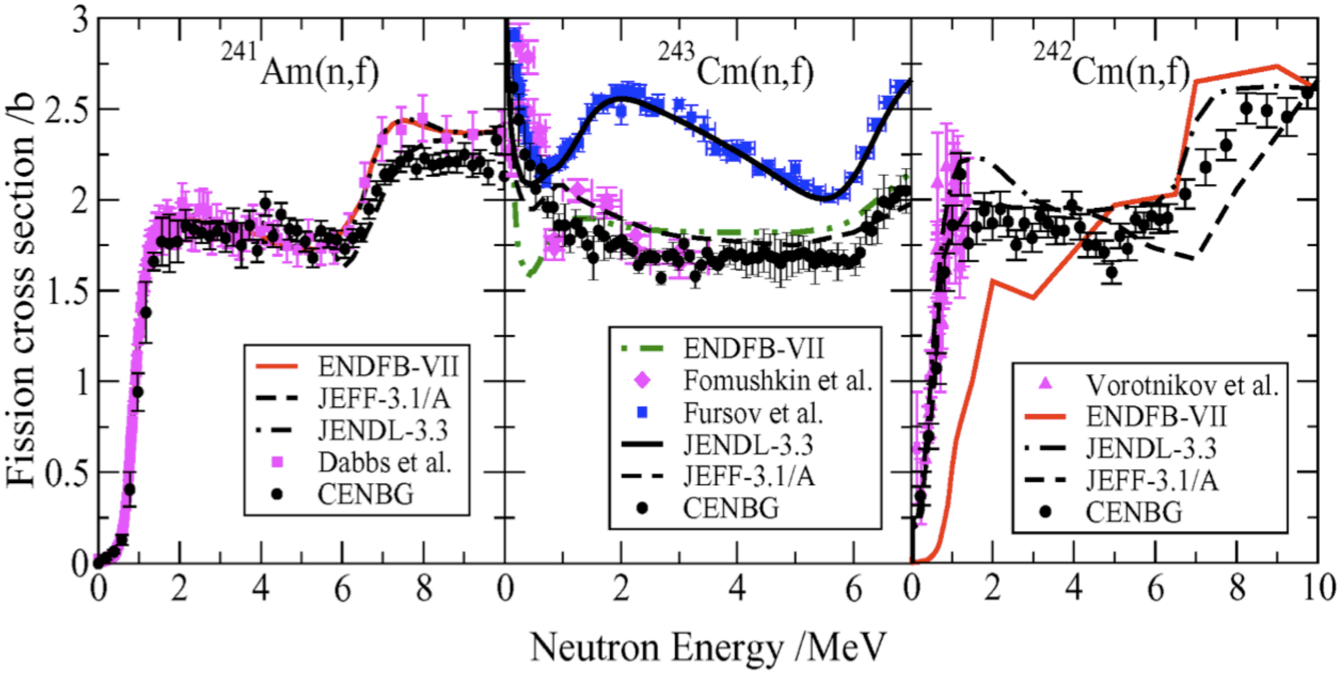

Figure 13: The preliminary results of the CENBG group are shown for ^{241}Am(n,f), ^{243}Cm(n,f) and ^{244}Cm(n,f). The results were determined from the ^{4}He, d and p exit channels from ^{3}He incident on ^{243}Am. The results are compared to direct measurements and evaluations [46] [50] [44] [47].

3.4 Surrogate experiments at STARS/LiBerACE

In 2003, LLNL nuclear physicists started a new effort to determine cross sections from Surrogate measurements. The first few experiments were carried out at the Wright Nuclear Structure Laboratory at Yale University. Following this experience the STARS/LIBERACE array was designed and assembled by a collaboration of scientists from Lawrence Livermore National Laboratory and Lawrence Berkeley National Laboratory. The Silicon Telescope Array for Reaction Studies (STARS) has been developed by a collaboration lead by Lawrence Livermore National Laboratory and Lawrence Berkeley National Laboratory. An auxillary array of high purity germanium (HPGe) detectors called the LIvermore BERkeley Array for Collaborative Experiments (LIBERACE) is used with STARS. The apparatus was installed at the 88 Inch Cyclotron at Lawrence Berkeley National Laboratory in Berkeley, California. The STARS/LIBERACE system has been used to study light ion reactions of various species of incident particle from protons to ^{18}O on targets spanning the periodic table of elements.

In a five-year period, over 55 experiment runs occurred investigating surrogate reactions, astrophysics, nuclear lifetimes and nuclear structure. In the following sections, the STARS/LIBERACE apparatus will be described as well as a few key experiments that employ variants of the Weisskopf-Ewing approach to analyze Surrogate data.

3.4.1 The STARS charged particle detector system

The Silicon Telescope for Reaction Studies (STARS) is a robust modular silicon telescope array. Using STARS to identify the outgoing particles, their scattering angle and energy, one can study a wide range of nuclear processes and reactions including surrogate reactions. A schematic drawing of the detector system is shown in Figure 14. The detector systems and components are described in the following sections.

Silicon Telescope Array for Reaction Studies - STARS. The STARS detector system consists of two or more Micron S1 or S2 silicon detectors arranged in a ΔE-E telescope configuration. The Micron S2 detectors consists of a silicon wafer with an active inner diameter of 22 mm, an active outer diameter of 70 mm and various thicknesses. The Micron S2 detectors currently available at STARS are nominal thicknesses of 65 μm, 140 μm, 300 μm, 500 μm and 1000 μm. The detectors are double sided and coated with 48 one mm wide aluminum rings on one side and 16 gold coated sectors on the other. The aluminum rings have an areal density of 27 μg/cm^2 and the gold sectors are 500 μg/cm^2. A Micron S2 detector has also been used upstream of the target location to detect fission fragments in coincidence with scattered particles. Typically a 140 μm thick S2 detector is used as the fission detector. This thickness is useful in that it separates the fission fragments from direct beam particles energetically. The most energy an alpha particle can deposit in a 140 μm thick silicon detector (normal incidence) is approximately 20 MeV. Fission fragments are typically more energetic even after taking into account energy down-scatter due to energy loss in the target prior to escape. The silicon telescope can be placed at various distances from the target. Typically the angle range covered by a telescope is from 35° to 65° when particles strike the inner and outer rings respectively.

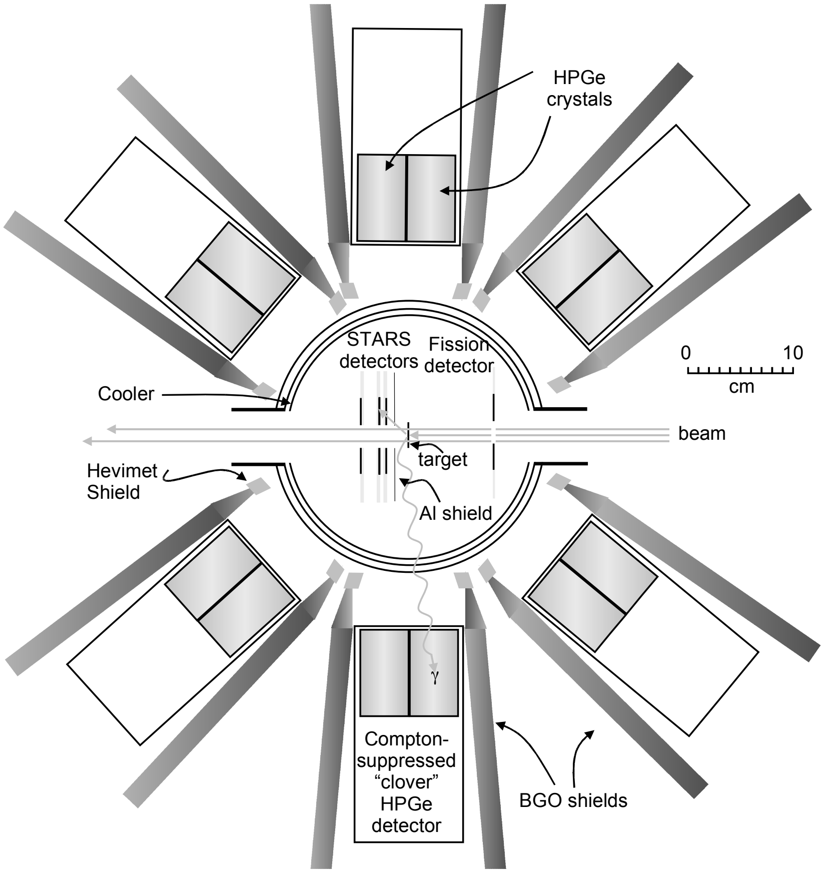

Figure 14: The top view of the STARS/LIBERACE detector system is shown. The HPGe clover detectors are surrounded by BGO Compton shields. The STARS target chamber contains the silicon telescope array, target wheel and optional fission detector. The Hevimet shields and copper cooler can also be used as needed.

When a charged-particle beam strikes a target it liberates electrons from the target. These electrons are called δ electrons. The electrons are attracted to the charged surfaces of the silicon detectors. Gradually during an experiment the δ electron flux can alter the leakage current of the silicon detector. Due to the way the resistor network is designed, as the current increases the bias voltage on the detector decreases, causing a gain shift. To mitigate the effect of δ electrons an aluminum shield is placed in front of the δE detector to reduce and eliminate the delta electron. The aluminum shield can be very thin and typically has an areal density of 200 μg/cm^2. Fission fragments that strike the δE detector slowly damage the detector and its energy resolution decreases. To stop the fission fragments a 4.4 mg/cm^2 thick aluminum shield is used. The fission fragments range out in the aluminum and never reach the silicon detector.

Scattering chamber. The aluminum target chamber is a cylinder, 23.50 cm high with a 25.08 cm diameter and 0.40 cm thick walls. The cylinder is oriented perpendicular to the beam axis and HPGe clover detector plane. The design of the detector mounts allows the Si detectors to be lowered in from the top of the chamber onto two alignment rails. The detector pack can then be positioned as close as 1.0 cm and as far as 12 cm from the target. The alignment rails are symmetric in the chamber and the silicon detectors can be position either downstream (forward angles) or upstream (backward angles) of the target. There is a view port on the top of the chamber which allows a camera to view a phosphor in a target position so that the beam profile can be observed during beam tuning. The square base that supports the target chamber contains several BNC vacuum feedthroughs through which high voltage is supplied to the silicon detectors. There are also two vacuum feedthroughs which contain four 34 pin ribbon cable feedthroughs. These feedthroughs connect the breakout boards to the preamplifiers located just outside the vacuum wall. A photo of the top view of the chamber loaded with a simple silicon detector is shown in Fig. 15.

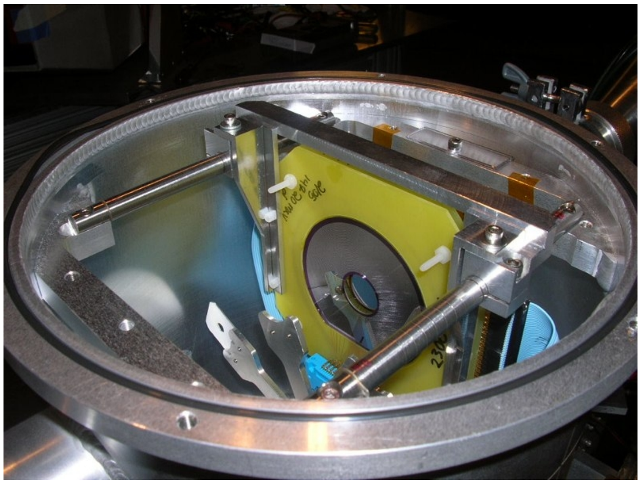

Figure 15: The photo shows a view of the STARS chamber without the top on. The target wheel is in the foreground and a closely packed silicon telescope (of S2 type) is shown behind, resting on the rails. Ribbon cables connect the detectors to motherboards located under the cylindrical chamber. The beam enters the chamber from the lower left and exits through the upper right.

Target Wheel. The target wheel has eight target positions with the ability to rotate (while maintaining vacuum) between various targets during an experiment as can be seen in Figure 16. Each 0.16 cm thick aluminum target frame is a 2.54 x 3.81 cm rectangle, with a variety of diameter holes 2.54 cm from the bottom for the placement of the target foil. There are two notches on the bottom of the target holder to secure it to the target wheel with hex head 4-40 screws. The target wheel was also designed to accommodate the GAMMASPHERE [68] target holders (with an adaptor) which increases availability of on-site targets.

The target wheel is sighted into the chamber by using a theodolite that looks along the beam axis starting from the beam dump and looking upstream. The left-right centering of the target wheel is accomplished with the theodolite and a special target frame with scribed centering marks on it. During an experiment, phosphor coated target frames with various holes sizes (6.4 mm, 9.5 mm and 12.7 mm diameter) are used to tune and focus the beam.

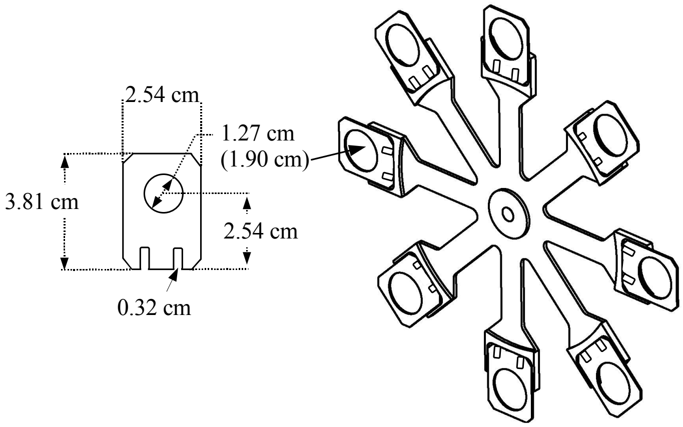

Figure 16: Schematic of the 8-position target holder. A typical target frame is also shown with a 1.27 cm diameter hole. The target wheel is shown loaded with target frames with a 1.90 cm diameter hole.

The beam intensity is dropped down to the sub-particle nA range for visual tuning. The next step is to reduce the scattered beam from the smallest tuning blank striking the silicon telescope. Once these steps are complete the experiment is then ready to proceed.

Targets can be self-supporting or backed with a rigid material. Examples of self-supporting targets are a 761 μg/cm^2 ^{238}U metallic foil [70, 8] and ^{9}Be foils [96]. Most of the actinide targets require a support backing. The thicknesses of backing materials are chosen to minimize the energy loss and straggle of the outgoing fission fragments. Examples of these targets include ^{235}U (720 μg/cm^2 thick) stippled onto a 100 μg/cm^2 natural C backing [70] and ^{234}U (253 μg/cm^2) electroplated on a 2.29 mg/cm^2 Ta foil [69].

Energy Calibration. The energy calibration of the rings and sectors of the silicon telescope is performed using a combination of the following; 1) α-lines from a standard ^{226}Ra source, 2) the energies of ground and excited states of low-mass contaminants such as carbon or oxygen, and 3) the elastic scattering peak from the target nuclei. A commercially available ^{226}Ra α source is used to calibrate the silicon detectors for energies less than 8 MeV. Energy resolution varies by experiment and is dependent on detector thickness and previous use. A representative spectrum is shown in Fig. 17 for a 140 μm detector [30]. As the energy of the detected particles can be $\gg$10 MeV, other methods must be used to reliably extend the calibration to higher energies.

The ground and excited state energies of target contaminants such as^{1}H, ^{12}C and ^{16}O are well known. If these peaks are observed in the silicon spectra, they can be used to calibrate higher energies. Also, elastic and inelastic scattering from discrete states in the target nucleus or calibration targets can be used as an *in situ* energy calibration.

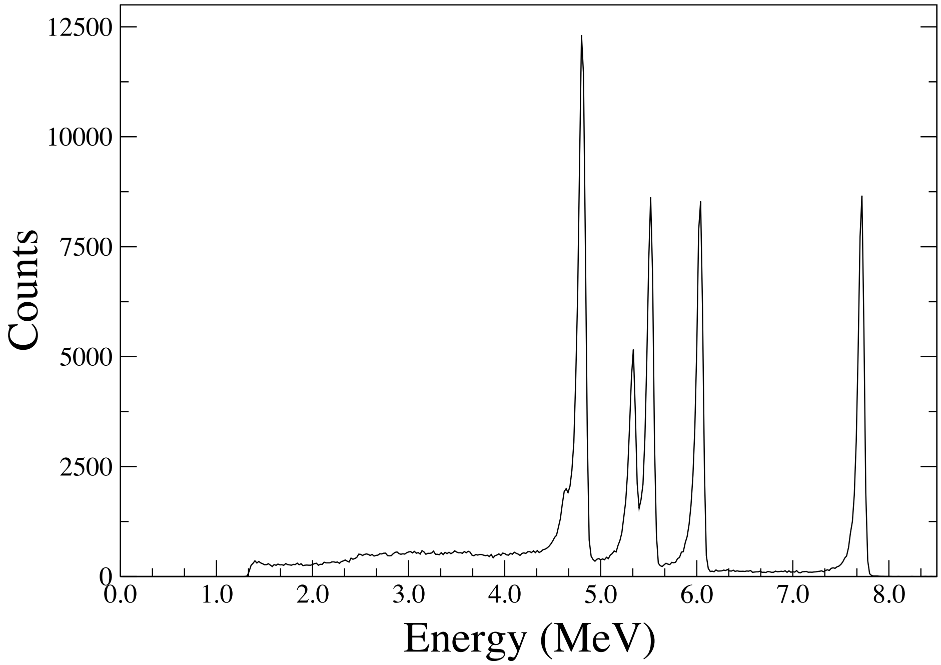

Figure 17: A typical ^{226}Ra calibration spectrum is shown for a 1000μm S2 detector. The FWHM for the 7.868 MeV peak is 60 keV.

Particle Identification. Particles are identified by the differential energy loss between the front ΔE ($E_{\Delta E}$) detector and the back E (E_{E1}) detector(s) of the telescope from their characteristic values:

$$a^{-1} = \frac{\cos\theta}{T}\Big((E_{\Delta E} + E_{E1})^{1.73} - E_{E1}^{1.73}\Big), \tag{15}$$

where $\frac{T}{\cos\theta}$ is the path length through the ΔE detector of thickness T and θ is the angle of incidence of the particle. This relation is based on the empirically-determined range of particles in matter of $aE^{1.73}$, where a is a constant that scales inversely with the rate of energy loss [57]. Fig. 18 shows a representative PID plot from the STARS/LIBERACE particle telescope used for charged particle identification. The same data can be converted to a range energy plot using equation 15. The resulting range versus energy histogram is shown in Fig. 19. If the incident particles are too energetic and manage to pass through the entire telescope then they are said to have "punched through" the detector. This is the origin of the backbend in the PID plot for the protons and deuterons shown in Fig. 18.

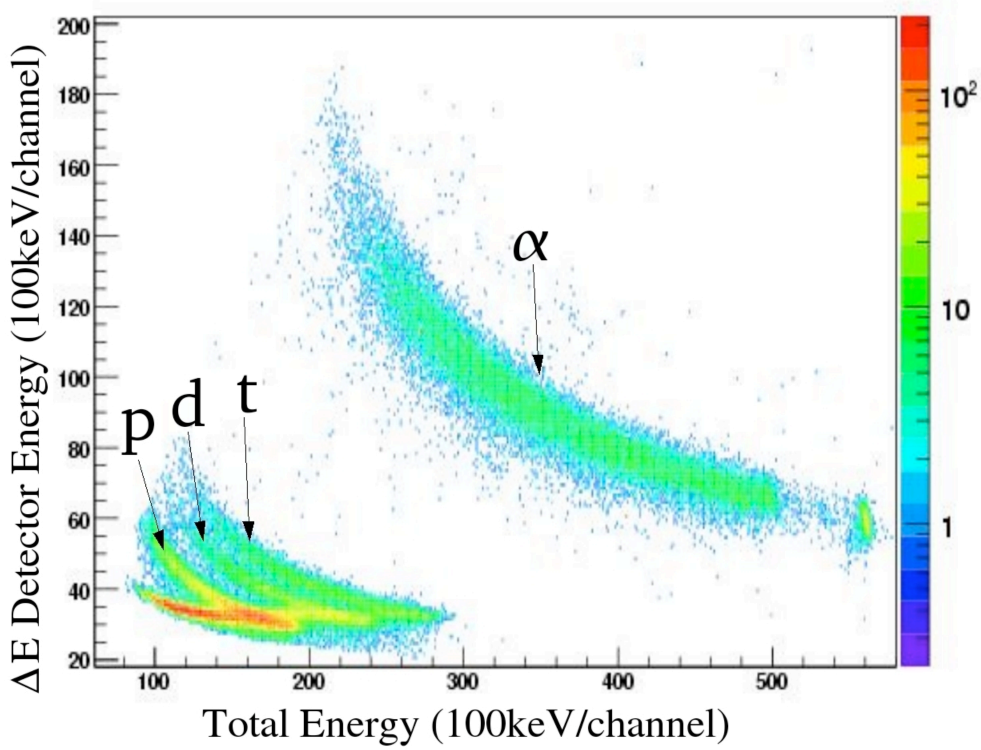

Figure 18: Shown here is a representative particle identification plot using the STARS detector array. The respective p,d,t and α particle bands are labeled.

Valid event identification To identify real particle events that originated from the target location a series of requirements are applied to the data. For each event the δE and E detector sectors had to match each others position. Only events which occur in the ΔE detector ring and a cluster of consecutive rings in the E detector are valid. This is determined from a ring-ring correlation matrix representing a "ray-trace" of the particle from the target to the detector. Only single signal events are considered, i.e. if an event triggers two sectors or rings which are not near each other, it is rejected. Generally the sectors are used to determine the energy of the event and the rings are only used for θ angular information.

Energy loss in the target material, dead layers of the detector and δ-shield which is not measured must be calculated and added back to obtain the correct particle energy. This is done by using the program *Elast* (Energy Loss and Straggling Tool) [1] or SRIM [106]. The energy loss due to the kinematic recoil of the target nucleus is also calculated based on the beam energy, scattered particle energy and angle of the scattered particle. This energy is also added back to obtain the true excitation energy of the target nucleus.

The Cooler. To improve the energy resolution of the silicon detectors, a thin copper heat shield may be placed inside the target chamber and used as a radiative cooling system. This copper is thermally insulated from the chamber and cooled to -10 to 0°C by flowing ethylene glycol through a closed circuit. This maintains the silicon detectors at a temperature of approximately 15°C and improves the intrinsic energy resolution of the silicon detectors.

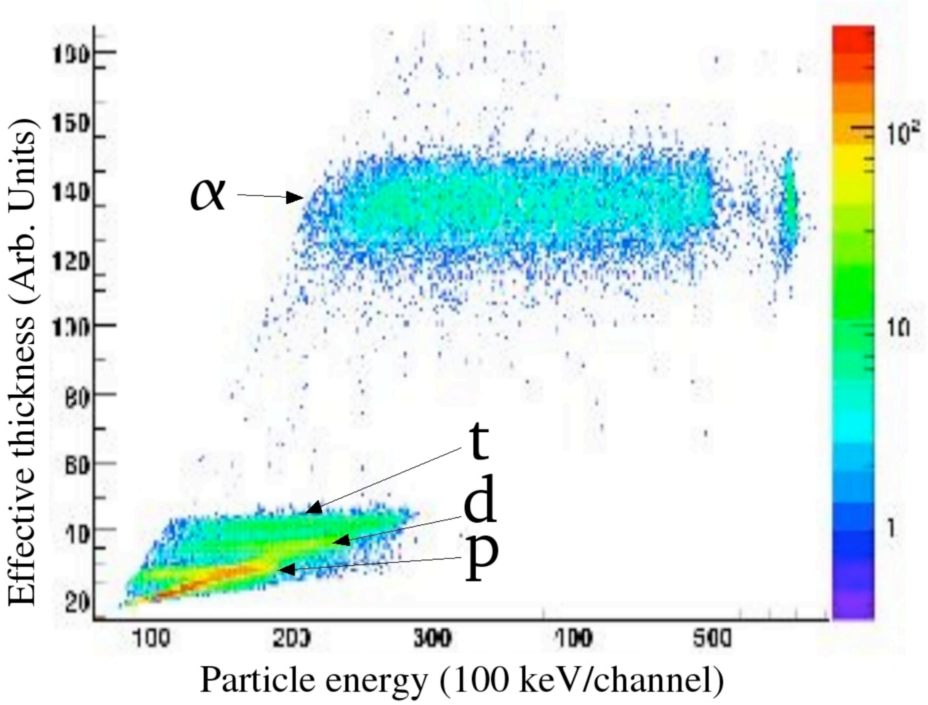

Figure 19: A representative range energy plot is shown with p,d,t and α particle ranges are identified.

However, the benefit of improved energy resolution of the silicon detectors comes at a cost: more material is introduced between the target and high purity germanium detectors so the detector efficiency for low-energy γ rays decreases.

Fission Detector. For surrogate measurements and other experiments which require fission particle energy or identification, a Micron S2 detector is placed in the STARS chamber upstream of the target position. The fission fragments gradually radiation damage the front surface of the detector and the energy resolution of the detector degrades over time.

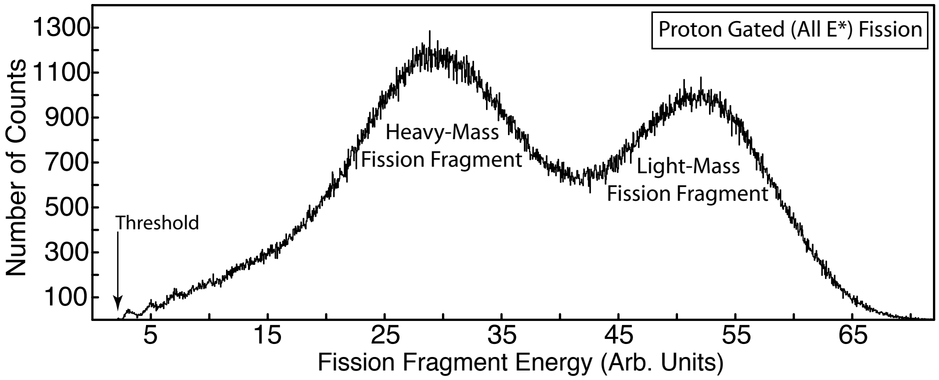

Figure 20: The proton-gated fission spectra from the ^{235}U(d,pf) surrogate experiment [3]. The light and heavy mass fission fragments peaks are indicated.

The fission detector in STARS is typically a 140 μm thick Micron S2 detector. The fission detector is usually located a distance of 12 mm upstream of the target with the ring side facing the target. The angular range for detecting fission fragments is $106-131^{\circ}$ [30, 70, 69] at this distance. Fig. 20 is an example of the fission fragment energy spectrum detected from the STARS/LIBERACE ^{235}U(d,pf) surrogate experiment [3].

STARS Signal Processing. The silicon detector signal processing by which energy is recorded for each event is described as follows. The detectors are fully depleted by applying a bias voltage to the ring side while the sector side is held at ground potential. The bias voltage and signal lines are coupled to the detector via a custom breakout board within the vacuum chamber. Breakout boards for the S2 detector have been designed in two different configurations; 24 rings and 8 sectors or 48 rings and 16 sectors. The first breakout board design combines adjacent rings and sectors through a 64 pin high-density Yamaichi connector from the detector into two 34 pin connectors for a total of 32 signals. The second breakout board design converts all 48 rings and 16 sectors to four 34 pin connectors for a total of 64 signals. A similar breakout board with 48 rings and 16 sectors is used for Micron S1 detectors. Bias voltage on each board is supplied via a LEMO connector.

The outputs from the breakout board is plugged into a custom made NEMA-G vacuum feedthrough that contains four 34 pin feed throughs for a total of 64 channels per feedthrough. There are two feedthroughs located in the base of the scattering chamber that can accommodate a total of 128 channels of silicon with the capacity to add more. The signal pulses are AC coupled through 1300 pF capacitors to the pre-amplifiers. The capacitors isolate the DC bias supply from the pre-amplifier signal inputs.

The silicon signals are amplified by Swan Charge 8 pre-amplifiers. The pre-amplifiers have gains of 8 mV/MeV, 20 mV/MeV and 45 mV/MeV. The appropriate gain for a given detector is chosen for each experiment depending on the dynamic range required. The pre-amplifers are plugged into a motherboard that provides power and the ability to test the pre-amplifers response to a pulser signal. The preamplifiers are located right next to the vacuum feedthrough on each side of the chamber.

The pre-amplifier signals are amplified and shaped by CAEN N568B shapers which have either a 1k Ohm or 50 Ohm input impedance. Each signal channel is attached to the shaper by individually shielded coaxial cables. Each shaper provides 16 individual fixed-gain fast outputs and 16 shaped slow output signals with approximately a 400ns delay. The fast output signals are discriminated using LeCroy 1806 CFDs which have been converted to leading edge discriminators. The OR output from the LeCroy 1806 discriminators are used to form a trigger as discussed below.

The particle trigger is formed from the overlap of the ΔE and E detector signals. The OR output signals from the two to four discriminators used for the ΔE detector are logically ORed together. The same process is followed for the E detector. An overlap circuit is created using a gate and delay generator which produces a 200 ns logic pulse from the OR input from the E detector and a separate gate and delay generator produces a 50 ns logic pulse from the ΔE detector OR input. The 50 ns pulse is delayed so it arrives in the middle of a logical AND whose output is the particle master trigger.

3.4.2 The LIBERACE γ-ray detector system

Detectors. The LiBerACE system consists of up to six Compton suppressed EURISYS HPGe 2-fold segmented Clover detectors on a horizontal plane in a close-packed configuration around the STARS target chamber as shown in Fig. 14. The four n-type germanium crystals, 50 mm in diameter and 80 mm in length, are arranged as a four-leaf Clover [38]. The crystals are mounted in a cryostat cap with a 0.6-mm gap between each side and 10 mm from the front face of the detector. Each Clover is surrounded by 16 optically-separated SCIONIX Bismuth-Germante (BGO) scintillation crystal detectors act as Compton suppression shields [39]. The detectors are positioned as close to the target chamber as possible at 40°, 90° and 140° (measured at the center of the Clover) relative to the beam. The center of each crystal of the Clover is offset by 2.5 cm from the centerline of the detector. When the detectors are flush against the chamber wall, this offset is ± 9°. Hevimet collimators may be attached to the front of the BGO detectors to decrease false vetoes due to high multiplicity events. The Hevimets have a trapezoidal cross-section thickness of either 40 mm or 26 mm. The thicker Hevimets change the angular offset of each crystal in the detector to ±7.0° and the thinner one to ±7.5° in the most forward position. In addition, the use of a LEPS (Low-Energy Photon Spectrometer) detector offers the ability to observe photons with less than 300 keV energy with higher efficiency.

Energy Calibration and Efficiency. For most experiments, the Clover-detector calibration is determined for each individual crystal: both the energy response and the photopeak efficiency for γ rays that originated from the target location. The energy response is determined from second-order polynomial fits to γ ray sources. For most experiments, energy calibrations are performed periodically during the experiment and efficiency calibrations are performed before and/or after data collection. Gain drifts can occur over the course of the experiment. These gain changes are apparent when the calibration is applied to determine the energy of known transitions and can be easily removed by re-calibrating. The energies of all the detectors can typically be aligned to within 0.2 keV at energies <400 keV, increasing to 1 keV at energies >1000 keV. The spectra from all the detectors can be summed together and the resulting resolution (FWHM) of 1.8 keV at 300 keV and 2.7 keV at 1000 keV is nearly identical to the energy resolution of the individual crystals.

The energy-dependent efficiency, $\epsilon_\gamma(E_\gamma)$, of the LiBerACE array is determined offline using standard ^{152}Eu (2.91 ± 0.10 μCi), ^{133}Ba (0.361 ± 0.007 μCi), and ^{207}Bi (4.85 ± 0.20 μCi) sealed sources placed at the target location. With these sources, the efficiency can be determined to ≈5–10% over an energy range of 45–1800 keV. The total efficiency of the array peaks at ≈3% near 200 keV and decreases at both higher and lower energies. The photopeak efficiency of the array can be greatly improved at higher energies by using an appropriate add-back routine [38] to sum together the energy deposited in the different crystals of the individual Clover detectors. The efficiency calibration from a recent experiment using five Clover detectors (without addback) is shown in Fig. 21. At the lowest energies, the efficiency depends sensitively on the material between the target and detector and can vary significantly from crystal to crystal even within the same Clover detector.

For example, *in situ* efficiency calibrations are performed to verify the efficiency calibra-

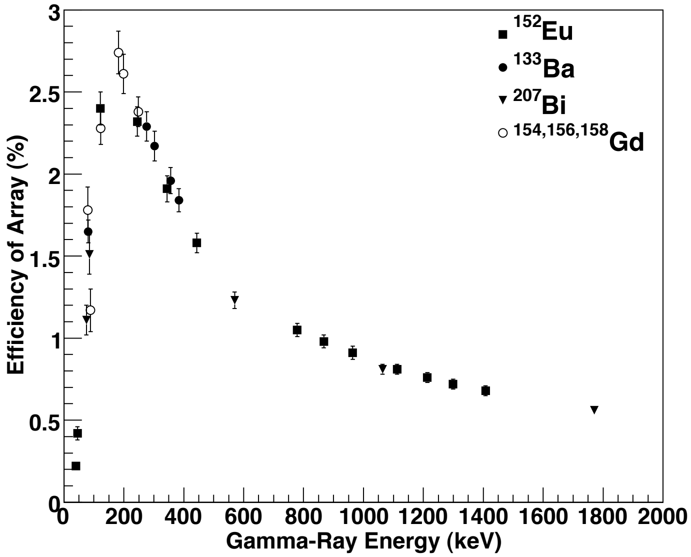

Figure 21: The efficiency of the LiBerACE HPGe array (using five Clover detectors and the copper cooler) determined using ^{152}Eu, ^{133}Ba, and ^{207}Bi sealed sources and transitions in ^{154,156,158}Gd measured *in situ.*

tion. In a recent experiment in which protons bombarded ^{154,156,158}Gd targets, $p-\gamma-\gamma$ coincidences in $6^+ \rightarrow 4^+ \rightarrow 2^+$ and $4^+ \rightarrow 2^+ \rightarrow 0^+$ ground-state band cascades of ^{154,156,158}Gd nuclei were analyzed. Absolute activities were determined by analyzing γ-ray cascades for which a pair of γ rays (denoted γ_1 and γ_2) were known to be emitted in coincidence. The efficiency, ϵ_2, for detecting γ_2 was determined from the ratio of the number of $\gamma_1 - \gamma_2$ coincidences, $N_{\gamma_2\gamma_1}$, relative to the total number of γ_1 events observed, N_{γ_1}, after accounting for the internal conversion coefficient α_2, and including small ($\sim$5%) corrections:

$$\epsilon_2 \approx \frac{N_{\gamma_2\gamma_1}}{N_{\gamma_1}} \times (1+\alpha_2) \times \frac{n}{n-1} \times (1+\Omega_C). \tag{16}$$

For the Gd measurements, $n = 19$ was the number of HPGe detector crystals (one leaf on one of five Clover detectors was not functional) so $\frac{n-1}{n}$ was the fraction of detectors available to detect γ_2 following the detection of γ_1 (assuming all elements have identical detection efficiency). Summing corrections were negligible because each detector element subtended only 0.3% of 4π. Ω_C allows for the change in efficiency because γ_2 is not emitted isotropically due to $\gamma-\gamma$ angular correlations. This term is < 0.04 even for large correlations because of the substantial in-plane coverage of the array. Once ϵ_2 is determined, the absolute activity was determined from the detection rate of γ_2.

LIBERACE Signal Processing. The signals from the Clover detectors and BGO shields are processed by a CAMAC based unit developed by RIS Corp. In total seven signals from the Clover detector are readout; leaf 1, leaf 2, leaf 3, leaf 4, left side channel, middle side channel and right side channel. The BGO shield PMT signals are also readout by the Clover Module. On the BGO shield, neighboring PMTs have their outputs summed together. Therefore the 16 PMT signals provide 8 inputs to the Clover Module. The BGO shield signals are discriminated internally in the Clover Module and an OR logic signal is generated, called the BGO VETO. Similarly, each Clover signal are discriminated internally by a CFD and a logic signal is generated. The Clover signals will only be digitized by the 14 bit ADCs in the Clover Module when there is no BGO VETO signal present that overlaps the Clover logic pulse. This creates Compton suppressed γ-ray spectra.

3.4.3 Results using the Weisskopf-Ewing approximation

In this section, the results from two absolute measurements of actinide fission cross sections are discussed. The absolute surrogate method is applied to obtain the cross sections for ^{237}Np(n,f) and ^{236}U(n,f). The technique used is nearly identical to that used in the 1960s and 1970s as well as the CENBG work discussed in Section 3.3. One notable difference for the two experiments discussed below is the use of highly-segmented silicon detectors which cover wide angle ranges of outgoing particles. In the early work from the 1960s and 1970s the experiments employed small area silicon detectors which usually only covered one or two angles for detecting the charged particle out channels. The CENBG work is very similar in this respect. The use of large area segmented detector systems allows one to explore the effects of the angular-momentum mismatch between the Surrogate and desired reactions.

^{238}U(^{3}He,tf) as a surrogate to measure the ^{237}Np(n,f) cross section. In order to determine the ^{237}Np(n,f) cross section, a surrogate experiment was performed using the STARS/LIBERACE apparatus [8]. The ^{237}Np(n,f) cross section was determined from an absolute surrogate measurement of ^{238}U(^{3}He,tf). A self-supporting 760 μg/cm^{2} ^{238}U target was used for this experiment. By using a self-supporting metallic target the particle singles background signal was greatly reduced compared to a carbon backed target. The target was impinged upon by a 42 MeV ^{3}He beam from the 88 Inch Cyclotron at the Lawrence Berkeley National Laboratory.

The STARS detector setup for this experiment consisted of a 140 μm thick δE detector and a 1000 μm E detector both were Micron S2 type detectors previously discussed. The target was at a distance of 15 mm from the front face of the δE detector. The angle range covered for the outgoing particles was 36° to 66°. A 140 μm thick Micron S2 detector was used to detect fission fragments. The fission detector was located 10 mm upstream of the target and covered an angular range from 106° to 131° with respect to the beam. The energy resolution of the particle detectors for this experiment was 120 keV.

Over a period of 4 days statistics were accumulated at a rate of approximately 4-8 kHz on this target. The triton particles were identified using standard particle identification plots. The particle singles and particle-fission coincidence spectra are shown in Fig. 22. The silicon telescope was not sufficiently thick enough to stop the higher energy tritons. Tritons with energy higher than 26.5 MeV punched through the E detector and their full energy was not recorded. The effective range of energy for this result is then 15.5 MeV to 25.5 MeV in excitation energy of the nucleus. The ^{238}Np nucleus has a neutron separation (Sn) energy of Sn = 5.49 MeV. The equivalent neutron energy range covered is then 10 MeV to 20 MeV.

The fission probability is obtained from the singles events, particle-fission coincidence events and the fission detector efficiency. The fission probability is determined as follows

$$P_f(E^*) = \frac{1}{\epsilon_{ff}(E^*)}\frac{N_{coinc}(E^*)}{N_{single}(E^*)} \tag{17}$$

where ϵ_{ff} is the fission fragment detection efficiency, $N_{coinc}(E^*)$ is the number of particle-fission coincident events at excitation energy E^* and $N_{single}(E^*)$ is the number of singles events at excitation energy E^*. The result is shown in Fig. 23.

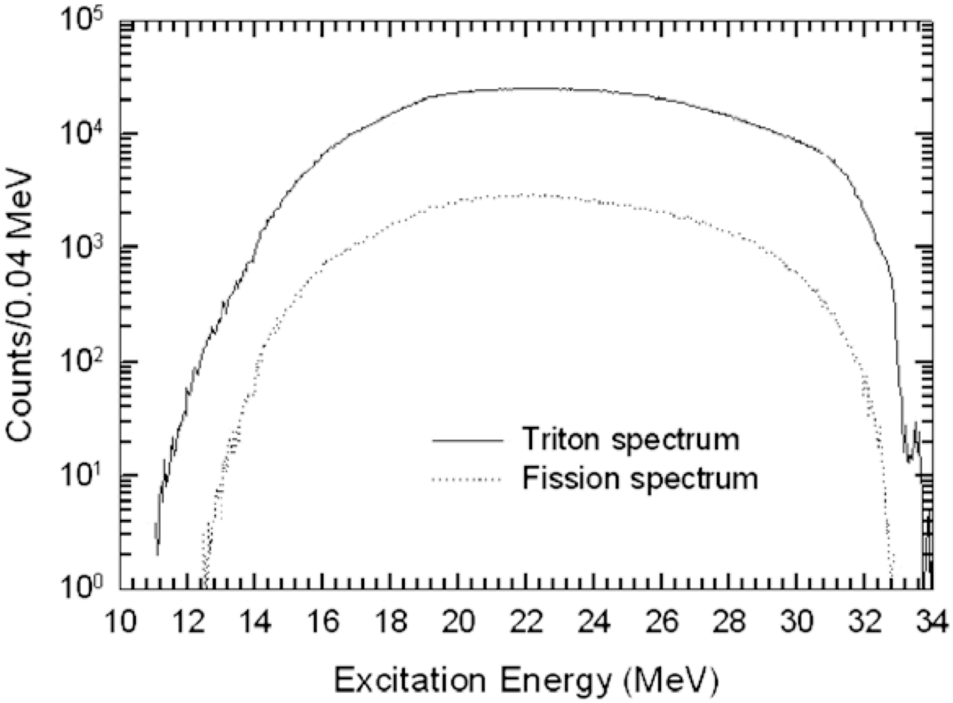

Figure 22: STARS/LiBerACE particle singles and coincidence spectra from a ^{238}U(^{3}He,α)Surrogate experiment. The solid line shows the triton singles spectrum as a function of excitation energy of the nucleus. The dashed line shows the triton-fission coincidence spectrum. The fission probability is the obtained from this data directly.

Once the fission probability has been determined as a function of energy it must be multiplied by the ^{237}Np+n Compound nucleus formation cross section as shown by

$$\sigma_{nf}(E_n) = \sigma_n^{CN}(E_n) P_f(E^* = S_n + \frac{A}{A+1} E_n) \tag{18}$$

where $\sigma_{nf}(E_n)$ is the neutron induced fission cross section as a function of incident neutron energy, P_f is the energy dependent fission probability and $\sigma_n^{CN}(E_n)$ is the energy dependent compound nucleus formation cross section.

The final cross section obtained is shown in Fig. 24 and compared to the absolute cross section obtained by Sherbakov [**?**] and the evaluations ENDF/B-VII.0 and JENDL3.3. Good agreement across the range of energy can be seen for this measurement however there appears to be a systematic offset in the data to a slightly higher value (0.1 barn) over most of the region. This could be due to a systematic error in the detector efficiency or the compound nucleus formation cross section. Comparison to the ratio results of Tovesson [**?**] who measured the ratio of ^{237}Np(n,f)/^{235}U(n,f). To make this comparison Basunia divides the absolute value of the surrogate result by the known directly measured ^{235}U(n,f) cross section. The results of the ratio comparison agree within the uncertainties of both measurements across

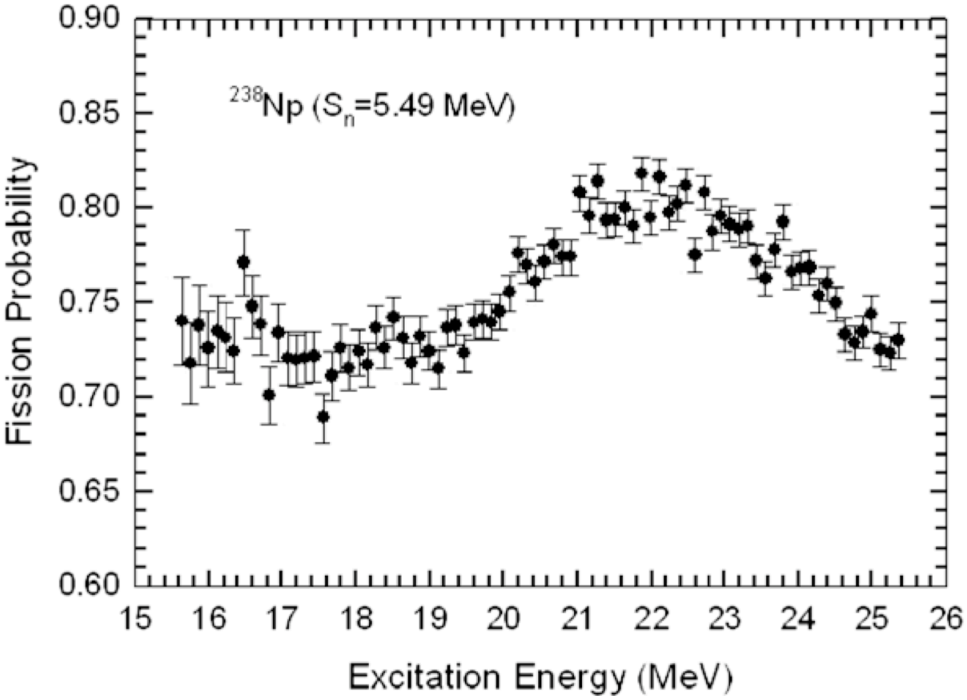

Figure 23: The fission probability for the ^{238}Np nucleus as a function of excitation energy from 15.5 MeV to 25.5 MeV is shown. The equivalent neutron energy for this range is 10 MeV to 20 MeV.

the entire energy range. By examining both these results one could draw the conclusion that the absolute neutron induced cross section from Sherbakov [**?**] contains a systematic offset not the surrogate result of Basunia [8]. The cross section obtained from this approach have uncertainties on the order of 10% once all sources of uncertainty are folded together.

At equivalent neutron energies greater than 10 MeV pre-equilibirum effects were thought to become significant contributors to the cross section. It has been proposed that the surrogate approach would expect to see approximately a 10 % to 20 % decrease in the cross section due to pre-equilibrium neutron emission prior to damping into the compound nucleus. The pre-equilibirum would reduce the fission cross section by this amount and occur specifically in the 10 MeV to 20 MeV range. This translates into a 0.2 barn to 0.4 barn reduction in the energy range measured here. No pre-equilibrium effect is seen for this reaction.

^{238}U(^{3}He,αf) as a surrogate to measure the ^{236}U(n,f) cross section. To study the effect of the angular-momentum mismatch on (n,f) cross sections extracted from Surrogate measurements, an experiment was performed by Lyles [70] using the ^{235}U(^{3}He,αf) and ^{238}U(^{3}He,αf) reactions as surrogates for ^{233}U(n,f) and ^{236}U(n,f) respectively. The experimental apparatus was identical to the one used above in the work of Basunia [8].

In this experiment a 42 MeV ^{3}He beam bombarded ^{235}U and ^{233}U targets. The STARS array recorded the outgoing scattered particles and recorded both their energies and angles.

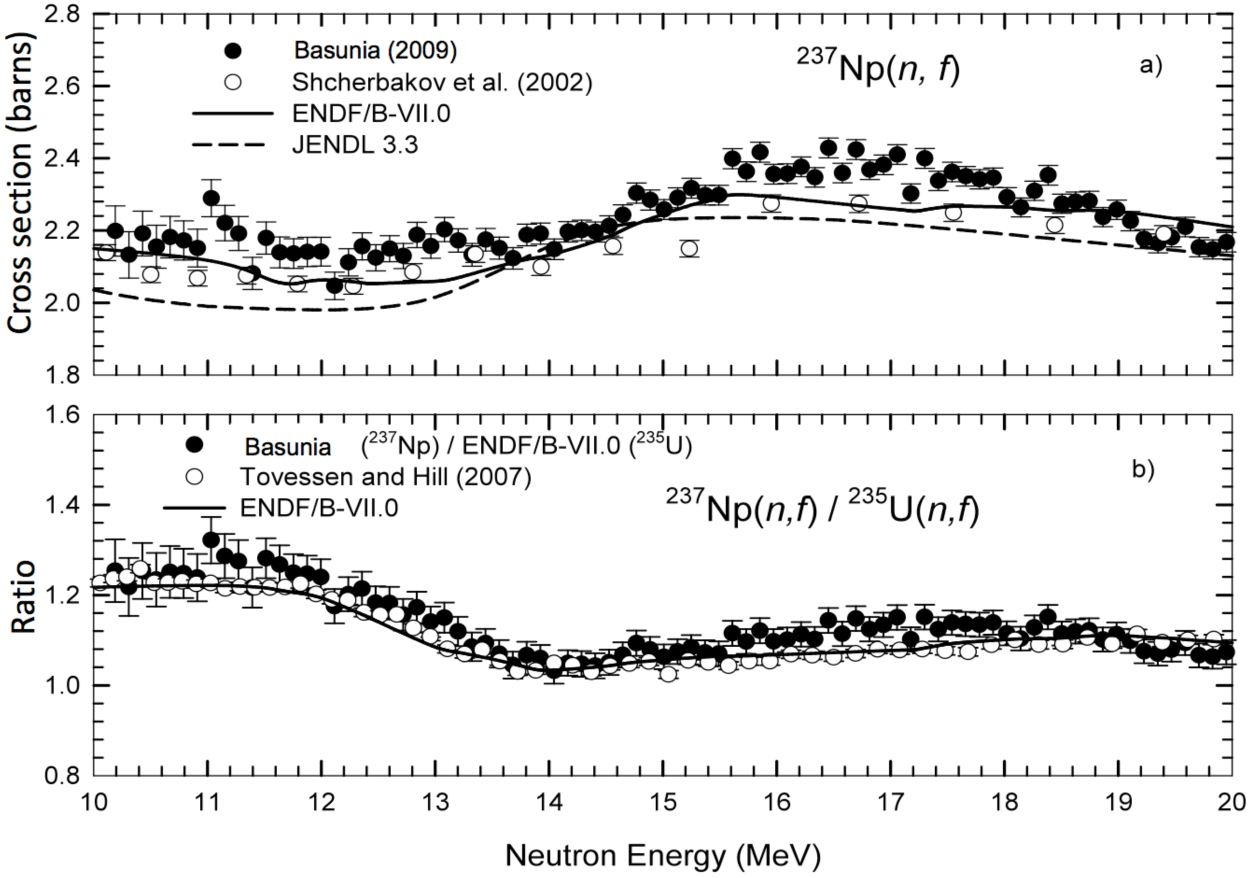

Figure 24: The ^{237}Np(n,f) cross section determined from a Surrogate experiment at STARS/LiBerACE]. Panel a) shows the results from Basunia [8], Sherbakov [?], ENDF/B-VII.0 and JENDL3.3 for the directly measured ^{237}Np(n,f) cross section from 10 MeV to 20 MeV. Panel b) shows a comparison of the ratio result to Tovesson [?]

The ^{236}U fission cross section was determined two different ways as an absolute surrogate and a surrogate ratio. Figure 25 shows the results of the absolute surrogate measurement which was the ^{238}U(^{3}He,αf) reaction. The ratio result will be discussed in Section 4.5.3. Notice the deviation of the surrogate reaction above 7 MeV equivalent neutron energy. This is a result of contamination of various light elements (C, N, and O) in the target which contribute to the singles rate and artificially reduce the cross section. The light contaminants increase the number of events that get included in the denominator of the fission probability artificially. This artificially suppresses the fission probability over a wide range of energy. In past experiments, some groups have only collected particle events at backward angles in an attempt to kinematically shift the light contaminants out of their region of interest.

A further test of the spin mismatch for the low energy region was examined by looking at the absolute surrogate cross section value as a function of the outgoing α particle angle.

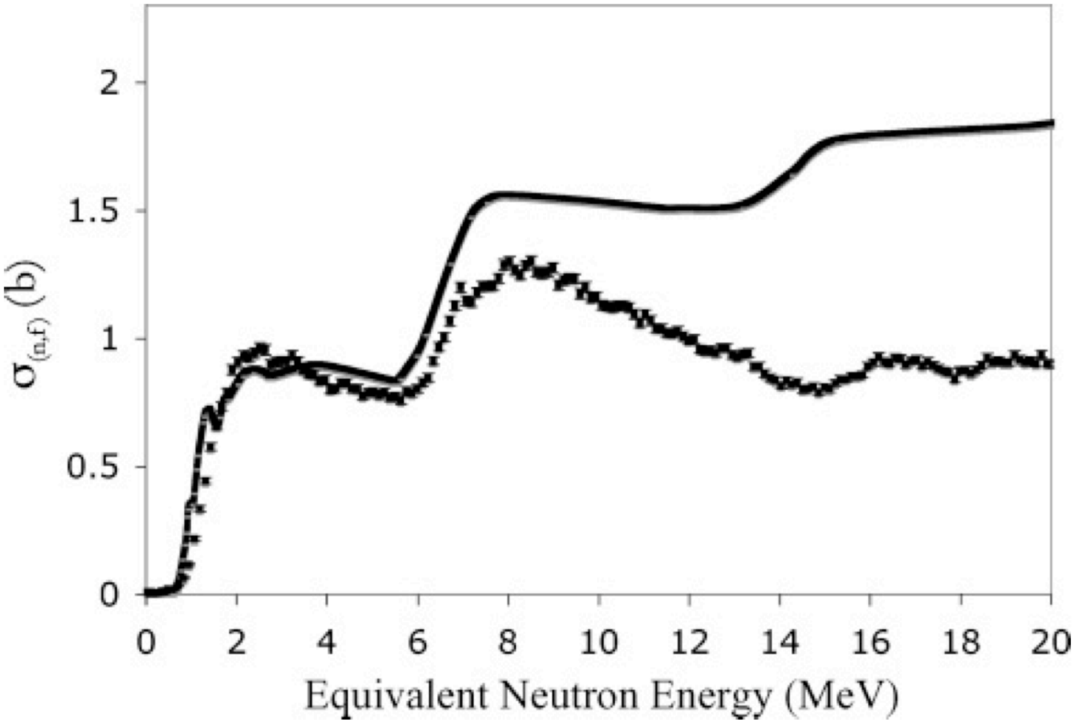

Figure 25: Results of the ^{236}U absolute surrogate measurement obtained by Lyles [70] from the ^{238}U(^{3}He,αf) surrogate reaction. The solid line is the ENDF/B-VII evaluation and the black squares are the experimental results. Deviation of the surrogate reaction above 7 MeV equivalent neutron energy is a result of contamination of various light elements (C, N, and O) in the target which contribute to the singles rate and artificially reduce the cross section.

To study the effect that the outgoing particle angle (angular momentum) has on the cross section, the absolute cross section was determined from different outgoing α particle angle ranges. The cross section for α particles in the 36°-45° range and 57°-62° was found to differ by up to a factor of two. This is taken as evidence of spin-mismatch effects, as is explained in Section 3.5.3.

3.5 Validity of the Weisskopf-Ewing Approximation

Unfortunately, it is not feasible to experimentally determine the branching ratios $G_\chi^{CN}(E, J, \pi)$ for individual $J\pi$ values and test under which conditions the Weisskopf-Ewing limit is applicable. The validity of the approximation is typically established by comparing cross sections obtained from Surrogate experiments that were analyzed in the Weisskopf-Ewing limit with independent direct measurements or cross section evaluations. However, it is possible to carry out calculations to predict the behavior of the branching ratios $G_\chi^{CN}(E, J, \pi)$ as a function of energy, angular momentum, and spin, and to draw some conclusions about the limitations of the Weisskopf-Ewing approximation. Such calculations have been carried out for the decay of the CN ^{235}U by fission and γ emission [43, 42], and for lighter systems (Zr and Gd) decaying via γ-emission [51, 83] . In Section 3.5.1 below, we summarize the main findings of that study. In Section 3.5.3, we will discuss an experimental test of the Weisskopf-Ewing approximation.

3.5.1 Fission probabilities and the WE approximation.

The branching ratios $G_{\chi=fission}^{CN}(E, J, \pi)$ can be extracted from a calculation of the (n,f) cross section and their $J\pi$-dependence can be studied. To this end, we simulated a nuclear reaction. We extracted the branching ratios from a full Hauser-Feshbach calculation of the ^{235}U(n,f) reaction that was calibrated to an evaluation of experimental data. The model used a deformed optical potential and the level schemes, level densities, gamma strength functions, fission-model parameters, and pre-equilibrium parameters were adjusted to reproduce the available data on n-induced fission for energies from E_n= 0 to 20 MeV. For more details on the calculations, and a figure demonstrating the quality of the fit, see Refs. [43, 42]. In Fig. 26 we present the extracted $G_{fission}^{CN}(E, J, \pi)$ for fission proceeding through positive parity states in the compound nucleus ^{236}U. The left panel shows the $G_{fission}^{CN}(E, J, \pi)$ for $J = 0, 5, 10, 15, 20$ for neutron energies $E_n = 0 - 20$ MeV, where $E_n = E(^{236}U) - S_n(^{236}U)$. We observe that the branching ratios exhibit a significant $J\pi$ dependence, in particular for low neutron energies, $E_n = 0 - 5$ MeV. With increasing energy, the differences decrease, although the discrepancies become more pronounced near the thresholds for second-chance and third-chance fission. The branching ratios for negative parity states (not shown) are very similar.

The calculated fission branching ratios $G_{\chi=fission}^{CN}(E, J, \pi)$ help us understand possible discrepancies between the directly-measured cross sections and those extracted from a Weisskopf-Ewing analysis of the Surrogate data: If the Surrogate reaction populates the relevant compound nucleus, e.g. ^{236}U, with a spin-parity distribution that contains larger angular-momentum values than the population relevant to the neutron-induced reaction, then the measured decay probability $P_{\delta,fission}(E_{ex})$ of Eq. 2 contains larger contributions from those $G_{\chi=fission}^{CN}(E, J, \pi)$ associated with large J values than the cross section expression for the desired (n,f) reaction does. Consequently, the cross section extracted by using the Weisskopf-Ewing assumption and approximating $P_{\delta,fission}(E_{ex}) \approx \mathcal{G}_{fission}^{CN}(E_{ex})$, gives too large a result. The opposite will hold true for Surrogate mechanisms that produce the compound nucleus with spin-parity distributions that are shifted to smaller J values relative to the distribution

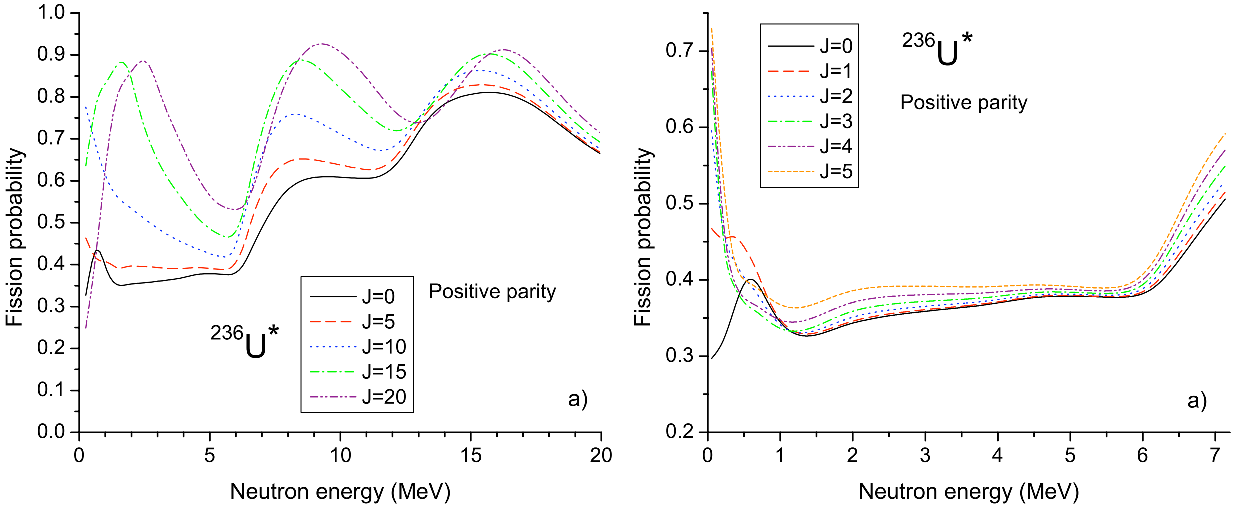

Figure 26: Calculated branching ratios $G^{CN}_{fission}(E, J, \pi)$ for fission of ^{236}U*, as a function of the laboratory neutron energy in the $^{235}\text{U} + n$ system. Results are shown for positive parity states with total angular momenta $J = 0, 5, 10, 15, 20$ (left panel) and $J = 0, 1, 2, 3, 4, 5$ (right panel) in the compound nucleus ^{236}U*.

found in the neutron-induced reaction. In Sec. 3.5.2, below, we illustrate this effect using schematic Surrogate spin-parity distributions.

In the right panel of Fig. 26, a narrower range of angular-momentum values is considered for neutron energies up to 7 MeV. The associated branching ratios are seen to be very similar to each other for all but the lowest energies. The comparison of the top and bottom panels illustrates an important point: It is not *a priori* clear whether the Weisskopf-Ewing limit applies to a particular reaction in a given energy regime. While the Weisskopf-Ewing approximation may break down for a reaction that populates a wide range of $J\pi$ states, it may provide a valid description for a reaction that populates a narrow range of angular-momentum values [1]. Thus, the spin-parity distributions for both the desired and Surrogate reactions have to be considered. For neutron-induced reactions, the spin and parity of the compound nucleus depends on the target spin and the energy of the neutron; the distribution can be calculated with an appropriate optical-model potential. An example for the case of n + ^{235}U is shown in the right panel if Fig. 27. The $J\pi$ population, which clearly depends on the energy, is different from that for a reaction on the excited state, n + ^{235m}U, as the spin of the former target is $J^\pi = 7/2^-$, while that of the latter has $J^\pi = 1/2^+$. For the Surrogate reaction, the spin-parity distribution depends on the reaction mechanism, the projectile-target combination considered, the energy of the projectile, and the angle of the outgoing direct-reaction particle. The ingredients needed for predicting the spin-parity populations for Surrogate are discussed in Section 7.

---

[1] In Appendix A.2, the relationship between the angular-momentum dependence of the calculated fission probabilities and the spin-cutoff parameter in the level-density expressions for the competing exit channels is investigated.

3.5.2 Impact on extracted fission cross sections

Employing the Weisskopf-Ewing assumption in the analysis of Surrogate reactions for which this approximation is not valid will result in extracted cross sections that deviate from the desired true cross section. The effect of the spin-parity mismatch between the desired and surrogate reactions on the cross section extracted from a Weisskopf-Ewing analysis can be simulated by employing the calculated $G^{CN}_{fission}(E_{ex}, J, \pi)$ of Fig. 26 and schematic surrogate spin-parity distributions. We consider the four schematic, energy-independent distributions $F^{CN(p)}_{\delta}(E_{ex}, J, \pi)$ shown in the left panel of Fig. 27, and calculate simulated surrogate coincidence probabilities $P_{\delta,fission}(E_{ex}) = \sum_{J,\pi} F^{CN}_{\delta}(E_{ex}, J, \pi)\ G^{CN}_{fission}(E_{ex}, J, \pi)$. Treating the latter like an experimental result, one obtains – in the Weisskopf-Ewing approximation – the ^{235}U(n,f) cross sections indicated in the right panel of Fig. 27. These cross section were obtained via the formula $\sigma^{WE}_{(n,f)}(E_{ex}) = \sigma^{CN}_{n+target}(E_{ex})\ \mathcal{G}^{CN}_{fission}(E_{ex})$, with $\mathcal{G}^{CN}_{fission}(E_{ex}) = P_{\delta,fission}(E_{ex})$, i.e. this corresponds to a Surrogate analysis in the Weisskopf-Ewing approximation. The compound-nucleus formation cross section is $\sigma^{CN}_{n+target}(E_{ex}) = \sum_{J\pi} \sigma^{CN}_{n+target}(E_{ex}, J, \pi)$, where the individual $\sigma^{CN}_{\alpha}(E_{ex}, J, \pi)$ were taken to be the formation cross sections that were used for the fit mentioned above.

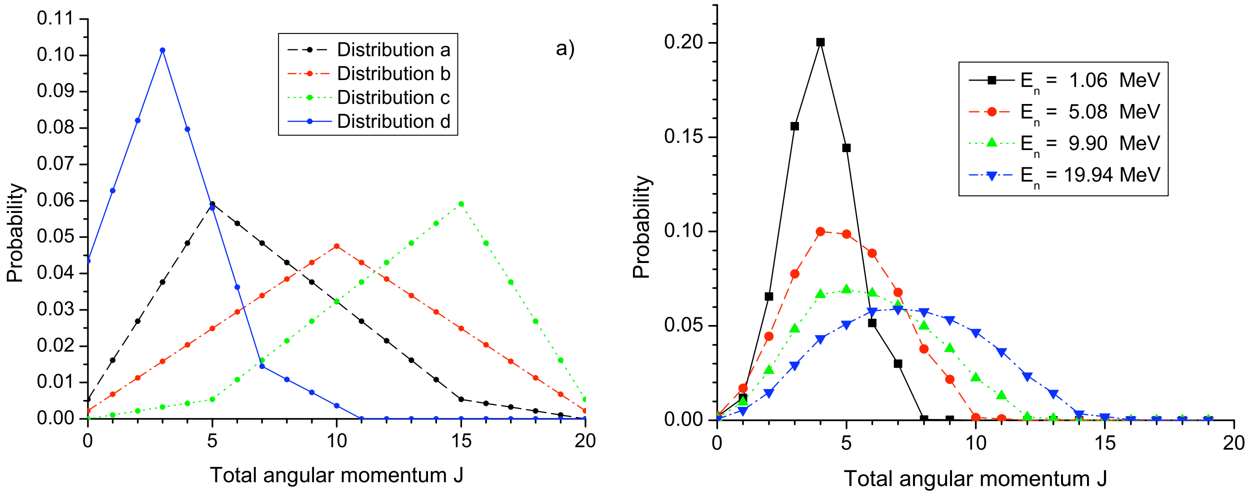

Figure 27: Left panel: Schematic distributions of total angular momentum for the compound nucleus ^{236}U*. The mean angular momentum is $\langle J \rangle = 7.03$, 10.0, 12.97, and 3.30 for distributions a, b, c, and d, respectively; positive and negative parities are taken to be equally probable. The distributions were chosen solely to perform a sensitivity study. Right panel: Distributions of total angular momentum for ^{236}U* produced in the neutron-induced reaction n+^{235}U(n,f), for selected neutron energies.

Results for the ^{235}U(n,f) cross section obtained from the simulated Surrogate experiment are compared to each other and to the "reference" cross section in Figure 27b. The influence of the spin-parity distribution in the compound nucleus on the extracted cross sections is

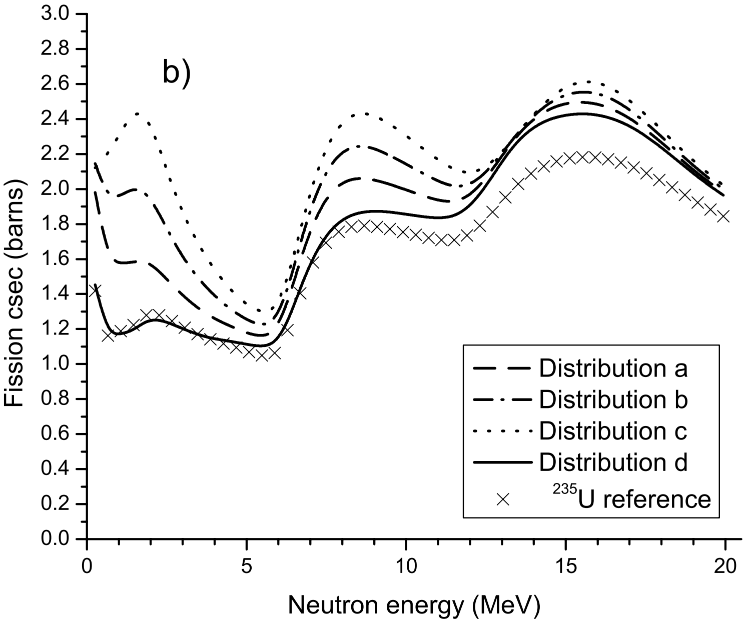

Figure 28: Weisskopf-Ewing estimates of the ^{235}U(n,f) cross section, using the distribution of angular momenta shown in Figure 27. The crosses represent the "reference" ^{235}U(n,f) cross section from the fit.

significant; again, this reflects the fact that the Weisskopf-Ewing approximation is not strictly valid in this case. We observe that the inferred cross sections for distributions a, b, and c are too large, by as much as 40% for energies above 5 MeV and up to a factor of two for smaller energies. It is clear that a larger mismatch between the $J\pi$ populations in the Surrogate and desired reactions leads to a larger discrepancy between the cross section extracted in the Weisskopf-Ewing approximation and the reference cross section. The curve associated with distribution c can be considered an extreme outer limit, as Surrogate reaction conditions employed in recent experiments tend to populate lower spins. The results for distribution d are in very close agreement with the expected cross section for $E_n = 0 - 8$ MeV, and too large by about 10-15% for higher energies. While the extracted cross sections are least sensitive to the underlying $J\pi$ distributions in the energy range $E_n = 13 - 20$ MeV, they consistently overestimate the cross section by 10-15%. These discrepancies are primarily due to preequilibrium neutron emission in the neutron-induced reaction. Preequilibrium effects for the desired reaction, which reduce the reference cross section, have been included in the fit mentioned above, but are not contained in the type of Surrogate measurements simulated here.

3.5.3 Experimental evidence for spin mismatch effects in (n,f) cross sections

Since the angular-momentum transfer between projectile and target in a direct (Surrogate) reaction $d + D \rightarrow b + B^*$ depends on the angle of the outgoing particle b, the measured coincidence probabilities $P_\chi(E)$ should depend on that angle if the Weisskopf-Ewing approximation is not valid. Such angular dependence was indeed observed in a recent experiment carried out at the 88-inch Cyclotron at Lawrence Berkeley National Laboratory: A 42-MeV ^{3}He beam was used to create the CN ^{237}U via the ^{238}U(^{3}He,α) Surrogate reaction [?]. The α-fission coincidence probabilities were measured and the ^{236}U(n,f) cross section was determined, using the Weisskopf-Ewing approximation. Restricting the analysis to α-fission coincidence events for which the outgoing α particle was observed at angles between 36° and 45° relative to the beam axis led to a cross section that is different from the cross section obtained for α particles observed in the 57° to 62° range, for neutron energies below about 1.5 MeV. This is illustrated in Fig. 29, where the cross sections extracted for the two angular ranges are compared to each other (they differ by up to 30%) and to the cross section that is obtained by averaging over the full angular range. The findings demonstrate that the spin-parity mismatch has to be minimized or corrected for theoretically in order to improve the accuracy and reliability of cross sections extracted from Surrogate experiments, in particular for low energies (below about 2 MeV).

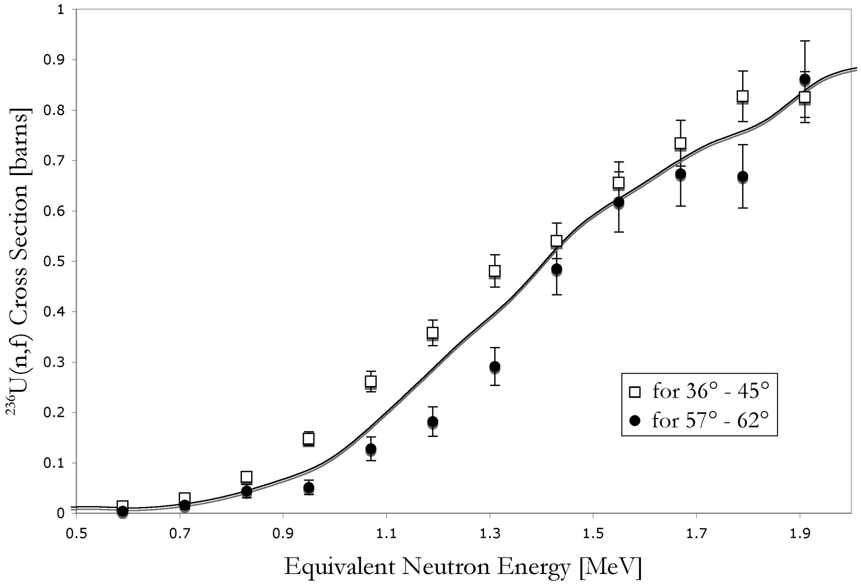

Figure 29: ^{236}U(n,f) cross section obtained from a Weisskopf-Ewing analysis of Surrogate ^{238}U(^{3}He,α) measurements. Data represented by open squares correspond to events for which the outgoing α particle was observed at 36° to 45°, while filled circles correspond to an angular range of 57° to 62°. The solid line is the cross section that results from averaging over all experimentally accessible angles, 36° to 62°.

4 Surrogate analyses using ratios

The *Surrogate Ratio approach* [43, 29] is an approximation that makes use of the Surrogate idea and requires the (approximate) validity of the Weisskopf-Ewing limit. In this approach, the ratio $R(E)$ of the cross sections of two compound-nuclear reactions is determined in two Surrogate experiments. An independent determination of one of the cross sections can then be used to deduce the other. One advantage of this method is that it eliminates the need to accurately measure N_δ, the total number of surrogate reaction events. There are also indications that small to moderate deviations from the Weisskopf-Ewing assumption might cancel [43]. Different variants of the Ratio approach have been employed in recent years. Cross sections for (n,f) reactions extracted in the *External* Ratio approximation have been tested for consistency with results from direct measurements as well as complementary surrogate experiments [29, 69]; the results, as well as theoretical simulations [43] confirm the validity and identify limitations of the Ratio approach for (n,f) reactions. In Sections 4.1 and 4.2 we will review the formalism of the Ratio approach and discuss a subtle issue in applications of the method that, if overlooked, can introduce additional uncertainties in the extracted cross sections. Applications of the Ratio method are discussed in Section 4.3, and theoretical as well as experimental investigations of its validity are summarized in Section 4.5. The focus of Sections 4.3–4.5 is on (n,f) cross sections; the (n,γ) case is investigated in Section 6.

4.1 The Ratio approach

The goal of the Ratio method is to experimentally determine the ratio

$$R(E) \quad = \quad \frac{\sigma_{\alpha_1\chi_1}(E)}{\sigma_{\alpha_2\chi_2}(E)} \tag{19}$$

of the cross sections of two compound-nucleus reactions, $a_1 + A_1 \rightarrow B_1^* \rightarrow c_1 + C_1$ and $a_2 + A_2 \rightarrow B_2^* \rightarrow c_2 + C_2$, where the two reactions have to be "similar" in a sense that remains to be specified. One of the cross sections, say $\sigma_{\alpha_2\chi_2}(E)$, needs to be known, and the other $\sigma_{\alpha_1\chi_1}(E)$ is then extracted from the ratio. In the Weisskopf-Ewing limit,

$$R(E) \quad = \quad \frac{\sigma_{\alpha_1}^{CN1}(E)\, \mathcal{G}_{\chi_1}^{CN1}(E)}{\sigma_{\alpha_2}^{CN2}(E)\, \mathcal{G}_{\chi_2}^{CN2}(E)}\,, \tag{20}$$

with branching ratios $\mathcal{G}_\chi^{CN}(E)$ that are independent of the $J\pi$ population of the compound nuclei under consideration. For most cases of interest the compound-nucleus formation cross sections $\sigma_{\alpha_1}^{CN1}$ and $\sigma_{\alpha_2}^{CN2}$ can be calculated reliably by using an optical model.

To determine $\mathcal{G}_{\chi_1}^{CN1}(E)$ / $\mathcal{G}_{\chi_2}^{CN2}(E)$, two experiments are carried out that create the relevant compound nuclei, $CN1$ and $CN2$, respectively. For each experiment, the number of coincidence events, $N_{\delta_1\chi_1}^{CN1}$ and $N_{\delta_2\gamma_2}^{CN2}$, is measured. The ratio of the branching ratios into the desired channels for the compound nuclei created in the two reactions is given by

$$\frac{\mathcal{G}_{\chi_1}^{CN2}(E)}{\mathcal{G}_{\chi_2}^{CN2}(E)} \quad = \quad \frac{P_{\delta_1\chi_1}^{CN1}(E)}{P_{\delta_2\chi_2}^{CN2}(E)} = \frac{N_{\delta_1\chi_1}^{CN1}(E)}{N_{\delta_2\chi_2}^{CN2}(E)}\,\frac{N_{\delta_2}^{CN2}(E)}{N_{\delta_1}^{CN1}(E)}\,\frac{\epsilon_{\chi_2}(E)}{\epsilon_{\chi_1}(E)}, \tag{21}$$

where ϵ_χ denotes the efficiency for detecting the relevant exit channel. The experimental conditions are adjusted such that the relative number of reaction events, $N_{\delta_1}^{CN1}/\ N_{\delta_2}^{CN2}$, can be determined from the relative beam intensities, target thickness, and livetimes of the two experiments. The ratio of detection efficiencies $\epsilon_{\chi 2}/\ \epsilon_{\chi_1}$ can typically be determined accurately and for fission measurements is nearly unity. The ratio of the decay probabilities then simply equals the ratio of the coincidence events and $R(E)$ becomes:

$$R^{exp}(E) \;=\; \frac{\sigma_{\alpha_1}^{CN1}(E)\ N_{\delta_1\chi_1}^{CN1}(E)}{\sigma_{\alpha_2}^{CN2}(E)\ N_{\delta_2\chi_2}^{CN2}(E)}\ , \tag{22}$$

where we have set $N_{\delta_1}^{CN1}/\ N_{\delta_2}^{CN2} = 1$ and $\epsilon_{\chi 2}/\ \epsilon_{\chi_1} = 1$ to simplify the notation.

The definition of the energy E in Eqs. 19–22 remains to be specified. Typically, the energy-dependence of a compound-nucleus formation cross section, $\sigma_\alpha^{CN} = \sigma(a + A \rightarrow B^*)$ is characterized by the kinetic energy of the projectile, E_a, while a branching ratio is normally given as a function of the excitation energy of the compound nucleus, $\mathcal{G}_\chi^{CN}(E_{ex})$. In a compound-nucleus reaction, those two values are related via the separation energy S_a of the particle a in B^*: $E_{ex} = S_a + E_a$. While either E_{ex} or E_a can be used to uniquely specify the energy-dependence of such a reaction, each choice of matching energy has certain advantages and disadvantages, which will be discussed in Section 22.

Different variants of the Surrogate Ratio approach can be considered, depending on the entrance and exit channels of interest. The *External Surrogate Ratio (ESR)* method, introduced in 2005 by the STARS/LiBERACE collaboration [79] is the most widely-employed variant. It has been tested theoretically [43], as well as experimentally [70, 69]. A few applications have made use of the *Internal Surrogate Ratio (ISR)* method, which was also first used by the STARS/LiBERACE collaboration [15, 16, 3]; a careful test remains to be carried out. More recently, an additional variant has been explored [74]. The discussions in this report will focus primarily on the External (ESR) method. The other approaches will be mentioned where appropriate.

ESR Approach. In this approach, the cross sections in $R(E) = \sigma_{\alpha_1\chi_1}/\sigma_{\alpha_2\chi_2}$ refer to two reactions with the same type of entrance channel and the same type of exit channel, $\alpha_1 = \alpha_2$ and $\chi_1 = \chi_2$, but different compound nuclei, $CN1 \neq CN2$. The ratio of the coincidence probabilities (Eq. 21) is determined from measurements of two Surrogate reactions that involve identical entrance channels, $\delta_1 = \delta_2$; the exit channels are identical as well. An example of an experiment employing the ESR method is given in Section 4.3. The ratio $\sigma[^{237}\mathrm{U(n,f)}]$ / $\sigma[^{235}\mathrm{U(n,f)}]$ was determined from measurements of $P[^{238}\mathrm{U}(\alpha,\alpha' f)]$ / $P[^{236}\mathrm{U}(\alpha,\alpha' f)]$, where α and α' refer to alpha particles, not channels. In this case, the entrance and exit channel were $\alpha_1 = \alpha_2 = n + target$, and $\chi_1 = \chi_2 = fission$, and the Surrogate reactions both measured (α, α') coincidence events. The absolute number of Surrogate events was not determined.

Note that in order to determine $R(E)$, it is necessary to take into account the ratio $\sigma_{\alpha_1}^{CN1}/\sigma_{\alpha_2}^{CN2}$. In many applications of the ESR method, this ratio has simply been set to one, but this is not necessarily a good approximation (see the discussion on energy matching in Section 4.2 below).

ISR Approach. In this variant, the compound nuclei created in the two reactions of interest (and hence also in the Surrogate reactions) are identical, $CN1 = CN2$, the entrance channels are identical, $\alpha_1 = \alpha_2$, but the decay channels differ in type, $\chi_1 \neq \chi_2$. The Surrogate measurement employs one projectile-target combination, $\delta_1 = \delta_2$. An example of an ISR measurement is given in Ref. [3], where the ratio $\sigma[^{235}\text{U(n},\gamma)]$ / $\sigma[^{235}\text{U(n,f)}]$ was determined from a measurement of $P[^{235}\text{U(d,p}\gamma)]$ / $\sigma[^{235}\text{U(d,pf)}]$, *i.e.* $\alpha_1 = \alpha_2 = \text{n} + {}^{235}\text{U}$, but $\chi_1 \neq \chi_2$, *i.e.* the Surrogate measurement considered the γ channel relative to the fission channel.

Since the entrance channels and compound nuclei involved are identical, one can set $\sigma^{CN1}_{\alpha_1}/\sigma^{CN2}_{\alpha_2} = 1$, provided the decay probabilities in Eq. 21 are compared at the proper energies (see also Section 4.2 below). The ISR approach is investigated in Section 6 for (n,γ) reactions.

Other variants. Another variant of the Ratio method used Surrogate $^{232}\text{Th}(^6\text{Li},\alpha)^{234}\text{Pa}$ and $^{232}\text{Th}(^6\text{Li,d})^{236}\text{U}$ reactions to infer information on the cross section ratio $\sigma[^{233}\text{Pa(n,f)}]$ / $\sigma[^{235}\text{U(n,f)}]$. In other words, the desired and reference reactions are both of the same type, namely (n,f), and thus $\alpha_1 = \alpha_2$ and $\chi_1 = \chi_2$. The Surrogate reactions, however, involved two different types of mechanisms for producing the compound nuclei, namely (^{6}Li,α) and (^{6}Li,d). For more details, see the discussion in Section 4.4.

4.2 Energy matching in the Ratio approach

In a surrogate ratio analysis, the choice of energy variable at which the data sets are compared introduces a subtle but important issue that can affect the results, even when the Weisskopf-Ewing approximation is valid. The comparison of the cross sections for the reactions $a_1 + A_1 \rightarrow B_1^* \rightarrow c_1 + C_1$ (numerator) and $a_2 + A_2 \rightarrow B_2^* \rightarrow c_2 + C_2$ (denominator) can be made either *at the same projectile energy* E_a or *at the same excitation energy* E_{ex}. Of course, in a compound-nucleus reaction, those two energies are related via the separation energy S_a of the particle a in B^*: $E_{ex} = S_a + E_a$. For a given projectile energy, $E_{a_1} = E_{a_2}$, small differences in the separation energies, S_{a_1} and S_{a_2}, will lead to different excitation energies in the compound nuclei, B_1^* and B_2^*, respectively. Thus, the choice of energy variable becomes important as it introduces additional uncertaintes in either the ratio of formation cross sections or the ratio of exit-channel branching ratios.

The energy-dependence of σ^{CN}_α is most naturally characterized by the kinetic energy of the projectile, E_a. When the cross sections in Eq. 19 are compared at the same projectile energy, the ratio $\sigma^{CN}_{\alpha_1}$ / $\sigma^{CN}_{\alpha_2}$ can sometimes be approximately set to one for the relevant energy range. This is convenient, as the calculation of two formation cross sections and the associated uncertainties can be avoided in this case. For the ESR method, this approximation is likely to be valid if *one* projectile type is considered, *i.e.* $a_1 = a_2$, hitting targets that are structurally similar (deformation, level structure), such as ^{233}U and ^{235}U. For the ISR method, this ratio is by definition one, provided the energies are matched at E_a. In the work by Nayak *et al.* [74], which compared (n,f) reactions on Pa and U targets, the ratio had to be explicitly calculated using optical potentials.

While matching the energies of numerator and denominator in Eq. 19 at the projectile energy has the advantage that the ratio of the formation cross sections can possibly be set to one, it also introduces challenges: In particlar, the quantitiy $\mathcal{G}^{CN}_{\chi_1}/\mathcal{G}^{CN}_{\chi_2}$ is obtained from the measured coincidence probabilties, $P_{\delta_1\chi_1}/P_{\delta_2\chi_2}$, given in Eq. 21 and it is assumed that $\epsilon_{\chi_2}N_{\delta_2}/\epsilon_{\chi_1}N_{\delta_1}$ can be accurately determined. However, when matching at projectile energy, this assumption may not be valid, since the efficiencies, ϵ_{χ_1} and ϵ_{χ_2}, for detecting the outgoing direct-reaction particles, are energy-dependent. A match at projectile energy results in kinetic energies for those particles that differ by $S_{n_1} - S_{n_2}$ which can be several MeV in extreme cases. Under those circumstances the approximation $\epsilon_{\chi_2}/\epsilon_{\chi_1} \approx 1$ will break down and the ratio in Eq. 21 can no longer be determined reliably. For this reason, recent Ratio analyses have made comparisons in excitation energy.

4.3 Surrogate ratio experiments at STARS/LiBerACE

In the past few years, new experiments have been performed to determine the ^{237}U(n,f) and ^{239}U(n,f) cross sections more accurately and over a wider energy range. These isotopes are particularly challenging to measure directly due to their short half-lives. The ^{237}U half-life is 6.75 days and ^{239}U half-life is 23.4 minutes. A direct measurement at typical neutron beam facilities would require samples with minimum masses of approximately 60 μg, resulting in sample activities of 5 and 2000 Curies for ^{237}U and ^{239}U, respectively. These target activities would make a direct measurement very difficult. There is only one, difficult direct measurement that has been attempted [64] to measure the cross section at energies below 2 MeV. Below, we discuss the surrogate ratio method experiments used to determine the ^{237}U(n,f) and ^{239}U(n,f) cross sections up to 20 MeV.

4.3.1 Determination of the ^{237}U(n,f) cross section

The ^{237}U(n,f) cross section was determined using the surrogate ratio technique. An (α,α') reaction was chosen as it allowed the use of ^{238}U and ^{236}U targets which have half-lives of 4.47×10^9 years and 2.34×10^7 years, respectively. Target activities were then manageable — 30 nCi and 6 μCi for the ^{238}U and ^{236}U targets, respectively.

The surrogate reaction for the ^{237}U(n,f) unknown cross section was ^{238}U(α,α'f). The surrogate for the known ^{235}U(n,f) cross section was ^{236}U(α,α'f). A 55-MeV α beam from the 88-Inch Cyclotron at Lawrence Berkeley National Laboratory was used to bombard the targets. Outgoing α particles were detected using the STARS detector array at forward angles from 35° to 60° relative to the beam direction. Fission fragments were detected at backward angles with respect to the beam in an additional silicon detector that covered an angular range of 106° to 131°. The Coulomb barrier for α particles in uranium is approximately 24 MeV. The neutron separation energy in ^{238}U is 6.152 MeV and ^{236}U is 6.544 MeV. The beam energy of 55 MeV was chosen so an equivalent neutron energy range of 0 to 20 MeV could be measured before the Coulomb barrier became a factor, E_{beam} - S_n - E_{range} > E_{coul}.

The ^{237}U(n,f) cross section was determined from the ratio of the number of α-fission coincident events at a given energy for each target multiplied by the known ^{235}U(n,f) cross section at that same equivalent neutron energy as given by

$$\sigma(^{237}U(n,f)) = \frac{N(^{238}U_{\alpha-f}, E_{ex})}{N(^{236}U_{\alpha-f}, E_{ex})}\sigma(^{235}U(n,f)); \tag{23}$$

The ^{237}U(n,f) cross section shows the structure of the first, second and third chance fission channels, see Fig. 30. Good agreement was found between the results of Younes and Britt citeyounes:05tr and this work.

4.3.2 Determination of the ^{239}U(n,f) cross section

The ^{239}U(n,f) cross section was determined using the surrogate ratio technique. The (^{18}O,^{16}O) reaction was used to transfer two neutrons to ^{234}U and ^{238}U which were used as surrogates

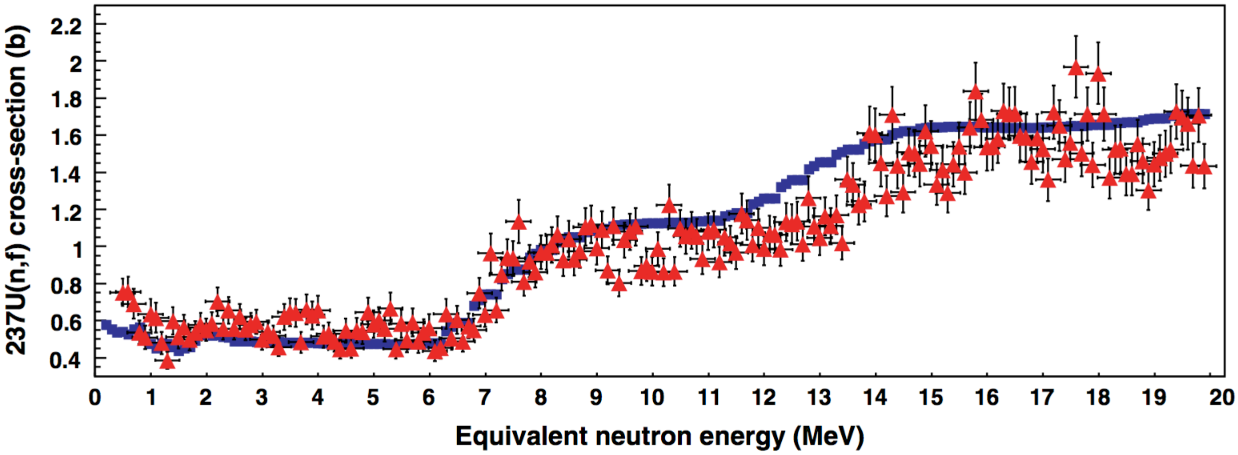

Figure 30: The ^{237}U(n,f) cross section from a ^{238}U(α,α'f) surrogate experiment from Burke et al. [28] are shown. The ^{237}U(n,f) surrogate cross section result is plotted with red triangles. For comparison, the previous result from Younes and Britt [102] is shown as blue squares. The uncertainties for Burke et al. include both statistical and systematic uncertainties. No uncertainties are quoted for the Younes and Britt result.

for ^{235}U(n,f) and ^{239}U(n,f). A 250 MeV ^{18}O beam was used to populate the two nuclei of interest. A 140 μm δE detector and a 1000 μm thick E detector were used to construct a silicon telescope suitable to stop the scattered oxygen isotopes. The silicon telescope covered a forward angular range from 19° to 26° overlapping the grazing angle of 23°. A Micron S2 detector was used upstream at a distance of 12 mm from the target to detect the fission fragments.

A disadvantage of this particular reaction mechanism is that the ^{18}O nucleus can interact with the target nuclei and transfer many nucleons. Outgoing particles detected from the reaction covered the range from protons to neon nuclei. This has the net effect of spreading out the strength of the reaction cross section and reducing the contribution of the rate to the desired ^{16}O nucleus. The second disadvantage comes from the fact that the ^{18}O beam radiation damages the δE and E detectors. The gain of the detectors then changes at a fairly rapid pace which causes a shift in the apparent energy of the detected ^{16}O nuclei.

In order to compensate for the gain shift, every one million events the elastic peak of the (^{18}O,^{18}O') reaction was fit and the centroid determined. In this way the centroid was tracked and the energy scale was appropriately corrected on a rolling one million event basis throughout the entire run. Once the data had been corrected for the gain shift throughout the experiment the ^{239}Ucross section was determined.

The ^{239}U(n,f) cross section was obtained by taking the ratio of the number of ^{16}O-fission coincident events that occurred for each target ^{234}Uand ^{238}Uas a function of energy.

$$\sigma(^{239}U(n,f)) = \frac{N(^{238}U_{^{16}O-f}, E_{ex})}{N(^{234}U_{^{16}O-f}, E_{ex})}\sigma(^{235}U(n,f)) \tag{24}$$

The cross section is shown in figure 31. The resulting cross section from Burke [27] agrees well with that of Younes over the energy range shown. The ENDF-BVII result currently used by the community is higher by 20% to 40% in the second and third chance regions respectively. A new evaluation of the ^{239}U(n,f) cross section is clearly needed at this time.

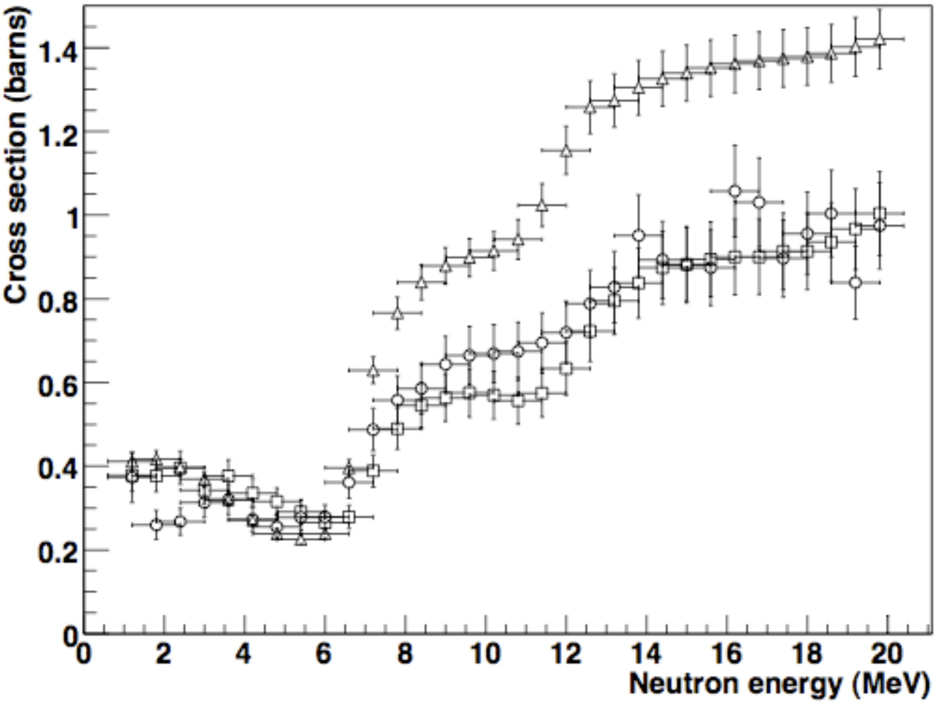

Figure 31: The ^{239}U(n,f) cross sections from two different Surrogate experiments compared to each other and to an evaluation. Results from the (^{18}O,^{16}O) experiment by Burke *et al.* [27] are plotted as open circles, the reanalyzed date by Younes *et al.* is shown as open squares, and the ENDF/B-VII evaluation is indicated as open triangles.

4.4 Other variants of the Surrogate Ratio method

A novel approach that combines the absolute and ratio surrogate reaction method was used by B. K. Nayak *et al.* to determine the ^{233}Pa(n,f) cross section at energies of 11.5–16.5 MeV [74]. In this experiment, a single self-supporting ^{232}Th target was bombarded by a 38-MeV ^{6}Li beam. By detecting d and α particles to identify ^{232}Th(^{6}Li,α)^{234}Pa and ^{232}Th(^{6}Li,d)^{236}U reactions, the ^{234}Pa and ^{236}U compound nuclei fission probabilities were measured. Although it would have been possible to independently infer the two (n,f) cross sections, a ratio of the two cross sections was used to determine the ^{233}Pa cross section relative to the known ^{235}U cross section. By taking a ratio of two reactions on the *same target*, systematic uncertainties due to target thickness, beam current, and deadtime were eliminated. It was also assumed by the authors of Ref. [74] that by taking a ratio of cross sections, spin-parity and pre-equilibrium effects were minimized. Although it seems to be the case that when two identical direct reactions on similar nuclei are compared that the spin-parity and pre-equilibrium effects are reduced, there is no evidence to suggest that this would be the case for two different transfer reactions which are likely to proceed through compound-nuclear states with different spin-parity distributions and have different pre-equilibrium contributions.

The ^{233}Pa$(n,f)^{234}$Pa cross section, $\sigma_{nf}^{^{233}Pa}$, was determined from

$$\sigma_{nf}^{^{233}Pa} = \frac{\sigma_n^{CN1}}{\sigma_n^{CN2}} \frac{G_f^{CN1}}{G_f^{CN2}} \times \sigma_{nf}^{^{235}U} \tag{25}$$

at excitation energies of 17–22 MeV. The ratio of entrance-channel cross sections was calculated using the EMPIRE-2.19 code [61] and the exit-channel probabilities were measured for ^{234}Pa and ^{236}U using the absolute surrogate reaction method. The results, shown in Fig. 32, seem consistent with the cross sections determined in Ref. [78, 90] and the output of the EMPIRE-2.19 code [74].

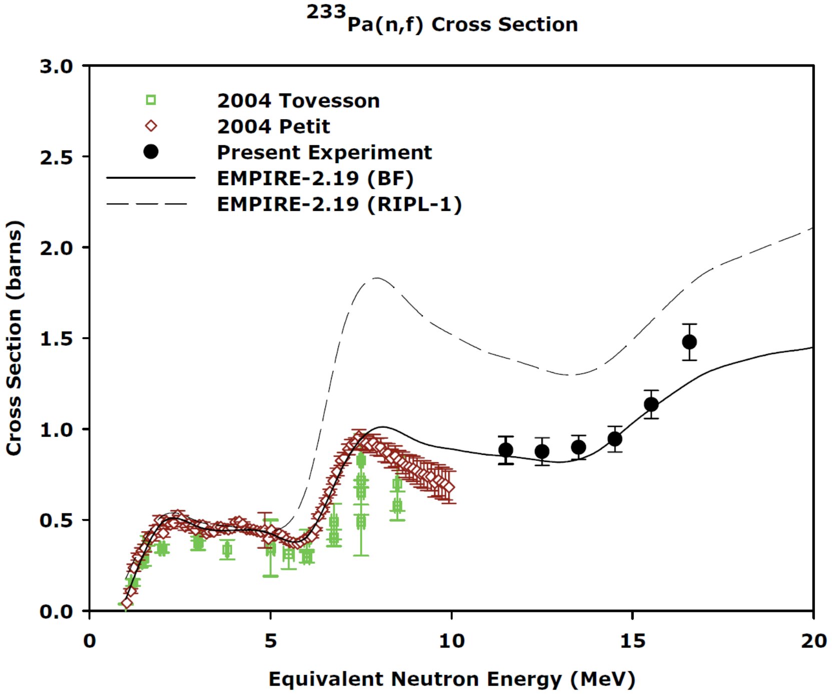

Figure 32: Cross section for ^{233}Pa(n,f) determined using a hybrid surrogate approach (black dots) and compared to other results from experiment and the EMPIRE-2.19 code. Figure taken from Ref. [74] Fig. 5.

4.5 Validity of the Ratio approach

Here, we investigate the assumptions underlying the Ratio method. Unless specified otherwise, we are considering the External Ratio method. In Section 4.5.1, we summarize the results of simulations carried out to assess the effect of neglecting the spin-parity mismatch on (n,f) cross sections obtained from a Ratio analysis of Surrogate data. In Sections 4.5.2 and 4.5.3, we discuss experiments that were carried out to test the level of agreement between cross sections extracted from ratio analyses of Surrogate data and directly-measurered cross sections.

4.5.1 Uncertainty assessment for (n,f) cross sections

To test the validity of the Ratio approach, we have carried out simulations similar to those employed for testing the Weisskopf-Ewing approximation (see Section 3.5). We consider the cross section ratio

$$R(E) \;=\; \frac{\sigma(^{235}\mathrm{U}(n,f))(E)}{\sigma(^{233}\mathrm{U}(n,f))(E)}\,. \tag{26}$$

where we treat $\sigma(^{235}\mathrm{U(n,f)})$ as the desired ('unknown') cross section and $\sigma(^{233}\mathrm{U(n,f)})$ as the known reference cross section. This choice has the advantage that all of the relevant cross sections are known from direct measurements. To simulate the quantity that is measured in a typical Surrogate Ratio experiment, namely the ratio of coincidence probabilities, we calculate

$$R^{sim,p} = \frac{P^{^{236}U(p)}_{\delta,fission}(E)}{P^{^{234}U(p)}_{\delta,fission}(E)} \;=\; \frac{\sum_{J,\pi} F^{^{236}U(p)}_{\delta}(E,J,\pi)G^{^{236}U}_{fission}(E,J,\pi)}{\sum_{J,\pi} F^{^{234}U(p)}_{\delta}(E,J,\pi)G^{^{234}U}_{fission}(E,J,\pi)}\,, \tag{27}$$

where the superscript p indicates that the simulation employed one of the four schematic spin distributions $F^{(p)}_{\delta}$ shown in the left panel of Fig. 27. The ^{236}U fission probabilities are those employed in Section 3.5 for simulating of the Weisskopf-Ewing approximation, they are plotted in Figure 26. The ^{234}U fission probabilities were taken from a Hauser-Feshbach calculation for the ^{233}U(n,f), carried out in analogy to the one for ^{235}U(n,f) case. More details and figures can be found in Ref. [43, 42]. For simplicity, we have taken the compound nucleus formation cross section to be independent of the target nucleus, $\sigma^{CN}_{n+^{233}U} = \sigma^{CN}_{n+^{235}U}$, and we consider the case where numerator and denominator of the all ratios are matched at the same projectile energy.

Each $J\pi$ distribution considered, $p = a, b, c, d$, yields a ratio $R^{(p)}$, from which we deduce the desired cross section $\sigma^{(p)}(^{235}\mathrm{U(n,f)}) = R^{(p)} \times \sigma(^{233}\mathrm{U(n,f)})$. The deviations of the resulting cross sections from each other provide a measure of how sensitive the Ratio approach is to violations of the Weisskopf-Ewing approximation, while the comparison with the reference cross section allows for an assessment of the overall quality of the cross sections obtained from a Ratio analysis.

Our results shown in Figure 33. We observe that the $J\pi$ distributions have a much smaller effect on the cross sections deduced here than on the cross sections obtained from a Surrogate analysis in the Weisskopf-Ewing limit; *i.e.* the Ratio method is less sensitive to the details of the spin-parity distributions. We find relatively good agreement between the simulated Ratio results and the expected cross sections for energies above about 3 MeV. The largest discrepancies, which may be as large as 50%, occur where the Weisskopf-Ewing approximation is no longer valid, *i.e.* at small energies ($E_n \leq 3$ MeV) and for angular-momentum distributions with high average J values. We also find differences of up to about 25% near the threshold for second-chance fission. As mentioned previously, the compound-nuclear spins populated in recent Surrogate experiments tend to be significantly lower than those of distribution c; thus, this distribution provides a useful outer limit for the uncertainty that results from neglecting the spin-parity mismatch. At the same time, the cross section associated with distribution d is in excellent agreement with the expected result for energies up to about 7-8 MeV, where preequilibrium effects set in.

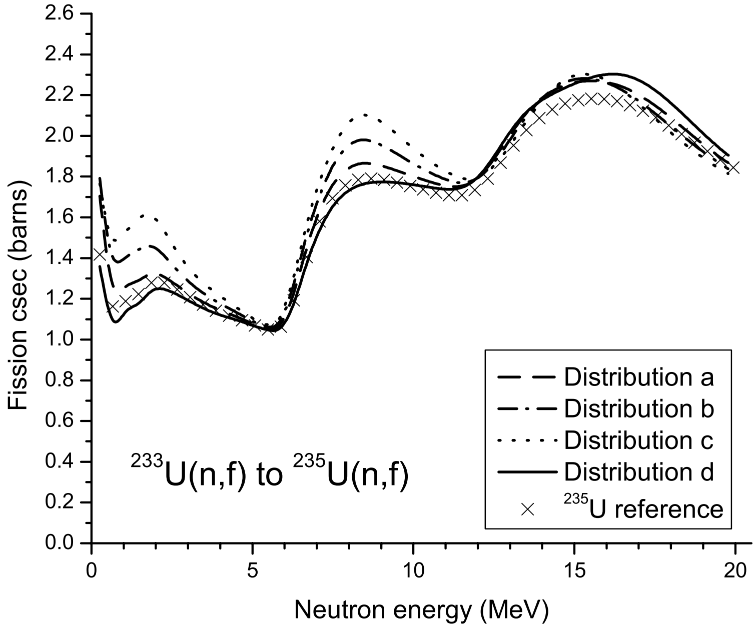

Figure 33: Estimates of the ^{235}U(n,f) cross section obtained from the Ratio method, using the distribution of angular momenta shown in Figure 27a. The crosses represent the "reference" ^{235}U(n,f) cross section from the fit.

For situations in which the Weisskopf-Ewing limit provides at least a rough approximation, *e.g.* for $E_n = 5$–20 MeV in the case considered here, the Ratio method further reduces the discrepancies between the extracted and expected cross sections, thus providing significantly improved results. Effects that, in the Surrogate Weisskopf-Ewing approach, cause deviations from the correct results seem to affect the ^{235}U(n,f) and ^{233}U(n,f) cross sections in a similar manner and hence cancel in part in the Surrogate Ratio treatment. This is in particular notable for the preequilibrium decays, the effects of which were pronounced in the Weisskopf-Ewing approach and are significantly smaller here.

4.5.2 Experimental benchmark for the Ratio Approach

As a complement to the simulations discussed in Section 4.5.1 above, Lesher *et al.* [69] carried out a set of experiments that allowed them to extract the known ^{235}U(n,f) cross section via the Surrogate Ratio approach, and to establish an experimental benchmark for the Ratio method. The experiment employed inelastic scattering by 55-MeV α particles as a mechanism to excite the target nuclei ^{234}U and ^{236}U from their ground state to excited states above the neutron-separation threshold. The STARS (Silicon Telescope Array for Reaction Studies) detector was used to detect the scattered α particles in coincidence with outgoing fission fragments. The outgoing α particles were identified in a standard ΔE-E plot and the ratio $R_f^{exp} = P^{exp}[^{234}\mathrm{U}(\alpha,\alpha'\mathrm{f})]/P^{exp}[^{236}\mathrm{U}(\alpha,\alpha'\mathrm{f})]$ of the fission probabilities associated with the decays of ^{234}U and ^{236}U nuclei, respectively, was obtained. In Figures 34 and 35, results from the analysis of this experiment are shown. The experimentally determined ratio R_f^{exp} is compared to the ratio of $\sigma(^{233}\mathrm{U(n,f)})$ / $\sigma(^{235}\mathrm{U(n,f)})$, with cross sections obtained from evaluations, as well as to simulated ratios obtained with the model of Ref. [43].

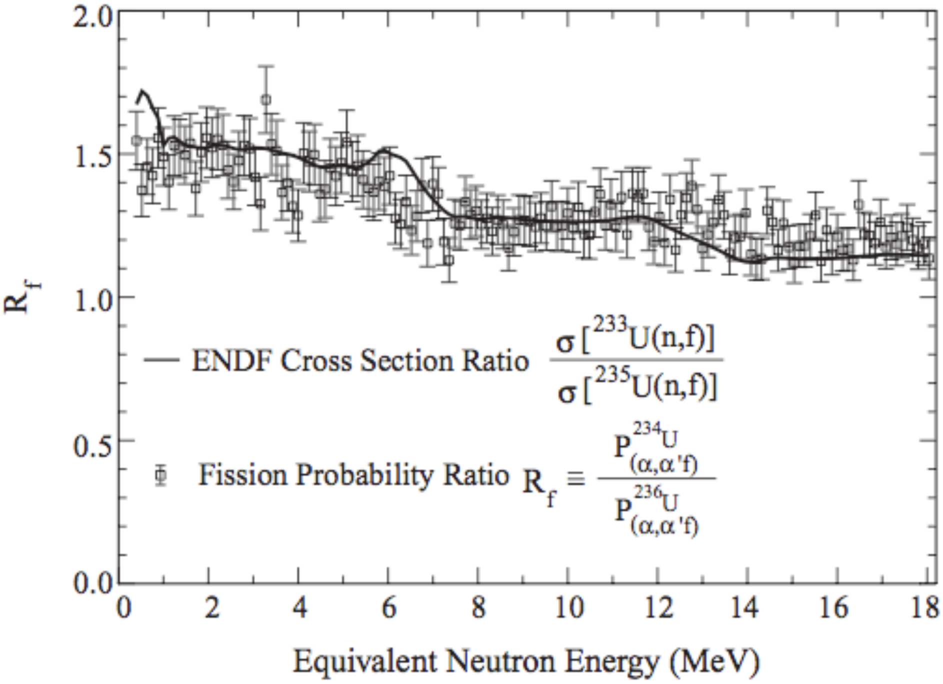

Figure 34: Experimental test of the External Surrogate Ratio method for fission. The ratio of measured fission (coincidence) probabilities (squares) is compared to the ratio $\sigma(^{233}\mathrm{U(n,f)})$ / $\sigma(^{235}\mathrm{U(n,f)})$ of evaluated fission cross sections (solid line). Figure taken from Ref. [69].

Overall, we find an acceptable level of agreement between the cross section ratio obtained from an ENDF evaluation [35] and the experimental ratio R_f^{exp}. The former lies clearly within the error bars of the latter, except for low energies, $E_n < 1$ MeV, see Fig. 34.

The ratios obtained from the simulations allow us to assess the effects of the neglected spin-parity mismatch on the extracted cross sections. Fig. 35 demonstrates rough agreement between the measured data and the calculated results for distributions a, b, and d, while distribution c produces a result that is in several energy regimes outside the range of the data. Based on insights from previous experiments [14], we expect that the $J\pi$ distributions with the smaller average J values, namely distributions a and d, are more likely to approximate the compound-nuclear spin-parity distribution obtained from inelastic scattering with 55-MeV α-particles than the other distributions shown in Fig. 27.

We can also identify energy regimes for which the measured fission probability ratio is sensitive to the spin distributions in the decaying compound nuclei, ^{234}U* and ^{236}U*. The largest variations in the calculated ratios occur for small equivalent neutron energies and near the onset of second-chance fission, as can be expected given the findings summarized in Refs. [42, 43]. At the higher energies ($E_{ex} \approx$ 18-20 MeV), we find little variation in the calculated ratios. Possible deviations of the extracted cross section from the expected cross section in that energy range are most likely be due to effects other than a mismatch between the compound-nuclear spin-parity distributions in the desired and Surrogate reactions.

The spin distribution of the compound nucleus produced in the Surrogate reaction depends not only on the projectile used (here α) and its energy, but also on the angle of the outgoing direct-reaction particle (here α'). Consequently, considering a narrow angular range for detecting the outgoing particle should reduce the scatter of the data points. Furthermore, varying the detection angle should result in changes in the ratio with the most pronounced changes occurring in those energy regimes that are expected to show an increased sensitivity to spin effects. Future experiments, if carried out with better statistical uncertainty, could look for such effects.

4.5.3 Testing the limits of the Ratio approach

An experiment aimed at exploring the limits of employing approximate methods in the analysis of Surrogate reactions was carried out by Lyles *et al.* [70], who studied the use of one-nucleon pickup reactions for obtaining cross sections for neutron-induced fission involving actinide targets. A 42-MeV ^{3}He beam was used to create the compound nuclei ^{237}U* and ^{234}U* via the ^{238}U(^{3}He,α) and ^{235}U(^{3}He,α) Surrogate reactions, respectively. Fission fragments of the decaying compound nuclei were detected in coincidence with the outgoing α particles. The ^{236}U(n,f) cross section was extracted from the data, via the Surrogate Ratio approach, relative to the known ^{233}U(n,f) cross section. The results were compared to the evaluated ^{236}U(n,f) cross section.

An important focal point of the work by Lyles *et al.* was the study of possible spin effects in applications of the Ratio method. For this reason, targets for the Surrogate reactions were selected in a manner that maximizes the spin mismatch between the two compound nuclei produced in the experiments: The ^{238}U ground state has J^π=0^+, while the ^{235}U ground state has J^π=$7/2^-$. Since the (^{3}He,α) transfer reactions were carried out with the same experimental setup and projectile energy, the resulting compound nuclei are expected to have spin-parity distributions that clearly differ from each other. The benchmark measurements described in the previous section, on the other hand, produced compound nuclei via inelastic α scattering on two even-even targets, which is expected to result in spin distributions that are very similar to each other.

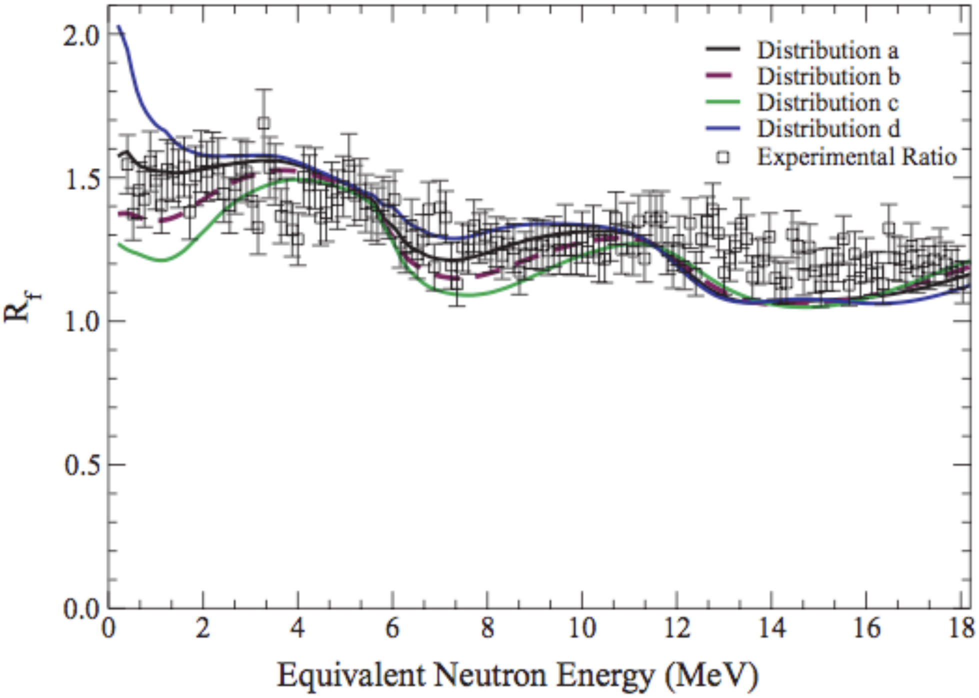

Figure 35: Comparison of measured fission (coincidence) probability ratios to simulated ratios, calculated for the schematic spin distributions shown in the left panel of Fig. 27. Calculated ratios are compared to experimental results. Figure taken from Ref. [69].

Figure 36 shows that the ^{236}U(n,f) cross section extracted from the Ratio analysis of the pair of Surrogate measurements agrees well with the expected result over an energy range from $E_n \approx 4$ MeV to $E_n \approx 20$ MeV. This figure demonstrates nicely that contaminants in the the Surrogate target pose no significant problem for the Ratio analysis. The presence of contaminants was clearly observed in a Weisskopf-Ewing analysis of the data; the extracted ^{236}U(n,f) cross section deviated significantly from the expected results for energies larger than about 7 MeV (for details, see Ref. [70]). This deviation is completely eliminated in the Ratio approach. However, for equivalent neutron energies below about 3 MeV, we find significant discrepancies between the expected cross section and that extracted from a Ratio analysis. The shape of the extracted cross section is very different from the evaluation, and the magnitude of the two differs by a factor of almost two. Possible reasons for the deviations between the low-energy extracted and evaluated cross sections include the spin-parity mismatch, as well as the energy mismatch discussed in Section 4.2. The spin-parity mismatch is expected to produce more dominant effects in this case than in earlier Ratio experiments, as the experiment compared the decays of an even-even and an odd compound nucleus, while the benchmark experiment (Section 4.5.2) and the simulations (Section 4.5.1) considered more benign cases: both target nuclei were even-even; in addition, the simulations employed very similar optical model potentials, level densities, strengths functions, etc., to model the structure and decay of the compound nuclei. The energy mismatch is also expected to contribute to discrepancies at low energies.

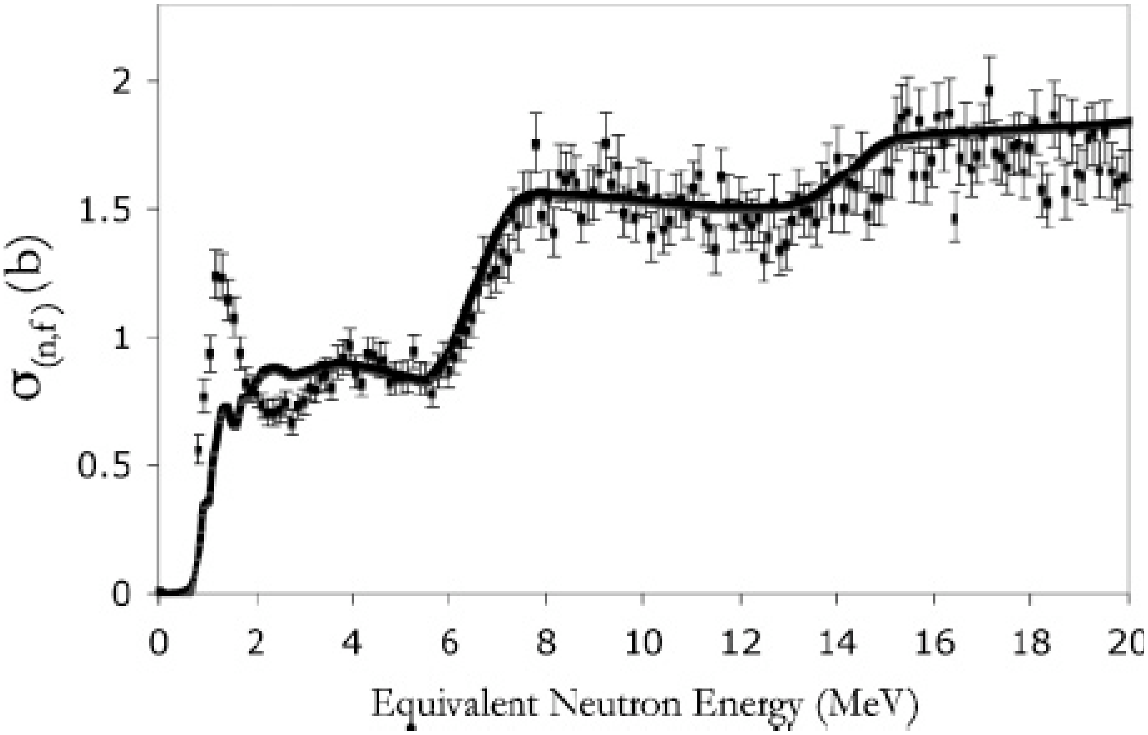

Figure 36: ^{236}U(n,f) cross section obtained from a Ratio analysis of Surrogate ^{238}U(^{3}He,αf) and ^{235}U(^{3}He,αf) measurements (filled symbols), compared to the evaluated cross section (solid line). Figure taken from Ref. [70].

5 Modeling approach

In the 'ideal approach' outlined in Section 2, one calculates the spin-parity distribution, $F_{\delta}^{CN}(E, J, \pi)$, and experimentally determines a set of coincidence data $P_{\delta\chi}(E)$, in order to extract the relevant $J\pi$ -dependent branching ratios $G_{\chi}^{CN}(E, J, \pi)$ from Eq. 2. In this approach, no assumptions about the form of the $G_{\chi}^{CN}(E, J, \pi)$ are made. Note that the $F_{\delta}^{CN}(E, J, \pi)$ depend not only on the direct-reaction mechanism selected, but also on the projectile energy and the angle of the outgoing direct-reaction particle. These quantities (beam energy and detection angle) have to be varied in order to provide sufficient complementary information on the $J\pi$-dependent branching ratios $G_{\chi}^{CN}(E, J, \pi)$. It is not *a priori* clear that experimental conditions can be selected that provide enough variation in the weights $F_{\delta}^{CN}(E, J, \pi)$ to allow for an unambiguous determination of the branching ratios. This fact makes this approach challenging.

While the 'modeling approach' is affected similarly by coincidence measurements that do not contain a wide range of complementary information on the $J\pi$-dependent branching ratios, it has the advantage that it can make use of independent information that constrains the $G_{\chi}^{CN}(E, J, \pi)$. Specifically, a sensible modeling approach should include a model for the decay of the compound nucleus under consideration that makes use of the available nuclear structure information for the region. In particular, neutron resonance spacings and average radiative widths may have been independently determined and there may be calculations or measurements for γ-ray strength functions and/or level densities. Reactions measured for nearby nuclei may also provide some constraints on the input parameters for the statistical reaction calculation. Combining such independent information with a Surrogate measurement in order to place stringent constraints on a Hauser-Feshbach calculation for the desired reaction is the objective of the modeling approach. The approach is somewhat similar to that employed in data evaluations, where model parameters which were adjusted to fit measured cross sections in one energy regime, are employed to calculate the cross section in another energy regime. In the Surrogate modeling approach, the parameters are adjusted to reproduce measured coincidence probabilities and subsequently used to calculate the desired reaction cross section.

Important steps towards developing the Surrogate modeling approach were taken by Back *et al.* [7, 6] and Younes and Britt [99, 100, 103]. Both groups employed simple models to predict the $J\pi$ distributions for compound nuclei formed in transfer reactions on actinide targets. Modeling the competition of the different decay channels for the relevant compound nuclei, and comparing the results to measured fission probabilities from direct-reaction experiments, allowed these authors to extract fission barrier parameters. Back *et al.* considered the energy region below the neutron separation energy; they did not attempt to determine fission cross sections, but focussed on the competition of γ-ray emission and fission and employed the modeling approach to determine barrier heights and curvatures.

5.1 Modeling approach for low-energy (n,f) reactions

Younes and Britt [99, 100, 103] built on the work of Back *et al.* [7, 6] and extended it higher energies in order to deduce (n,f) cross sections from existing (t,pf), (^{3}He,df) and (^{3}He,tf) measurements. They revisited older data sets, published by Britt *et al.* in 1968 [23], Cramer *et al.* [34, 33], and by Back *et al.* in 1974 [7], with the goal to improve on the previous Surrogate analyses that had employed the Weisskopf-Ewing approximation.

In Refs. [99, 100], the Surrogate (t,pf) fission probabilities, $P_{(t,pf)}(E)$ were calculated as a function of energy by summing over the contributions from the individual $J\pi$ compound states, $F^{CN}_{(t,p)}(E, J, \pi)\ G^{CN}_{fission}(E, J, \pi)$ (see Eq. 2). The (t,p)-induced spin-parity distributions, $F^{CN}_{(t,p)}(E, J, \pi)$, were taken to be independent of energy and calculated in a distorted-wave Born approximation approach that followed the procedure used by Back *et al.* in their study of fission-barrier parameters. Younes and Britt modeled the decay of the compound nucleus of interest by developing a description for the statistical competition between γ-decay, neutron emission, and fission. The γ-decay was assumed to proceed solely by E1 transitions; the neutron emission description employed a modern optical-model potential developed by Dietrich (see Appendix A.3). For the fission channel, a standard Hill-Wheeler formalism was employed, which included an inner barrier and two outer barriers with differing symmetry properties, discrete states in the first and second wells and on top of the fission barriers. Width fluctuation corrections were included as well.

In fitting their calculated $P_{(t,pf)}(E)$ to the Surrogate data, Younes and Britt only allowed the heights of the fission barriers to vary. Level densities, γ-ray strength functions, and the neutron transmission coefficients were considered to be fixed. This somewhat constrained approach minimized the number of adjustable parameters. It produced calculated coincidence probabilities, that, after fitting the barrier heights, were in good agreement with the measured $P_{(t,pf)}$ for energies below the neutron separation energy, but showed deviations on the order of xxx% from the data above that energy. A renormalization procedure was introduced to account for the differences. In particular, the branching ratios $G^{CN}_{fission}(E, J, \pi)$ that resulted from the fitting procedure, were renormalized by an energy-dependent, but $J\pi$-independent factor. The so renormalized quantities where subsequently employed to deduce the desired (n,f) cross sections.

For the ^{235}U(n,f) test case considered, Younes and Britt deduced a cross section which is in good agreement with the ENDF/B-VI evaluation [95] for neutron energies in the range of 0.5-2.5 MeV and too large by about 20% for energies from 0.1 to 0.5 MeV (see Fig. 37). The evaluated cross section was estimated to be accurate within 2%. Overall, the approach developed by Younes and Britt, which includes corrections for the spin-parity mismatch, resulted in significantly improved low-energy (n,f) cross sections when compared to the earlier work [33] that relied on the Weisskopf-Ewing approximation (see, for example, the ^{235}U(n,f) cross section in the upper right panel of Fig. 37). The method tested for the ^{235}U(n,f) case was subsequently applied to other available Surrogate data. In Ref. [99], it was used to predict the (n,f) cross section for the short-lived (26 min) isomeric state ^{235m}U at $E = 77$eV. In Ref. [100], (n,f) cross sections were extracted from (t,pf) data for neutron targets ^{240,241,243}Pu, ^{234,236,237,239}U, and ^{231,232}Th, for energies $E_n = 0.1$ - 2.5 MeV. All applications made use of the same approach, including the normalization procedure; all results were considered to be accurate to within 20% below $E_n \approx 0.5$ MeV, and 10% at higher energies.

In subsequent work, Younes, Britt, and Becker [103] covered Surrogate data from (^{3}He,df) and (^{3}He,tf) experiments carried out by Gavron *et al.* in 1976 [55, 25]. They deduced (n,f) cross sections for neutron targets ^{236,236m,237,238}Np, ^{237,237m}Pu, and ^{240,241,242,242m,243,244,244m}Am, for energies $E_n =$ 0-6 MeV. An example is shown in Figure 39. For those cases for which direct measurements exist, the directly-determined (n,f) cross section and the Surrogate result agree within about 10%.

5.2 Extension of the method to higher neutron energy

A procedure was developed [104, 102] to extrapolate the surrogate results to higher energies, and applied to estimating the $^{235,237,239}\mathrm{U}\,(n,f)$ cross sections for incident energies of up to 20 MeV. The procedure combines the surrogate predictions for the mass-A nucleus, which provide an estimate of the first-chance fission cross section, with known (n,f) cross sections on the $A-1$ nucleus, which give the second- and higher-chance contributions.

For the first-chance cross section, the surrogate predictions usually stop at a few MeV in equivalent neutron energy. In order to extend the predictions to 20 MeV, a linear extrapolation of the surrogate result was used. The surrogate data were used to fix the intercept of the linear extrapolation, and the slope was obtained from the ENDF/B-VI evaluation of the (n,f) cross section.

The second-chance fission cross section was decomposed into contributions from equilibrium and pre-equilibrium reactions. The second-chance equilibrium cross section was approximated as the difference between the compound formation and first-chance (n,f) cross sections. This difference gives the cross section for the equilibrium (n,n') process, which may then be followed by further neutron emission, γ decay, or fission. The pre-equilibrium (n,n') process was calculated using the code DDHMS [31], and its cross section was added to the equilibrium one. To extract the $(n,n'f)$ cross section, the total (n,n') cross section (equilibrium plus pre-equilibrium contributions) was multiplied by the conditional probability $P_{f|(n,n')}$ that the nucleus fissions given that an (n,n') reaction has occurred. This conditional probability was calculated by invoking the Bohr hypothesis and assuming that the probability $P_{f|(n,n')}\,(A)$ for a target nucleus A is equal to the probability $P_{f|(n)}\,(A-1)$ of fission following neutron absorption on a target with mass $A-1$, provided the same excitation energy is reached in both reactions. In practice, the probability $P_{f|(n)}\,(A-1)$ was obtained from the measured (n,f) cross section on the $A-1$ nucleus. In principle this procedure is designed to give the second-chance contribution to the cross section, but the use of the measured $A-1$ cross section introduces contributions from third- and higher-chance fission as well.

The dependence on emitted neutron energy for the second-chance fission process was assumed to follow a Maxwell distribution. The effective temperature in the distribution was the only adjustable parameter in the model. In a systematic study of the $^{235,237,239}\mathrm{U}\,(n,f)$ cross sections, the Maxwell-distribution temperature was fixed by fitting the known $^{235}\mathrm{U}\,(n,f)$ cross section with the model described above, and that same temperature was used to pre-

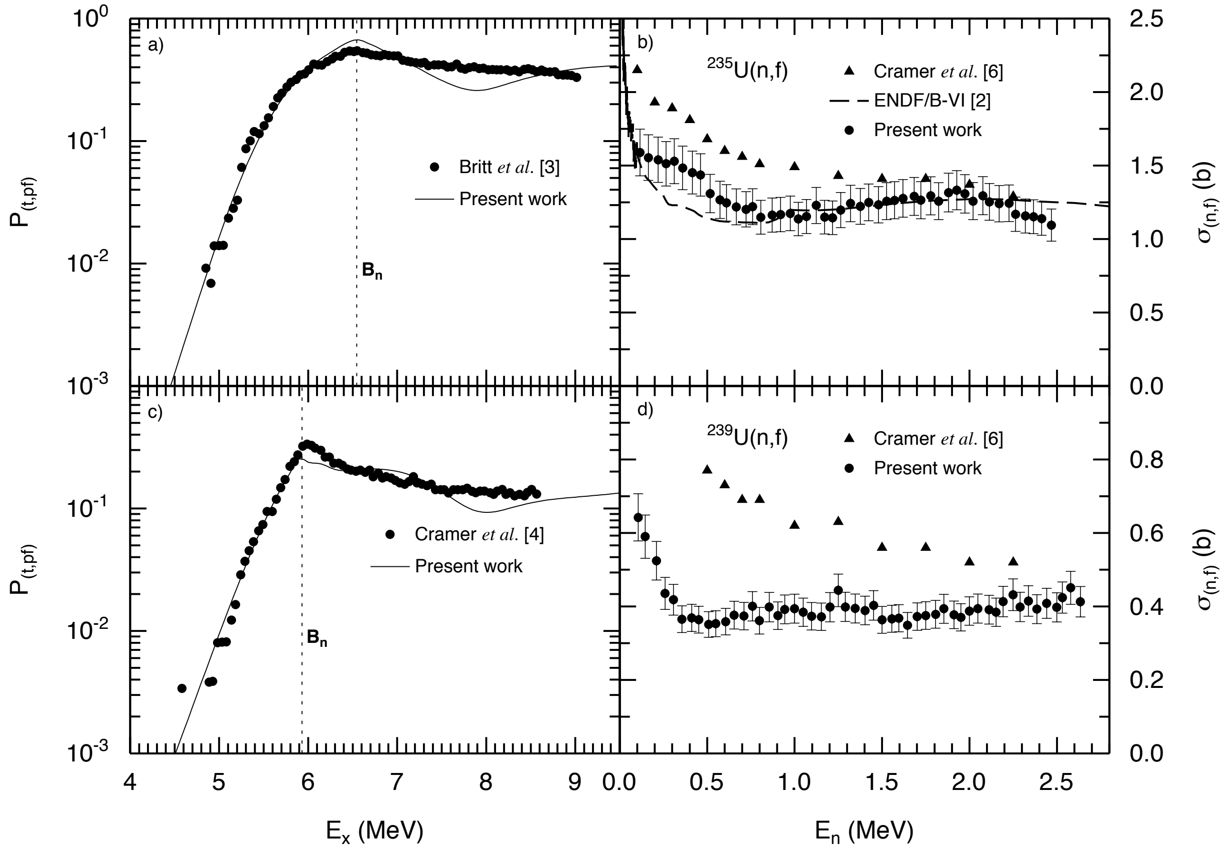

Figure 37: Surrogate fission probabilities and (n,f) cross sections for ^{235}U (top) and ^{239}U (bottom). Panels a) and c) show measured and predicted (t,pf) coincidence probabilities and panels b) and d) give the extracted cross sections. Panel b) compares results by Younes and Britt, whose analysis accounted for spin-parity differences between the desired and Surrogate reactions, to the earlier analysis by Cramer *et al.*, which employed the Weisskopf-Ewing approximation, and to the ENDF/B-VI evaluation [95]. Panel d) gives the ^{239}U(n,f) cross section, compared to the Weisskopf-Ewing result from Cramer *et al.*. Figure taken from Ref. [100].

dict the $^{235}\mathrm{U}\,(n,f)$ cross section. The fit to the $^{235}\mathrm{U}\,(n,f)$ cross-section evaluation is shown in Fig. 41. The deduced $^{237}\mathrm{U}\,(n,f)$ and $^{237}\mathrm{U}\,(n,f)$ cross sections are shown in Figs. 42 and **??**, respectively, where they are compared to the ENDF/B-VI evaluation.

5.3 Comments on the modeling approach

The work by Younes and collaborators demonstrates clearly that the accuracy of low-energy (n,f) cross sections can be improved by theoretically accounting for the spin-parity mismatch between the desired and Surrogate reactions, and by using high-quality optical-model potentials. The cross sections deduced in their modeling approach is in much better agreements with direct measurements (where available) than the older result, which employed the Weisskopf-Ewing approximation.

While the bulk of the work by Younes and Britt allowed only for a variation of very few parameters, namely the fission barrier heights, a full modeling approach should relax the constraints on the level densities, strength functions, etc. Variation of some additional parameters was part of a sensitivity study carried out by Younes *et al.* in Ref. [99]. Overall, it becomes important to balance the freedom gained by allowing additional parameters to vary, against the typically limited data that can be used to provide the necessary constraints.

The models used to predict $J\pi$ distributions of the compound nucleus were very simple, but seemed effective. The models did not take into account that nucleons were transfered to unbound states, nor did they include the possibility that the highly-excited intermediate system might decay without forming a compound nucleus. The predicted $J\pi$ distributions were independent of energy, which might be a reasonable approximation for the 2.5 MeV range populated in the (t,pf) reactions, but might lead to additional uncertainties when considering wider energy ranges.

The calculated fission probabilities that resulted from the fitting procedure showed deviations from the Surrogate data that had to be corrected for via an energy-independent, but $J\pi$ -dependent normalization factor. The factor, which was seen to deviate from one by as much as 15% for the ^{235}U(n,f) test case and 35% for the ^{235m}U application, indicates that further improvements in the method are possible. The goodness of the fit to the measured coincidence probabilities is an indication of how well the physics of the Surrogate reaction, including the decay, is described by theory. Having an accurate description that requires no additional normalization factors is particularly important if one wants to apply the method to reactions on nuclei which are a few nucleons off stability.

The predicted $J\pi$ populations were not independently tested. For the cases where directly-measured (n,f) cross section data was available, the agreement between the Surrogate results and the direct measurements was taken as an indication of the overall consistency of the approach and the models employed. However, developing experimental signatures that can test the predicted $J\pi$ populations would be useful for further tests and improvements of the Surrogate method. Such signatures might be found in the γ-ray transitions of a decaying compound nucleus that was created in a Surrogate reaction. This issue is currently being explored [41].

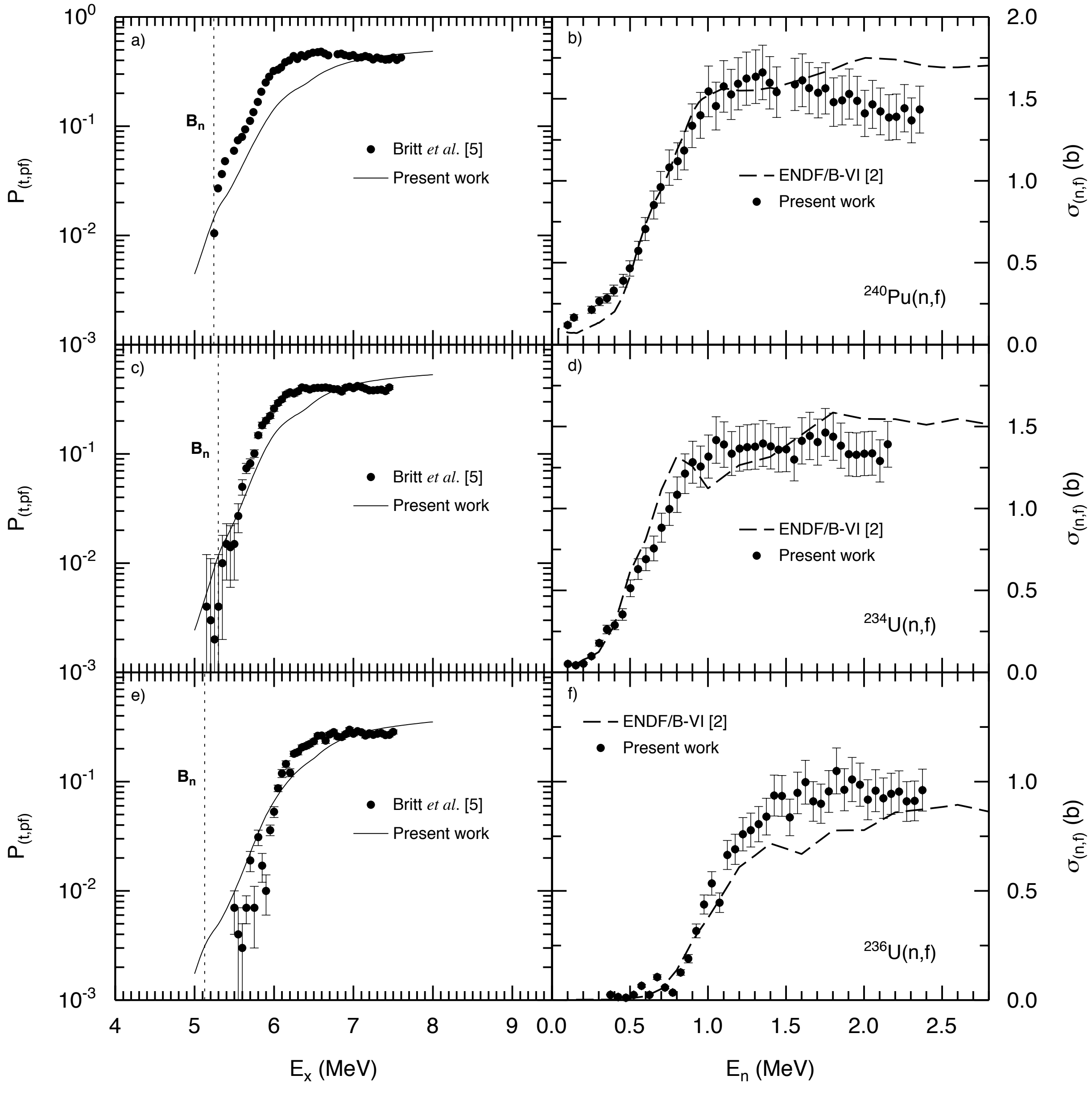

Figure 38: Surrogate fission probabilities and (n,f) cross sections for ^{236}U, ^{234}U, and ^{240}Pu. Figure taken from Ref. [100].

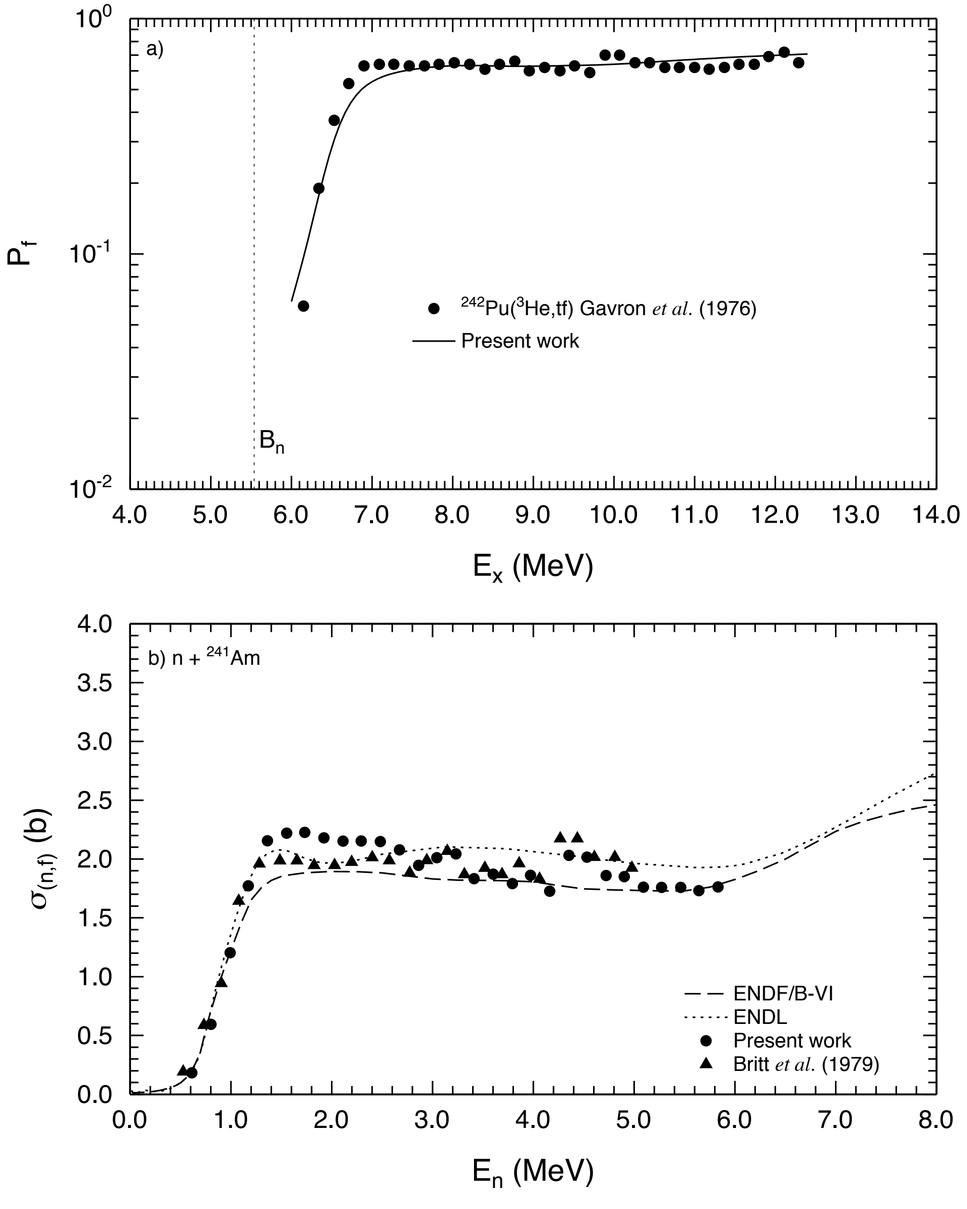

Figure 39: Surrogate fission probabilities and (n,f) cross sections for ^{241}Am. Figure taken from Ref. [103]

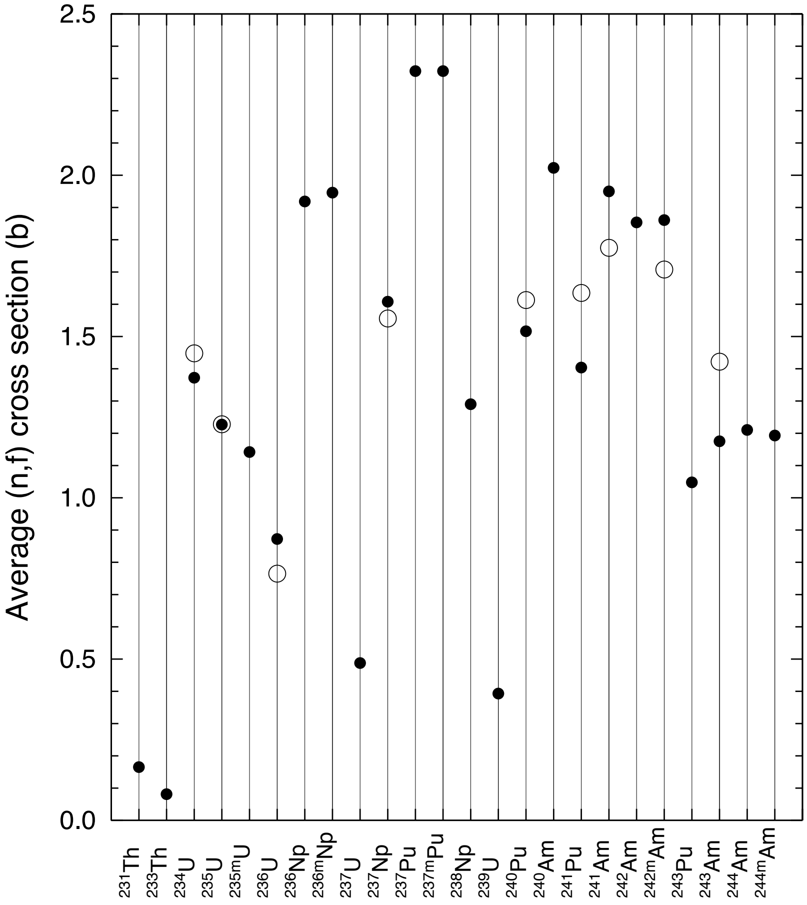

Figure 40: Summary of low-energy (n,f) cross section averages. Surrogate results (open circles) are compared to available data (filled circles). Figure taken from Ref. [101]

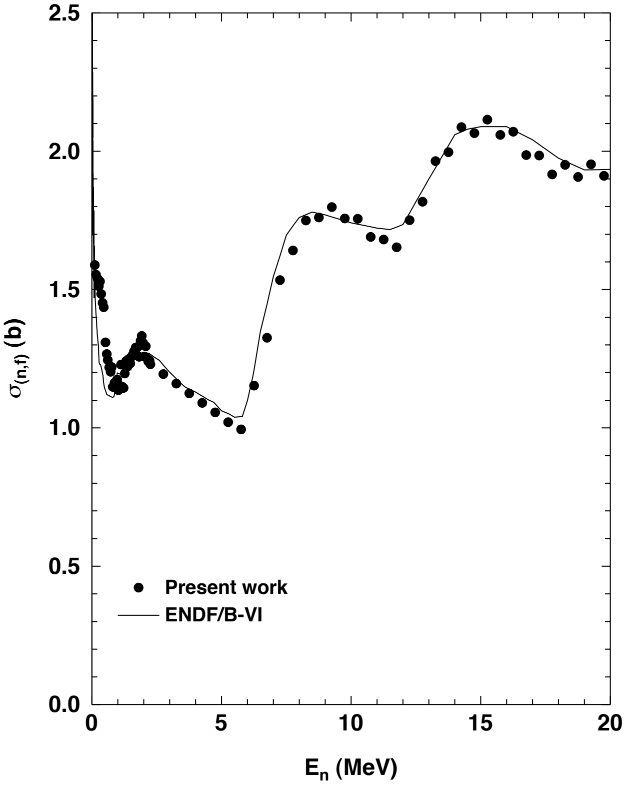

Figure 41: Comparison of the calculated $^{235}\mathrm{U}\,(n,f)$ cross section with the ENDF/B-VI evaluation.

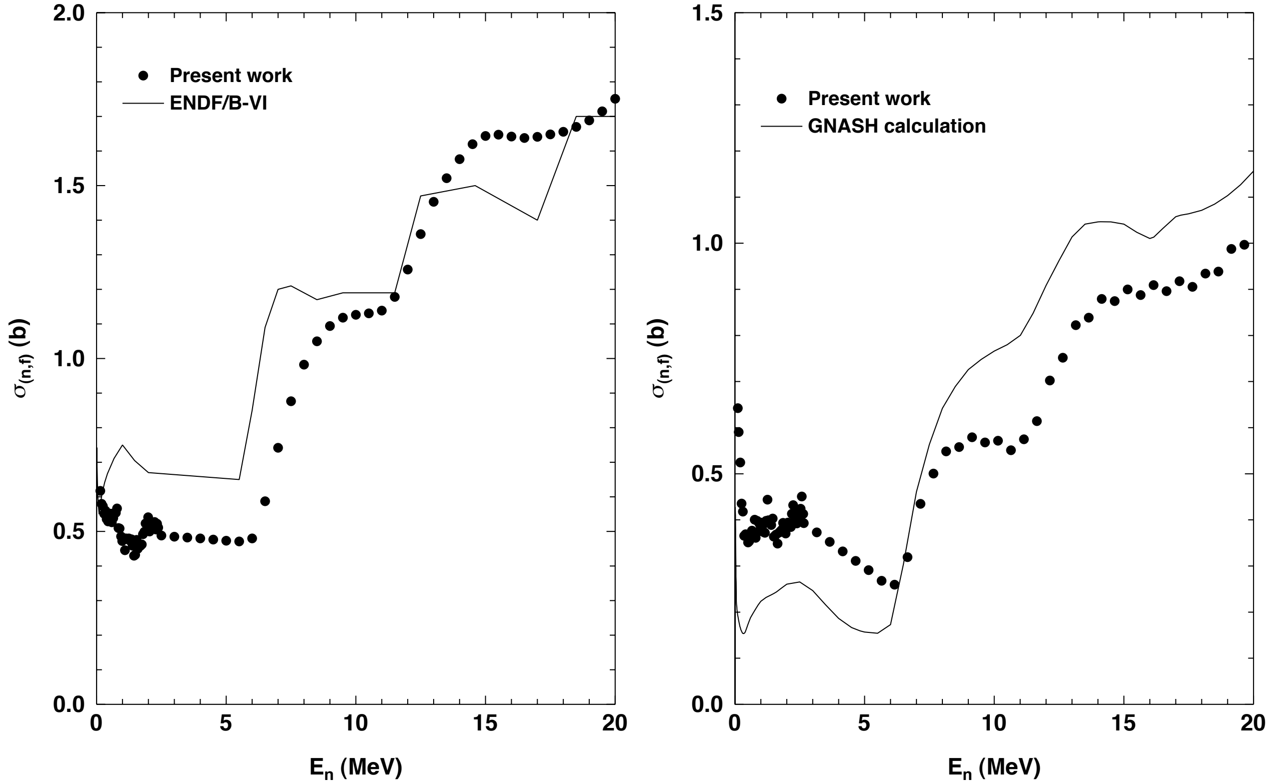

Figure 42: Comparison of the calculated $^{237}\mathrm{U}\,(n,f)$ and $^{239}\mathrm{U}\,(n,f)$ cross sections with the ENDF/B-VI evaluations.

6 Surrogate reactions for (n,γ)

While a large number of Surrogate experiments aimed at obtaining (n,f) cross sections have been carried out over the years, few experiments have been designed to determine (n,γ) cross sections. Still fewer experiments have attempted to provide information about the charged-particle or two-neutron exit channels. In this section, we focus on the prospects of determining (n,γ) cross sections from Surrogate experiments. The γ exit channel is very important, not only because cross sections for low-energy neutron capture ($E_n < 1$ MeV) play a crucial role for many applications, but also since the observables used to tag the γ exit channel in Surrogate experiments can provide valuable information on the spin-parity distributions present in the compound nucleus prior to decay. This is significant, as it can help to test theoretical predictions of the $J\pi$ distributions, which in turn are required for improving the accuracy of (n,f) cross section determined from Surrogate experiments and for enabling the extraction of (n,2n), (n,p), and other cross sections.

In Section 6.1 we describe the challenges that particularly affect the determination of (n,γ) reaction cross sections from Surrogate measurements. Specifically, we illustrate the sensitivity of the observables used to tag the γ exit channel to spin effects. In Section 6.2, we show simulations analogous to those employed to study the fission case (cf. Section 3.5) and test the validity of using the Weisskopf-Ewing approximation when extracting (n,γ) cross sections from Surrogate experiments. We demonstrate that, in general, it is not sufficient to rely on the Weisskopf-Ewing approach. The External Surrogate Ratio method, when used in the same straightforward manner that worked well for the fission case, is seen in Section 6.3 to provide some improvements over the (absolute) Weisskopf-Ewing approach, but the overall accuracy of the results is, in general, not found to be satisfactory. A brief summary of some experimental results for (n,γ) reactions is given in Section 6.4.

6.1 Challenges for Surrogate measurements of (n,γ) cross sections

For (n,f) reactions, the spin mismatch between the Surrogate and desired reactions was seen to primarily affect the accuracy of the extracted cross sections at low energies ($E_n < 1$ MeV), and, to a lesser extent, at the onset of first and second-chance fission (see Sections 3.5.2 and 3.5.3). Since the energy region of interest to many applications that require neutron-capture cross sections lies below about 1 MeV, accounting for this mismatch is expected to be very important for (n,γ) reactions. To investigate this, we have calculated the γ-decay probabilities $G_\gamma^{CN}(E, J, \pi)$ for the compound nucleus ^{236}U. We started from the simulations used for the (n,f) case discussed in Section 3.5.1, and slightly adjusted the Hauser-Feshbach parameters to better reproduce the available (n,γ) data and ENDF/B-VII evaluation for the ^{233}U(n,γ) and ^{235}U(n,γ) cross sections (the resulting fission cross sections did not differ much from the previous fit). Selected γ branching ratios $G_\gamma^{CN}(E, J, \pi)$ for the decay of ^{236}U are shown in Fig. 43; results for positive-parity states with $J = 0, 3, 6, 9, 12$, and 18 are shown in the left panel of the figure, and those for negative-parity states are given in the right panel, for ^{236}U excitation energies E_{ex} = 6.55-10.5 MeV, which corresponds to neutron energies of 0-4 MeV.

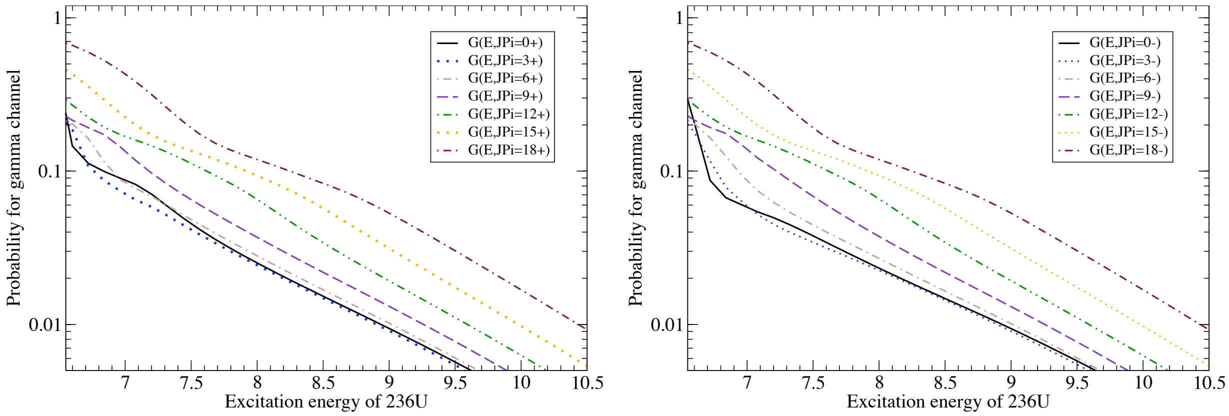

Figure 43: Calculated γ-decay probabilities $G_{\gamma}^{CN}(E, J, \pi)$, for ^{236}U . Shown is the probability that the compound nucleus, when produced with a specific $J\pi$ combination, decays via the γ channel. Positive-parity decay probabilities are shown in the left panel, and negative-parity decay probabilities are shown on the right.

While the $G_{\gamma}^{CN}(E, J, \pi)$ for $J = 0 - 6$ are very similar to each other for $E > 1$ MeV, they differ more significantly from each other below 1 MeV. For energies above about 1.5 MeV, all branching ratios exhibit roughly the same energy dependence, but the $G_{\gamma}^{CN}(E, J, \pi)$ associated with the higher angular-momentum values $J = 15, 18$ differ from those for $J = 0, 3$ by a factor of about 3-6. Even for $J = 9, 12$, the $G_{\gamma}^{CN}(E, J, \pi)$ differ from those for the low spins by factors of 0.5 to 3. Given the interest in the low-energy region, $E < 1$ MeV, and the fact that the compound nucleus ^{236}U can ^{236}U can exhibit spin-parity distributions peaked at various ranges of spins, depending on the reaction that produces it, we expect, based on these calculations, the cross sections obtained in the Weisskopf-Ewing approximation to be very limited in accuracy. This issues is investigated in more detail in Section 6.2.

A closely related challenge that has to be addressed when determining (n,γ) cross sections from Surrogate experiments lies in the identification of the γ exit channel. Surrogate experiments that aim at determining compound-nuclear (n,γ) cross sections have to detect the outgoing direct-reaction particle b in coincidence with an observable that identifies the γ-emission decay channel. In current applications of the Surrogate reaction technique, this is typically accomplished by gating on coincidences between the outgoing particle b and individual γ rays that are characteristic of transitions between low-lying levels of the decaying nucleus. The experiments measure the yields of individual gammas in the gamma cascade rather than the quantity that is wanted, which is the sum of all cascades. This differs from the fission case, in which observation of fission fragments provides a direct measure of the desired quantity. For capture, a reaction-model calculation of the gamma cascade must be used to connect the observed gamma yields with the desired cross section.

The effect is illustrated in Fig. 44 for the decay of the compound nucleus ^{236}U, formed in the n+^{235}U and n+^{235m}U channels, respectively. The plot shows the ratio of the calculated intensity of a particular γ transition to the total intensity of γ cascades that eventually reach the ground state of ^{236}U. The simulation described above was employed to calculate the relevant intensities; internal conversion, which affects the γ yield measured in any experiment that focuses on γ cascades has not been considered here, but has to be accounted for in actual measurements. Both panels of Fig. 44 show relative γ yields for the decay of the compound nucleus ^{236}U as a function of energy. Apart from the intensities for the $2^+ \rightarrow 0^+$ transition, the yields shown in the two panels of the figure are very different from each other. This difference can be attributed to a difference in the $J\pi$ distribution in the decaying compound nucleus. The compound nucleus ^{236}U associated with the upper panel is expected to have a spin distribution that is peaked at higher angular-momentum values than the compound nucleus ^{236}U associated with the lower panel. The former nucleus was produced in a reaction in which a neutron was absorbed by the $J\pi = 7/2^-$ ground state of ^{235}U, while the latter was produced in a reaction involving the first excited state of ^{235}U, which has angular momentum and parity $J\pi = 1/2^+$. The energy difference between these two target states is very small, less than 100 eV, thus the only significant difference between the compound nuclei ^{236}U produced in these reactions is the spin-parity population of the decaying nucleus. It is clear that the ratios-to-total are highly dependent on the spin-parity distribution for all of the transitions except the $2^+ \rightarrow 0^+$. This transition is dominated by internal conversion and is therefore very difficult to measure by gamma detection in the experimental setup currently being used for Surrogate reaction studies. Overall, it is evident that the compound-nucleus spin distribution has a significant influence on the observed quantities and thus on cross sections that are extracted if these aspects are not properly modeled.

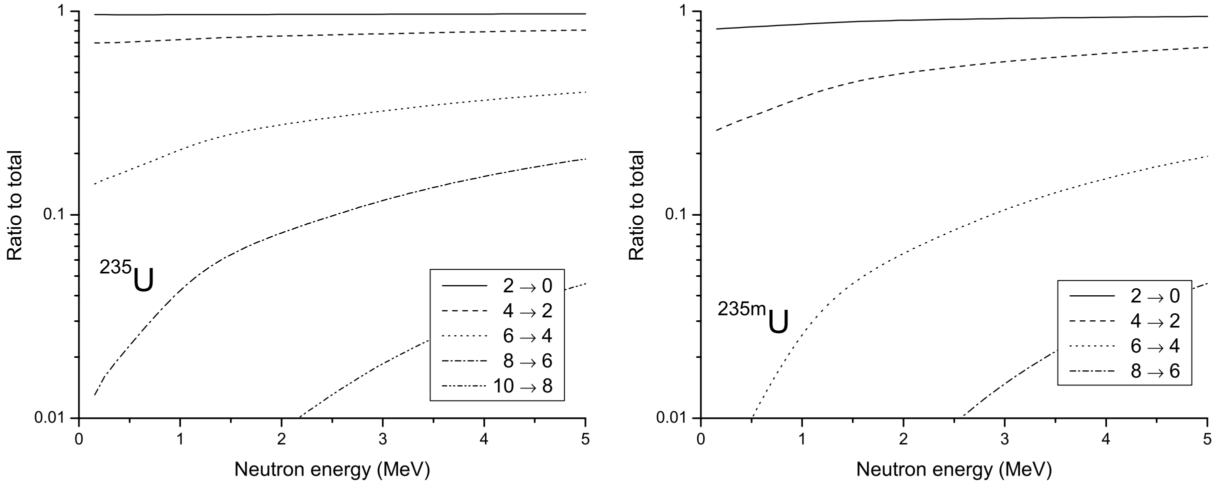

Figure 44: Ratio of yields of various γ rays for transitions in the ground-state band of ^{236}U to the total production of ^{236}U. The left panel shows results for the decay of ^{236}U following its production in the $n + ^{235}$U channel, while the right panel is for the $n + ^{235m}$U channel.

While the strong dependence of the γ ray yields on the $J\pi$ distribution of the compound nucleus makes the extraction of a (n, γ) cross section from a Surrogate experiment difficult, this sensitivity also provides an opportunity for obtaining information on the spin-parity distribution of the decaying nucleus from an observation of the associated γ rays. Measurements of yields for various individual γ rays will provide stringent tests for theoretical predictions of the formation and decay of a compound nucleus produced in a Surrogate reaction. This issue is currently being explored in an analysis of (p,p'γ) Surrogate experiments that were carried out to determine (n,γ) cross sections for gadolinium targets [41].

The application of the surrogate nuclear reaction method to (n,γ) cross sections poses challenges not only for interpreting the results, but also for obtaining high-quality experimental data. The signature of the γ-ray channel is a complex γ-ray cascade from a highly-excited compound nucleus. Compared to fission-fragment detection, γ-ray spectroscopy is less efficient and prone to backgrounds from the neutron-emission exit channel and impurities in the target. For example, backgrounds from target impurities (even if only at the percent level) are a concern because the γ-ray exit channel decreases rapidly with energy and can be orders of magnitude smaller than the cross section for unwanted nuclear reactions occurring within the target material. In addition, the excitation energy of the compound nucleus must be precisely determined to avoid washing out the strong energy-dependence of most (n,γ) cross sections. The resolution and calibration of the excitation-energy measurement also dictates how low in energy the experiment can probe before events from below the neutron separation energy compromise the Surrogate data.

6.2 Validity of the Weisskopf-Ewing approximation for (n,γ)

The effect of the spin-parity mismatch between the desired and surrogate reactions on the cross section extracted from a Weisskopf-Ewing analysis can be simulated by employing the calculated $G_{\gamma}^{CN}(E,J,\pi)$ of Fig. 43 and schematic surrogate spin-parity distributions. We consider four schematic, energy-independent distributions $F_{\delta}^{CN(p)}(E,J,\pi)$. The first three are distributions A, B, D employed in the study of the fission channel, as discussed in Section 3.5. They are shown in Fig. 27. Distribution C of that study is not considered here, as the reaction mechanisms employed in most recent Surrogate experiments are not expected to populate such high angular-momentum states. Instead, we have added distribution ABB, which we extracted from a (d,p) prediction made by Andersen *et al.* [4]. This distribution is shown in Fig. 45. We calculate simulated surrogate coincidence probabilities $P_{\delta\gamma}^{(p)}(E) = \sum_{J,\pi} F_{\delta}^{CN(p)}(E,J,\pi) G_{\gamma}^{CN}(E,J,\pi)$ for the four different distributions ($p = ABB, D, A, B$). Treating the latter like an experimental result, one obtains – in the Weisskopf-Ewing approximation – the ^{235}U(n,γ) cross sections indicated in Fig. 46 (left panel). Analogously, one obtains the ^{233}U(n,γ) cross sections shown in the right panel of the figure. In both cases the compound-nuclear formation cross section of Fig. 57 was used. These calculations are compared with the "reference cross section", which is the full Hauser-Feshbach calculation of the correct result using the same parameters, except that the spin-parity distribution in the gamma-emitting compound nucleus is determined by the entrance-channel transmission coefficients.

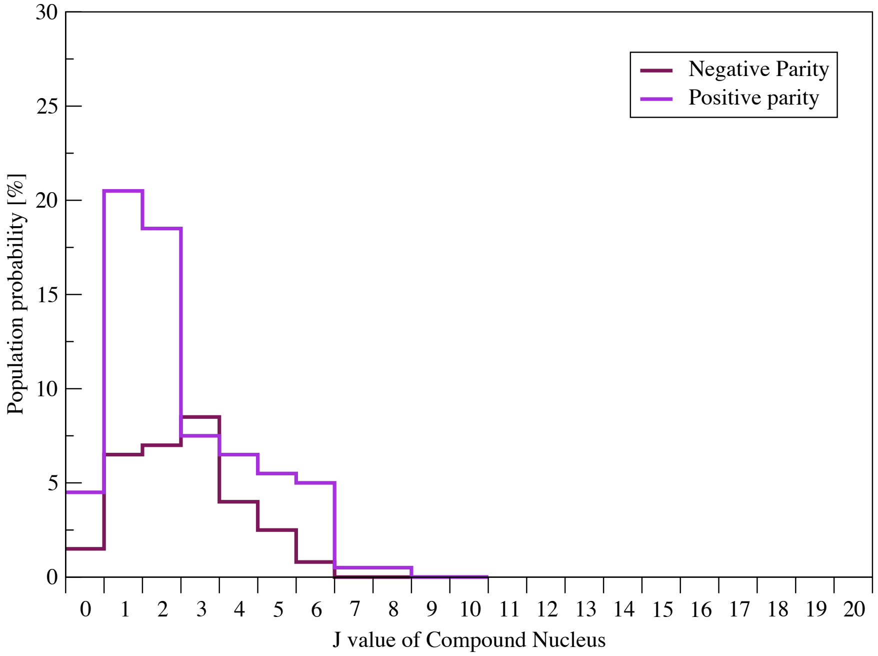

Figure 45: Schematic spin-parity distribution ABB.

We observe that for energies above $E_n \approx 0.6$ MeV the energy dependence of the radiative capture cross section is reasonably well reproduced by the Weisskopf-Ewing simulation, while the absolute magnitudes are strongly dependent on the assumed spin-parity distribution in the Surrogate reaction. Distributions ABB and D lead to results that are very close to the ^{235}U(n,f) reference cross section, while the cross sections associated with distributions A and B are too large by about 40% and 200%, respectively. Distributions ABB and D also yield very good agreement with the ^{233}U(n,f) cross section, but the cross sections extracted for distributions A and B are too large by roughly 20% and 50%, respectively.

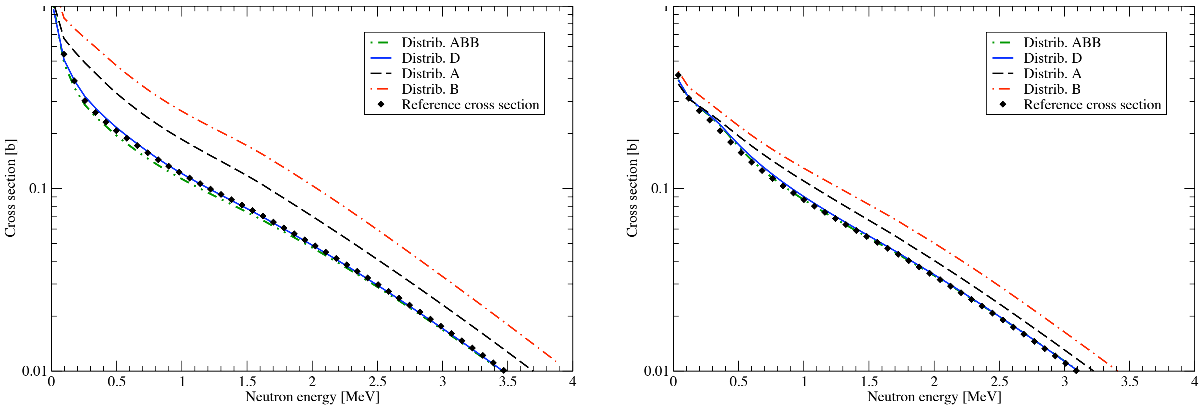

Figure 46: Weisskopf-Ewing estimates for the ^{235}U(n,γ) and ^{233}U(n,γ) cross sections, extracted from analyses of simulated Surrogate experiments, for four different compound-nuclear $J\pi$ distributions. For comparison, the reference cross section, which was obtained by adjusting the parameters for the Hauser-Feshbach calculation to reproduce direct measurements and evaluated results is shown as well.

The calculated γ-decay probabilities $G_{\gamma}^{CN}(E, J, \pi)$ shown in Fig. 43 help us understand discrepancies between the reference cross section and those extracted from a Weisskopf-Ewing analysis of the Surrogate data: If the Surrogate reaction populates the relevant compound nucleus, e.g. ^{236}U, with a spin-parity distribution that contains larger angular-momentum values than the population relevant to the neutron-induced reaction, then the measured decay probability $P_{\delta\gamma}(E)$ of Eq. 2 contains larger contributions from those $G_{\gamma}^{CN}(E, J, \pi)$ associated with large J values than the cross section expression for the desired (n, γ) reaction does. Consequently, the cross section extracted by using the Weisskopf-Ewing assumption and approximating $P_{\delta\gamma}(E) \approx G_{\gamma}^{CN}(E)$, gives too large a result. The same will hold true for other Surrogate mechanisms that produce the compound nucleus with spin-parity distributions that are shifted to larger J values relative to the distribution found in the neutron-induced reaction.

We conclude that the Weiskopf-Ewing approximation does not lead to a satisfactory estimate of the radiative capture cross section unless the spin-parity distribution in the compound nucleus is well known and a Surrogate reaction mechanism and experimental conditions can be identified and devised that approximately reproduce the spin-parity distribution of the desired reaction.

6.3 Validity of the Ratio approximations for (n,γ)

One may try to reduce the uncertainties seen in the cross sections obtained using the Weisskopf-Ewing analysis by employing the Surrogate Ratio method.

External Surrogate Ratio for (n,γ) cross sections. For the External Ratio (ESR) method, this amounts to dividing the results shown in the left panel of Fig. 46 by those in the right panel of the same figure and multiplying by the reference cross section, defined as above. The results are shown in the left panel of Fig. 47 for ^{235}U(n,γ). In order to better display the differences for the selected spin-parity distributions, we also show the cross section ratios $\sigma[^{235}\text{U(n,}\gamma)]$ / $\sigma[^{233}\text{U(n,}\gamma)]$ obtained for the four schematic $J\pi$ distributions and the reference cross sections (see Fig. 47, right panel). The dependence on the spin-parity distribution is reduced relative to the results for the Weisskopf-Ewing approximation but is still significant. In particular, the shape of the reference cross section is approximately reproduced for $E_n >$ 1 MeV, but the magnitudes of the results extracted from the External Ratio analysis are too large by roughly 20% (for distribution A) to 40% (for distribution B); the results for distributions ABB and D are within 5% of the reference ratio. The disagreement between the cross sections extracted using the ESR analysis and the reference result decreases with increasing energy, but even at $E_n \approx 3-4$ MeV, the Weisskopf-Ewing limit does not apply. This is different from what has been found in simulations of (n,γ) cross sections for lighter targets, such as zirconium [51] and gadolinium [83]. (For those cases, the Weisskopf-Ewing limit was reached around 2.5-3 MeV for Zr and 1.5-2 MeV for Gd.) For lower energies, $E_n <$ 0.5 MeV, the discrepancies increase, even the shape of the cross section is no longer properly reproduced.

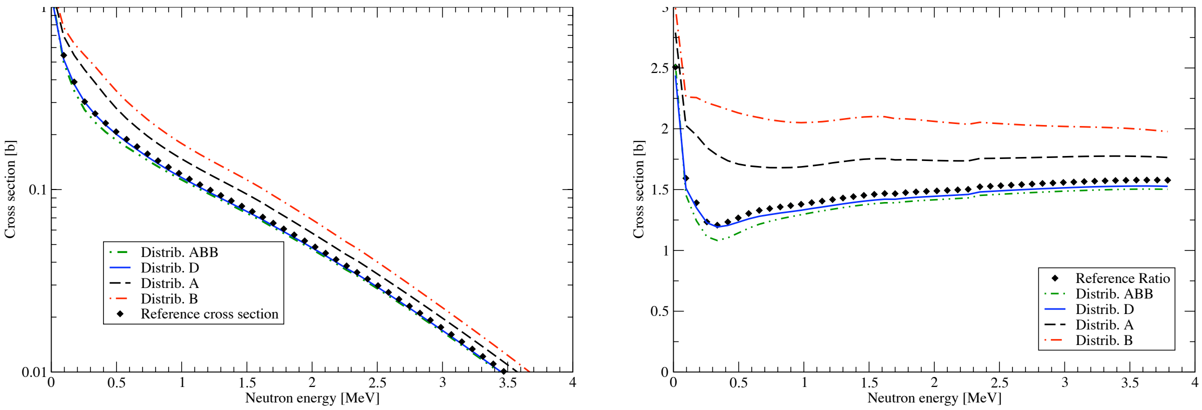

Figure 47: External Surrogate Ratio estimates for the ^{235}U(n,γ) cross section, extracted from analyses of simulated Surrogate experiments, compared to the reference cross section. The left panel shows the cross section result of a simulated External Surrogate Ratio analysis, while the right panel shows the ratio of the cross sections. Four different compound-nuclear $J\pi$ distributions were considered.

Internal Surrogate Ratio for (n,γ) cross sections. The results obtained by using the Internal Ratio method are shown in the Fig. 48. The left panel gives the ^{235}U(n,γ) cross sections extracted from the ISR analysis of simulated Surrogate experiments, compared to the reference cross section. For $E_n > 1$ MeV, the pattern is similar to that found for the (absolute) Weisskopf-Ewing analysis, No improvement over the Weisskopf-Ewing result is found and the spin-parity dependence of the cross section is stronger than that seen for the ESR case. Furthermore, the right panel illustrates that the cross sections do not simply differ by an approximately constant factor, *i.e.* the ISR analysis does, in general, not reproduce the shape of the cross section. For energies below 0.5 MeV, even the results for distributions D and ABB differ from the reference cross section.

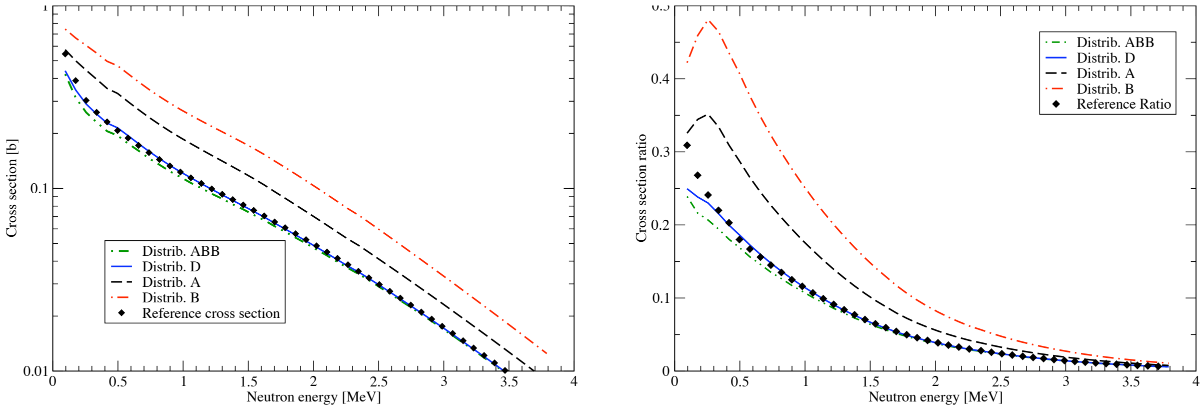

Figure 48: Internal Surrogate Ratio estimates for the ^{235}U(n,γ) cross section, extracted from analyses of simulated Surrogate experiments, compared to the reference cross section. The left panel shows the cross section result of a simulated Internal Surrogate Ratio analysis, while the right panel shows the ratio of the cross sections.

Overall, we find that the extracted (n,γ) cross sections are very sensitive to the compound-nucleus spin-parity distribution of the Surrogate reaction. The uncertainty is greater than that found for the (n,f) cross sections and – unlike in the fission case – is not significantly reduced when a Ratio approach is used. For the cases studied here, neither the ESR nor the ISR method yields a satisfactory agreement with the reference cross section unless the Surrogate experiment produces a compound-nucleus spin-parity distribution similar to that found in the desired reaction. The results shown here have not taken into account the further complication that arises when individual gammas rather than a total yield are measured, as discussed in the previous section; this provides an additional uncertainty.

6.4 Experimental efforts for (n,γ)

There have been several attempts to determine (n,γ) cross sections from Surrogate measurements. Here we will focus on those aimed at determining (n,γ) cross sections for actinide nuclei and mention only briefly those experiments that studied reactions in other mass regions.

CENBG studies of ^{233}Pa(n,γ). The CENBG collaboration extracted the ^{233}Pa(n,γ) cross section from two separate Surrogate experiments.

The first experiment [78] employed the (^{3}He,p) reaction on a ^{232}Th target and was designed to yield the ^{233}Pa(n,f) cross section, which was extracted from a Weisskopf-Ewing analysis of the data. A Hauser-Feshbach evaluation of the ^{233}Pa(n,f), ^{233}Pa(n,n$'$), and ^{233}Pa(n,γ) cross sections was carried out, with parameters adjusted to reproduce the new (n,f) data. In Fig. 49, the result of the ^{233}Pa(n,γ) cross section calculation is compared to prior evaluations. The setup of the experiment is discussed in Section 3.3 and the ^{233}Pa(n,f) cross section obtained is compared to direct measurements in Fig. 12. More details can be found in the publication by Petit *et al.* [78].

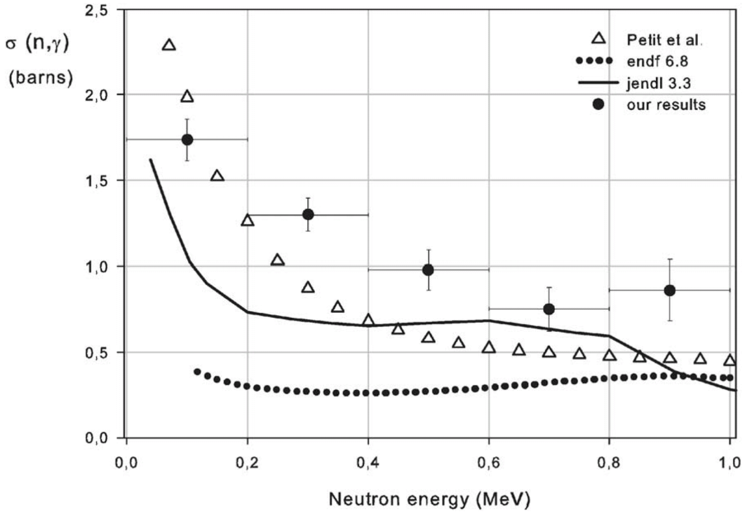

Figure 49: ^{233}Pa(n,γ) cross section from two separate Surrogate experiments, compared to evaluations. The triangles show the result of a Hauser-Feshbach calculation with parameters adjusted to fit the ^{233}Pa(n,f) cross section that was obtained from a ^{232}Th(^{3}He,pf) Surrogate experiment. The large, filled circles show the results of a Weisskopf-Ewing analysis of a ^{232}Th(^{3}He,pγ) Surrogate measurement. The solid and dotted curves show prior JENDL3.3 and ENDF/B-VI.6 results. Figure taken from Ref. [18].

The second experiment was specfically designed to determine the ^{233}Pa(n,γ) cross section. Boyer *et al.* [18] measured p-γ coincidence probabilities in a ^{232}Th(^{3}He,pγ) experiment with a 24-MeV ^{3}He beam at the IPN Orsay Tandem facility. Their experimental setup included four liquid scintillator C_6D_6 detectors and four Si telescopes. Details of the experiment are given in Ref. [18]. The ^{233}Pa(n,γ) result from this experiment is indicated in Figure 49 as well.

Given the simulations shown in Section 6.2, as well as similar calculations for Zr [51] and Gd [83], one might expect the cross section extracted from a Weisskopf-Ewing analysis of the Surrogate (^{3}He,pγ) data to be too large. As there are no direct ^{233}Pa(n,γ) cross section measurements, this hypothesis can currently not be tested. However, it is interesting to note that four of the five data points from the (^{3}He,pγ) experiment (the four points above $E_n = 0.2$ MeV) are about 50% higher than the (n,γ) cross section that was calculated by adjusting Hauser-Feshbach parameters to reproduce the (n,f) cross section obtained from the (^{3}He,pf) experiment.

STARS/LiBerACE study of the ^{235}U(n,γ) cross section using (α, α'). Bernstein *et al.* [15] employed inelastic scattering with 55-MeV α-particles as a Surrogate mechanism to produce the ^{238}U compound nucleus. Both α-fission and α-γ coincidence probabilities were measured. This made it possible to extract the ^{237}U(n,γ) cross section relative to the ^{237}U(n,f) cross section, using an Internal Ratio analysis and the ^{237}U(n,f) cross section determined by Burke *et al.* [29] (for information on the measurement of the ^{237}U(n,f) cross section, see Section 4.3.1 and Fig. 30). A set of characteristic γ-ray transitions was used to construct the total γ-channel probability, relative to the fission probability. Since the number of α-singles events was also determined, Bernstein *et al.* were also able to determine the ^{237}U(n,γ) cross section from a Weisskopf-Ewing analysis of the data. The results of both procedures are compared to each other in the top panel of Fig. 50; a comparison to several evaluations is found in the bottom panel of the same figure. For this case, as for the ^{233}Pa(n,γ) case, there exists no direct cross section measurement, so assessing the success of employing the Weisskopf-Ewing and Ratio approximations is difficult. However, the extracted cross sections are larger than the evaluations, by a factor of about 2-4, for energies below 1 MeV. While they seem to converge (within the experimental error bars) to the evaluated values, the shape of the deduced cross section differs from the evaluations.

STARS/LiBerACE study of the ^{235}U(n,γ) cross section using (d,p). Allmond *et al.* [3] employed the (d,p) stripping reaction with 21-MeV deuterons on a ^{235}U target to produce the ^{236}U compound nucleus. Both p-fission and p-γ coincidence probabilities were measured, as the objective of the experiment was to extract the ^{235}U(n,γ) cross section from an Internal Surrogate Ratio analysis. A strong γ-ray transition in the γ-decay of the ^{236}U compound nucleus was selected in order to infer the probability of the γ-channel relative to the fission channel. The fraction of the γ-cascade that proceeds through the transition studied was estimated by investigating the decay of the compound nucleus from excitation energies slightly below the neutron separation threshold and was accounted for in the ISR analysis.

The resulting ^{235}U(n,γ) cross section is in rough agreement with the ENDF/B-VII evaluation, as is shown in Fig. 51. The authors estimate the average deviation of the cross section to be somewhat less than 25%.

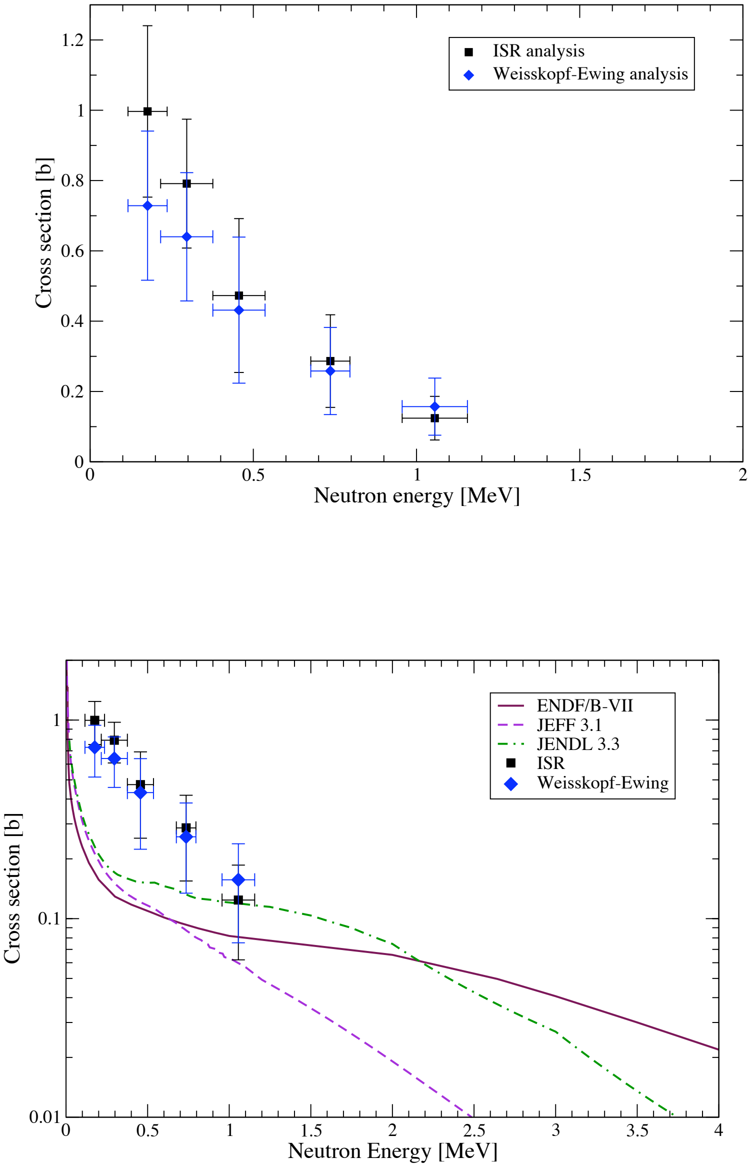

Figure 50: ^{237}U(n,γ) cross section extracted from two different analysis of a Surrogate ^{238}U(α, α') experiment, compared to evaluations. The top panel shows the ^{237}U(n,γ) cross section deduced using the Internal Surrogate Ratio (black squares) and (absolute) Weisskopf-Ewing approach (blue diamonds). The bottom panel shows a comparison of the extracted cross sections to various evaluations. Experimental data from L.A. Bernstein [14], evaluations from the NNDC web site (http://www.nndc.bnl.gov/).

Surrogate measurements of (n,γ) cross sections in other mass regions Several attempts have been made to determine (n,γ) cross sections for non-fissioning nuclei via the Surrogate approach. Hatarik *et al.* [59] studied the ^{171,173}Yb(n,γ) reactions using (d,pγ) as a Surrogate reaction mechanism. Goldblum *et al.* [56] investigated the ^{171}Yb(n,γ) cross section with (^{3}He,^{3}He$'$) and (^{3}He,α)Surrogate reactions. Scielzo *et al.* [83] carried out inelastic proton scattering experiments on $154, 156, 158$Gd targets in order to investigate the validity

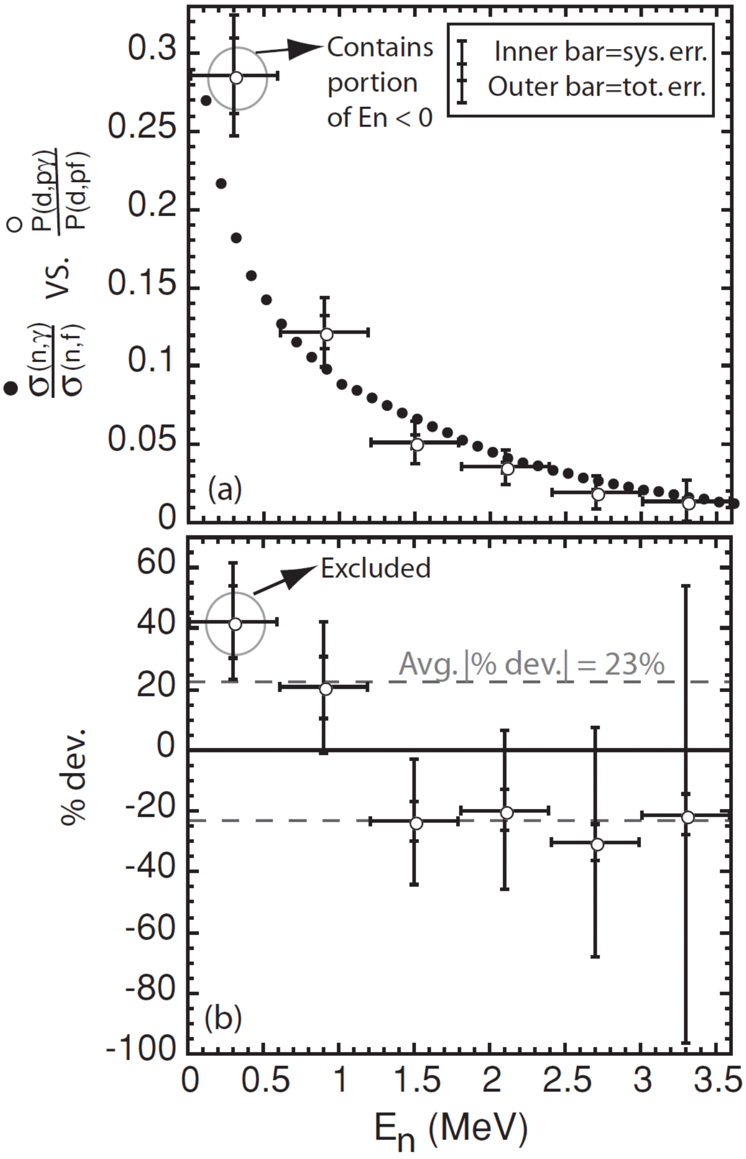

Figure 51: ^{235}U(n,γ) cross section extracted from an Internal Ratio analysis of a Surrogate ^{235}U(d,p) experiment. The top panel shows a comparison of the measured coincidence ratio $P_{(d,p),\gamma}(E)$ / $P_{(d,p),f}(E)$, compared to the ratio $\sigma[^{235}$U(n,γ)] / $\sigma[^{235}$U(n,f)] of cross sections from the ENDF/B-VII evaluation. The bottom panel gives the difference between these ratios as a percentage. Figure taken from Allmond *et al.* [3].

and limitations of the Weisskopf-Ewing and ESR approaches. The results of the latter work is in line with what we observed in Sections 6.2–6.3; the cross sections extracted from the Weisskopf-Ewing and ESR analyses were not found to be in satisfactory agreement with directly-measured reference results.

6.5 Comments on (n,γ) cross sections

Both the calculations presented in this section and the experiments summarized here illustrate that (n,γ) cross sections determined from Surrogate measurements are very sensitive to the spin-pairty distribution of the decaying compound nucleus. Consequently, employing the Weisskopf-Ewing approximation, or Ratio analyses based on the approximate validity of the Weisskopf-Ewing limit, will not lead to reliable cross sections.

While the strong dependence of the observables used to tag the exit channel makes extracting (n,γ) cross sections from Surrogate measurements very challenging, it also provides valuable information. In particular, simultaneously measuring the yields of several γ-ray transitions of a decaying compound nucleus can provide signatures for the spin-parity distribution of the compound nucleus prior to decay. An example for this is shown in Fig. 52, where we have plotted the relative yields of several ground band transitions for ^{236}U, for the four schematic $J\pi$ distributions considered in Sections 6.2 and 6.3. We find that different $J\pi$ distributions lead to markedly different relative γ-ray yields. These observables can be employed to test and constrain theories that predict compound nucleus spin-parity distributions. Relative γ-ray yields for the decay of even-even gadolinium nuclei have recently been measured [83] and methods are being developed to use this information in order to improve the (n,γ) cross sections determined from Surrogate experiments. This will also help to improve the accuracy of low-energy fission cross sections extracted from Surrogate experiments.

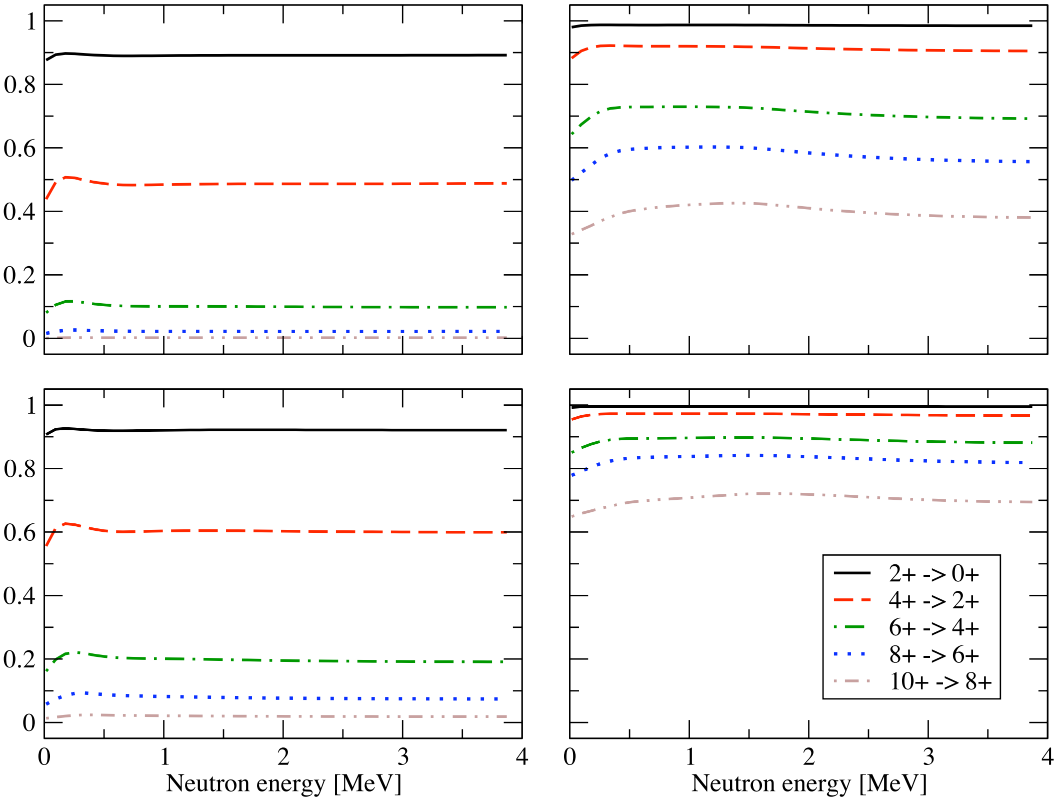

Figure 52: Ratio of the yields of various gammas in the ground-state band of ^{236}U to the total production of ^{236}U for the schematic spin distributions studied in Sections 6.2 and 6.3. The two graphs on the left show results for the ABB (top panel) and D (bottom panel) distributions, and the two graphs on the right show the results for the A (top panel) and B (bottom panel) distributions.

7 Moving beyond current approximations

7.1 Spin-parity mismatch and related challenges

The most significant limitation of the method at this time is the fact that the Surrogate reaction populates the states in the intermediate nucleus differently than the desired channel, i.e. the weights $F_\delta^{CN}(E_{ex}, J, \pi)$ by which the decay probabilities $G_\chi^{CN}(E_{ex}, J, \pi)$ are multiplied in Eq. 2 are different from the relative formation cross sections $f_\alpha^{CN}(E_{ex}, J, \pi)$ $= \sigma_\alpha^{CN}(E_{ex}, J, \pi)/\sum_{J'\pi'} \sigma_\alpha^{CN}(E_{ex}, J', \pi')$ of Eq. 31, and depend on the direct reaction under consideration. This diffference is often referred to as the *spin-parity population mismatch.*

Currently, our understanding of the spin-parity mismatch and its effect on cross sections extracted from Surrogate experiments is quite incomplete. When optical-model potentials are available, one can obtain fairly reliable spin-parity information for the desired reaction from optical-model calculations. However, no tools are currently available for formulating accurate predictions of the spin-parity distributions for compound nuclei produced in Surrogate reactions. This situation does not merely reflect an absence of useful reaction codes, but points to an incomplete picture of the reaction mechanisms that produce the compound nucleus in a Surrogate reaction.

Predicting the spin-parity distribution for a compound nucleus produced in a Surrogate reaction requires a careful consideration of the reaction mechanisms that are involved in the formation of the compound nucleus. In the absence of width fluctuation corrections, the challenge of describing the relevant reaction mechanisms can be divided into two separate problems:

1) the formation of a highly-excited nucleus in a direct reaction, and
2) the damping of the excited states into the compound nucleus.

The separation of the Surrogate reaction into two separate sub-processes is somewhat artificial, but may be useful conceptually. The Surrogate reaction is viewed as a mechanism that produces initially a highly-excited intermediate system. The system might consist, for instance, of a nucleon N (stripped from the projectile d in the reaction $d + D \rightarrow b + B^*$) plus the Surrogate target nucleus D. For the Surrogate approach to be valid, the $D + N$ system must subsequently fuse to produce the compound nucleus B^*, the decay of which one is interested in measuring. Decay of the intermediate system ($D + N$ in the example) by particle emission prior to reaching the equilibrated stage would invalidate the Surrogate approach, since the measured coincidence probabilities would no longer be associated with the decay of the compound nucleus of interest, B^*. It is thus important to understand how the configurations that are produced in the initial step evolve. Specifically, one needs to determine the probability for forming the desired compound nucleus B^*.

The above considerations do not include correlations between the incident and outgoing reaction channels, which in principle affect both the desired and Surrogate reactions. For the desired reaction, Eq. 31, these correlations can be taken into account formally by including width fluctuation corrections [53], while a similar simple solution is not readily available for the Hauser-Feshbach-type expression describing the Surrogate reaction, Eq. 2. Therefore, a comprehensive theoretical treatment of the Surrogate method also requires an assessment of the importance of

3) width fluctuation correlations to the Surrogate reaction formalism and possibly an extension of the formalism to account for these correlations.

7.2 Addressing the theory challenges: present status

In this section, we summarize some of the work done to address the challenges discussed above. A more detailed discussion of the developments needed for each reaction mechanism considered (pickup, stripping, inelastic scattering, etc.) will be given in the next section, Sec. 7.3.

7.2.1 Direct reaction to the continuum

Addressing the first problem necessitates developing a quantitative description of the direct-reaction process that allows for a prediction of the spin-parity distribution in the highly-excited intermediate nucleus, immediately following the direct reaction. Such a description is nontrivial since it requires a framework for calculating cross sections of different reactions (stripping, pick-up, charge exchange, and inelastic scattering) to continuum states, for a variety of projectiles (p, d, t, α, etc.) and targets (spherical, deformed, and transitional).

First steps towards predicting the spin-parity population following the initial step of a Surrogate reaction were taken by Andersen *et al.* [4], Back *et al.* [7], and, more recently, by Younes and Britt [99, 100]. These authors employed simple transfer calculations to estimate compound-nucleus spin-parity distributions following various stripping reactions on actinide targets. They neglected the possibility that the intermediate nucleus might decay prior to reaching equilibrium and took the resulting spin-parity distributions to be representative of those present in the compound nucleus created in the Surrogate reaction of interest. Younes and Britt used the calculated distributions to re-analyze Surrogate (t,pf), (^{3}He,df), and (^{3}He,tf) fission-correlation measurements from the 1970s [33, 25] in order to extract (n,f) cross sections. Compared to earlier Surrogate analyses of the data, which ignored spin effects, their estimated (n,f) cross sections showed significantly improved agreement with evaluated results, where available. Their findings underscore the importance of accounting for the spin-parity mismatch between the desired and Surrogate reactions.

Inelastic scattering is potentially an important Surrogate mechanism for determining cross sections relevant to the astrophysical s process: (n,γ) reactions on unstable s-process branch-point nuclei proceed through compound states of nuclei with stable ground states. Consequently, the compound states of interest can in principle be produced via an inelastic scattering reaction on a stable target. In Ref. [40], a simple model for predicting the spin-parity distribution of ^{90}Zr, produced via inelastic α scattering, was developed. The model was based on the assumption that the inelastic scattering cross section for a (near-)spherical nucleus can be approximately expressed in terms of cross sections for producing uncorrelated particle-hole excitations in the target nucleus. Information on such $J\pi$ distributions, their angular and energy dependence, is important for planning and interpreting Surrogate experiments.

7.2.2 Damping into the compound nucleus

The second problem to be addressed is associated with the evolution of the highly-excited intermediate system that is created in the initial stage of the Surrogate reaction. The assumption that a compound (i.e. equilibrated) nucleus is formed is central to the Surrogate method. Rapid decay of the intermediate configuration before a compound nucleus can be formed, which would invalidate the Surrogate analysis, needs to be excluded experimentally, or accounted for theoretically[2].

New theory development is needed in order to determine to what extent those configurations that are produced in the initial step of a Surrogate reaction damp into a compound state. The competition between particle emission and equilibration is expected to not only depend on the direct reaction and energy chosen, but also on the spin and parity of the intermediate nucleus.

First steps towards understanding the evolution of the intermediate, highly-excited, system following a direct reaction have been taken by F.S. Dietrich. In Ref. [37], he considered the case of direct-semidirect neutron capture, employing the formalism developed by Parker *et al.* [77]. While direct (or direct-semidirect) nucleon capture is not typically considered in practical applications of the Surrogate method, the insights gained from studying this process have implications for the Surrogate approach. In particular, there is an obvious connection between direct radiative neutron capture to a highly-excited region of the intermediate nucleus and the deposition of a neutron to that region via a direct (d,p) reaction. In the former case, the energy of the γ-ray determines the excitation energy of the intermediate system, while in the latter case, the outgoing proton can be used to tag the energy of the nucleus. The formalism developed in Ref. [77] allows one to calculate the cross sections for both capture to unbound states (and thus for escape of the nucleon from the combined target-plus-nucleon system immediately after capture) and capture followed by absorption via an imaginary potential (which represents the formation of a compound nucleus). In Ref. [37], Dietrich studies the evolution of the ^{90}Y* system following radiative capture of 19.6 MeV neutrons on ^{89}Y. He finds that the reaction fails to form a compound nucleus at the 10%-15% level. Furthermore, he demonstrates that the probability for forming a compound nucleus depends on both the energy of the intermediate system, and on the angular-momentum distribution present following the direct reaction. These findings underscore the need to carefully study the competition between particle emission and equilibration following other direct reactions, in particular one-neutron stripping reactions, such as (d,p).

---

[2] This process should not be confused with pre-equilibrium emission of particles in the desired reaction, $a + A \to c + C$; contributions from the latter cannot be determined via the Surrogate approach and need to be calculated separately and added to the desired cross section.

7.2.3 Width fluctuation corrections

Incorporating width fluctuation correlations will introduce additional complications. In the desired reaction, they are known to enhance the elastic scattering cross section and reduce the inelastic and reaction cross sections, although this depletion rarely exceeds 10-20% (even at energies below approximately 2 MeV) and becomes negligible as the excitation energy of the compound nucleus increases [53]. An examination of the role of width fluctuation correlations for Surrogate reactions has not yet been undertaken, but should be part of a comprehensive investigation of the formalism associated with the Surrogate approach.

7.3 Addressing the challenges for each Surrogate reaction mechanism

Often, a desired compound nucleus can be reached by several possible surrogate reactions, but these are not all equivalent when it comes to extracting the desired reaction rate from the cross sections observed in the surrogate reaction. In this subsection, therefore, we review the different kinds of reaction mechanisms that could be used in surrogate reactions, and discuss the strengths and weaknesses of each. We see how each reaction mechanism is capable of populating continuum energies for each spin and parity $J\pi$ of the intermediate nucleus left by the direct reaction, and also some considerations for the probability with which these intermediate states damps into a statistical average of compound nucleus states.

7.3.1 Reaction theory requirements

There are necessarily different experimental advantages of various surrogate reactions. It is always necessary reach the desired compound nucleus with available beams and targets, and it is necessary to measure the energies E_{ex} and of all outgoing particles x from reactions leading up to the formation of the compound nucleus. The measurements of these reactions must be kinematically complete, and hence also include angles θ_x, if we are to reconstruct the excitation energy E^* of the compound nuclear states that have been produced by $E_{ex} = E_{\text{tot}} - E_x$.

If a reaction mechanism is to be analyzed more accurately than by the Weisskopf-Ewing approximation, it is also necessary to have a reaction theory to predict the spin and parity distributions of the compound nuclei produced. That is, it should give us the cross sections $\sigma_{\text{CN}}(J^\pi, \theta_x, E_{ex})$ as a function of the momenta of the outgoing particle x. In terms of these cross sections, the surrogate weights are the CN formation probabilities

$$F_\delta^{CN}(E_{ex}, J, \pi) = \frac{\sigma_{\text{CN}}(J^\pi, \theta_x, E_x)}{\sum_{J\pi} \sigma_{\text{CN}}(J^\pi, \theta_x, E_x)} \tag{28}$$

for each measured outgoing angle θ_x.

A reaction is only suitable from the theoretical point of view, therefore, when we have some reaction model for the surrogate reaction, and when also we have a good idea of the various optical potentials and effective nucleon-projectile interactions that enter into the reaction model. A ideal 'reaction model' should be specified in terms of some Hamiltonian describing the essential few degrees of freedom in the reaction, in such a way that multi-step corrections become well defined within the model. The higher-order effects of target collective rotational or vibrational excitations should also be clear from the model, and the collective strengths known, so that these effects can be calculated if desired. Optical potentials for nucleons may be estimated from regional or global parameterizations, and ideally these should be checked by elastic scattering measurements at the proposed energies of the surrogate reaction beam.

By the 'effective nucleon-projectile interactions' needed, we refer for example to the np vertex function within the projectile in transfer reactions induced by a deuteron, or to the effective interaction between the projectile and a target nucleon that would create a particle-hole excitation in the target. The transfer vertex functions are well known for deuterons and other s-shell projectiles. The effective interactions for particle-hole creation have in general an energy- and density-dependence, but that is not so well determined. The relative cross sections for different excited states are probably well predicted, but the absolute magnitudes of cross sections should be checked where possible by comparison with other inelastic models, such as collective models.

In the following paragraphs, we discuss pickup, inelastic, transfer, charge-exchange and two-nucleon transfer reactions. This order is chosen as that from the simpler to the more complicated, measured both by the amount of detailed target structure required, and by the complexity of the required reaction model. In each case, we consider the kind of surrogate reaction to produce excited states in the target that have sufficient excitation energy to give some neutron escape width: just those states as if produced by a low-energy incident neutron. (If a typical target has a neutron separation energy of say 8 MeV, then the Fermi level would be at $E_F = -8$ MeV, and excitation energies of 8–9 MeV would be required to correspond to a neutron energy between 0 and 1 MeV of energy.) We also discuss in each case how the CN spin-parity distribution is influenced by the shell structures of the target at various binding energies.

7.3.2 Pickup reactions

In pickup reactions, a nucleon deeply bound in the target is removed by the projectile, and is carried away in a bound ejectile state. For example, beams of ^{3}He incident on a ^{238}U target may pick up a neutron from the target to form an outgoing α particle, and leave an excited ^{237}U* nucleus. If this reaction is to be a surrogate for n + ^{236}U, then, as $S_n \approx 6$ MeV, the excitation energy in ^{237}U* needs to be at least 6–7 MeV. That requires the hole state created by the pickup reaction to have a single-particle energy more than 12 MeV bound in the mean field of the target. The spin and parities J^π of the resulting ^{237}U* CN states are therefore determined by the kind of shell structure we find in the target at ≈ -12 MeV. That structure may be estimated by filling neutrons in a Hartree-Fock or Woods-Saxon mean field. The actinide and many rare-earth nuclei are well deformed, so it would be better, if we know the target deformation, to fill the neutrons within a deformed mean field. The binding energies E_i in a mean field, whether spherical or deformed, do not however take into account the residual interactions between the nucleons. Those residual interactions give a finite lifetime to any hole states, and that lifetime is shorter, the deeper the hole state. These lifetimes translate into non-zero widths Γ_s for the hole states, and hence the mean-field eigenstates should be smoothed out by convolution with (e.g.) a Lorentzian form with that width. This width is also called the 'spreading width', since it describes how the initial pure-single-particle hole states are 'spread out' into the much more complicated CN states.

In practice [88], we use the theory of Brown and Rho [26], which estimates these widths in terms of the energy distance e from the Fermi level as $\Gamma_s(e) = 24e^2/(e^2 + 500)$ for Γ_s and e in MeV. The Lorentzian spreading function is

$$L(E - E_i, \Gamma_s) = \frac{1}{2\pi} \frac{\Gamma_s/2}{(E - E_i)^2 + \Gamma_s^2/4} \ . \tag{29}$$

One advantage of pickup reactions are that the initial states produced in such reactions consist entirely of bound particle states, so there is no significant escape of neutrons before the compound nucleus is formed. Another is that the reaction does not depend on the details of correlations in excited states of the target. And finally, deep hole energies mean that there is reasonable to good energy matching in (^{3}He,α) pickup reactions, as the neutron separation energies in the α particle is 20.6 MeV. Deep hole states can only weakly be created in (p,d) reactions, by contrast, as there the separation energy is only 2.22 MeV.

7.3.3 Inelastic reactions

In an inelastic reaction processes, nucleons in the target are excited from occupied to unoccupied states: from below the Fermi level to above it, either to unoccupied bound states or to continuum states (where the nucleons may escape). For example, beams of protons may excite neutrons in ^{156}Dy* by at least 10 MeV, so that compound nucleus states are produced which have some probability of neutron escape, and hence enable predictions to be made for the desired reaction n + ^{155}Dy. The incident proton could have been replaced by an incident α-particle: the reaction dynamics would be somewhat changed, but sets of excited states would be produced over similar ranges of energy.

The incident projectile may excite rotational bands or vibrational phonon states, but, especially for light projectiles, this is not sufficient to reach 10 MeV of excitation. Instead, we rely on the projectile exciting particle-hole pairs in the target. In order to reach $E^* = 10-11$ MeV, the ph pairs must typically have their holes at deep energies $E_h \lesssim E_F - 5$ MeV, and particles at the higher energies $E_p \gtrsim E_F + 5$ MeV, so that $E^* \equiv E_p - E_h > 10$ MeV. In general the particle states at $E_p \approx E_F + 5$ MeV will still be bound, so again here here is no significant escape of neutrons before the compound nucleus is formed. The spin of the resulting compound nuclei will be the vector sum of $[I_h \otimes I_p]_J$ of the hole and particle spin states. Using spinless α-particle projectiles would imply that only natural-parity states $(-1)^J = \pi$ would be excited, whereas using proton projectiles allows the proton spin-dependent forces to also excit non-natural parity states, albeit more weakly.

In nature, inelastic excitations are not individual particle-hole pairs, but linear combinations of all possible ph combinations that can couple to a given spin and parity of the excited nuclear state. Individual ph excitations may be calculated using uncorrelated levels in a spherical or (better) a deformed mean field, but to describe all the more realistic linear combinations at least a RPA (Random Phase Approximation) excitation model will be needed. The RPA theory is designed to describe inelastic excitations up towards 100 MeV as general superpositions of all particle-hole excitations of an initial mean-field structure. The RPA calculations may use a spherical potential, or better a deformed potential; they may use harmonic-oscillator basis functions, or better the eigenstates in a box of some radius larger than the nucleus; they may be built on Hartree-Fock mean fields, or better (as QRPA) on HFB structures that include the effects of pairing on the mean field. These successive models have progressively higher level densities, and hence move the explicit nuclear descriptions from direct reactions to a little more towards a realistic level density. At present, we have some spherical RPA results, and a code from Chapel Hill [87] which calculates QRPA excitations of nuclei described by spherical mean field potentials. In all cases, energy spreading using a Lorentzian spreading function of Eq. (29) will be be necessary.

7.3.4 Stripping (transfer) reactions

Transfer reactions which strip a neutron from a projectile can add that neutron onto the target nucleus. For example we may populate states in ^{240}Pu* by the ^{239}Pu(d,p) reaction. As well as going into the unoccupied bound states of the target (as transfer reactions are traditionally performed), the neutron may now also be directly placed in a continuum state at exactly the low energies required to simulate the desired effects of an incident neutron. This transfer to the continuum is similar in mechanism to the well-established transfer reactions, and may be treated initially by the same DWBA method used for bound states, but more care is needed to obtain converged results because the continuum wave functions do not strictly have a square norm: either a continuum bins method [82] or complex contour integrations [94] will be necessary for convergence. Transfers to narrow resonances may be described as transfers to the pseudostates obtained by removing the exterior wave function, but for surrogate reactions we will also have to model transfers to the non-resonant continuum.

The reaction model for deuteron stripping is well defined in terms of the Hamiltonian for a three-body model of a proton, a neutron, and the target nucleus. Higher-order effects such as deuteron breakup, and couplings between transfer states can therefore be modeled easily by currently available reaction codes. We may also generalize the model to include rotational excited states of the core, and the XCDCC model of Summers et al [86, 85], though computationally more demanding, may be useful in this case.

The spin-parity structure therefore depends on the shell structure of the target in the energy range for unbound neutron states: this is at considerably higher energies in the mean field compared with the pickup and inelastic reactions described above. No structure information about occupied states in the target is needed to model these transfer reactions, in part because the stripping reaction is gentle with respect to target. We may think that neutron-transfer reactions are very much closer to being direct reactions than CN reactions. A consequence of this is that the neutron may well escape from the target, even before the CN states are equilibrated. This is the problem that damping into the compound nucleus will usually be less than 100%. In these reactions, we have therefore to consider the competition between the equilibration (spreading) of the neutron and its escape into the breakup phase space. This is identically the problem of *partial fusion*, for which several models have been proposed: by Udagawa & Tamura[91, 92], of Kerman & McVoy [67] (based on [66]), and of Baur & Trautman [12], as well as a proposal by one of us [89]. These models, however, do not all give the same results, and none have been systematically tested.

The partial fusion problem arises when there is a coincidence of absorption of one part of a composite system and the need for quantum-mechanical scattering amplitudes for another part. A theoretical model of few-body dynamics needs to be able to distinguish complete and no fusion from incomplete fusion. To do this, it is clear that we need to follow correlations after breakup, so we need either time-dependent or multistep breakup calculations as a starting point. The need is still, after absorption of one fragment, to follow the evolution of remaining part x, in order to see whether it escapes (yielding incomplete fusion) or fuses with the target (yielding complete fusion). When it may escape, we want a model to predict

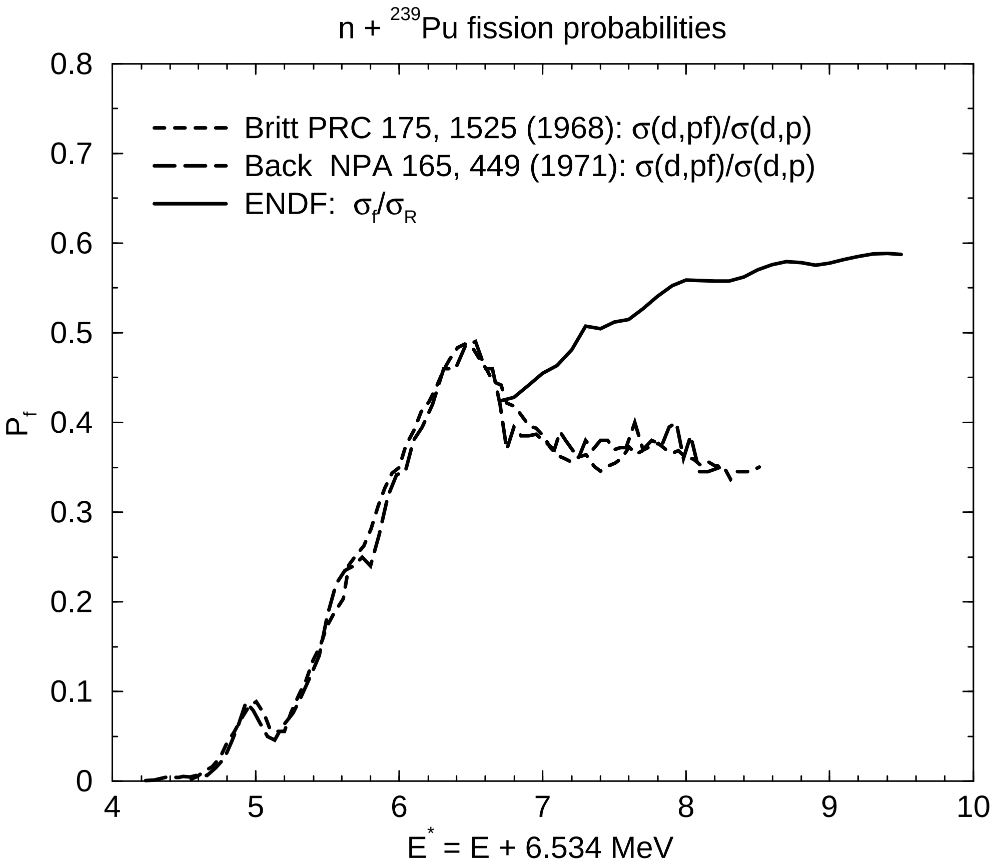

Figure 53: Fission probabilities for ^{239}Pu as extracted from (d,p) experiments, compared with that in the ENDF evaluation from direct measurements, as a function of excitation energy in ^{240}Pu.

its cross section distribution as a function of θ_x. We see from Figure 53, for example, that using fission probabilities from ^{239}Pu(d,pf) does not give correct (n,f) cross sections when it was assumed that all (d,p) transfer reactions lead to compound nucleus formation [5, 23]. The results can differ by up to 40% even at 2 MeV of equivalent neutron energy, and this is precisely the kind and direction of difference we expect to correct with a good theory of partial fusion. Similar fractions have been calculated by Dietrich [37], as described in section 7.2.2. To calculate the damping in our surrogate reactions, these escape fractions will have to be evaluated for each outgoing angle θ_x, a project we presently have underway.

7.3.5 Charge-exchange reactions

Reactions such as (^{3}He,t) may be used to replace a neutron in the target by a proton, most directly by pion transfer. For example, excited states in ^{240}Am* may be produced by the reaction ^{240}Pu(^{3}He,t)^{240}Am*, in order to indirectly measure reactions produced by neutrons incident on ^{239}Am. This approach has been used [33] to predict (n,f) cross sections. These early results, however, used the Weisskopf-Ewing approximation, without the effect of any spin-parity distribution.

These spin-parity distributions from charge-exchange reactions are more complicated to calculate than from the previously discussed inelastic and transfer processes, as the needed effective interaction has many components [76]. The charge-exchange cross section for light nuclei is also known to depend on a large number of shell-model matrix elements that all contribute coherently [58], and for heavy nuclei we would need at least (Q)RPA models [87] for all the particle-hole excited states that would be produced. In both cases there are as yet no implemented reaction models to predict the spin distributions. In addition to the above matrix elements for the one-step process, at beam energies below 50 MeV/u we should also include two-step transfer contributions. For the (^{3}He,t) reactions, these two-step routes would be via (^{3}He,d,t) and (^{3}He,α,t). Calculation of these routes would require knowledge of one-nucleon overlap functions for the several neighboring nuclei.

7.3.6 Two-nucleon transfer reactions

Lastly, two-nucleon transfer may be used to travel further from the target nucleus in the Segré chart. For example, the fission cross section for neutrons incident on ^{239}U has been extracted by using a (t,p) reaction to transfer two neutrons from ^{238}U to make excited states in ^{240}U* [100]. The (^{18}O,^{16}O) process has also been used [?] for the same purpose.

In principle, all the previous comments about transfer reactions apply here also, because this reaction can be modeled as a di-neutron transfer, but with additional complications since the di-neutron is not strictly a particle. Transfer cross sections are small ($\approx 1-10$ mb), so two-neutron transfers are even smaller ($\approx 10-100$ μb). We would need to populate continuum states with excitation energies of the order of 16 MeV above ground state in the ^{240}U case, and we should calculate the escape probabilities again for the neutrons appearing as breakup rather than in compound nuclei after their transfer. We should also calculate two-step contributions from sequential transfers, the (t,d,p) or (^{18}O,^{17}O,^{16}O) routes, which again add coherently to the direct 'simultaneous' transfer matrix element.

The pair of transferred nucleons keeps (to first order) the same configuration that they have in the projectile: the same relative angular momentum, and the same distribution of radial separations. This means that (t,p) reactions, for example, where initially the two neutrons are almost entirely in a singlet ^{1}S$_0$ state, only populate target states where they have the same relative motion. The angular momentum between the 2n and the target is not constrained, but, as in normal transfer reactions, may have any value as determined by the shell structure of the composite nucleus at the measured energies.

The reaction models for calculating nn, np or pp two-nucleon transfers are available in principle for both simultaneous and sequential transfers, as long as we have available some structure models to calculate the several one- and two-nucleon overlap functions. Some additional work, though, may be need to ensure convergence when we include continuum states as intermediates in the sequential transfer of the nucleons.

8 Summary and recommendations

Surrogate experiments carried out so far illustrate both the potential and the current limitations of the method. In this report, we have summarized the present status of the Surrogate method for applications involving neutron-induced reactions on actinide targets. We showed successful applications from the early Surrogate experiments, carried out at Los Alamos in the 1970s, and more recent experiments carried out by the CENBG group in France and the STARS/LiBerACE collaboration led by scientists from LLNL and LBNL. In particular, we have seen that (n,f) cross sections extracted from Surrogate measurement show reasonable agreement with directly-measured cross sections for neutron energies above 1-2 MeV, can help to distinguish discrepancies between different direct measurements and extend known cross sections to energy regimes for which no data exist. Moreover, they are able to provide cross sections for reactions that cannot be measured directly.

We have also discussed the limitations of the Surrogate method as it is presently implemented. Almost all applications of the method so far have relied on approximation schemes which ignore the fact that the compound nucleus that is produced in the Surrogate reaction is characterized by a spin-parity distribution that can be very different from the spin-parity distribution of the compound nucleus occurring in the desired, neutron-induced reaction. Ignoring this "spin-parity mismatch" is not only formally incorrect, it also has practical implications: it reduces the accuracy of the cross sections extracted from Surrogate measurements and it limits the reach of the Surrogate approach. We have illustrated this with examples of measured low-energy (n,f) cross sections and theoretical sensitivity studies. We have also shown the improvements that can be attained when correcting for the spin-parity mismatch. We have furthermore demonstrated that (n,γ) cross sections extracted from Surrogate experiments tend to be much more sensitive to the spin-parity distribution of the compound nucleus than (n,f) cross sections. The calculations carried out here, and available Surrogate data indicate that it is crucially important to correct for the spin-parity mismatch when considering (n,γ) reactions.

A comprehensive theoretical treatment of the Surrogate approach involves a description of direct reactions that populate highly-excited, unbound states, the damping of these doorway states into more complicated configurations that lead to a compound nucleus (or non-equilibrium particle emission), the dependence and influence of these processes on angular momentum, parity, and energy, and possible width fluctuation corrections to the standard Hauser-Feshbach-type formalism. We have outlined the steps that will improve the accuracy and reliability of the Surrogate approach and extend its applicability to reactions that cannot be approached with the present implementation of the method. Renewed interest in the Surrogate method over the last few years has led to significant improvements in our understanding of the method as well as to a deeper appreciation of what remains to be done. Efforts to move beyond the present limitations have shown promise. Some of the recent accomplishments, outstanding problems, and recommendations are the following:

- Recent experiments have been largely devoted to fission. The Weisskopf-Ewing method appears to be satisfactory above 1 to 2 MeV, but a full Hauser-Feshbach treatment may be needed at lower energies. This is confirmed by the modeling work of Younes and Britt [99, 100, 105], as well as the sensitivity studies carried out by Escher and Dietrich [43].

- The Surrogate Ratio method was originally introduced to mitigate experimental difficulties, but has since evolved into a practical approach for certain cross section measurements. Several variants of the Ratio method have been developed in recent years. The External Surrogate Ratio method is useful in reducing errors in certain cases when the conditions for validity of the Weisskopf-Ewing approximation are not well satisfied, as was shown through simulations [43, 42] and in benchmark experiments [69, 70]. The efficacy of the other variants (Internal Surrogate Ratio, etc.) has not been sufficiently established, as was discussed in the present report.

- In order to move beyond the Weisskopf-Ewing and Ratio approximations, a modeling approach can be introduced, which includes descriptions of both the formation of the compound nucleus in the Surrogate reaction and of its decay. In this context, information on compound-nucleus $J\pi$ distributions prior to decay is crucial. This must be supplied by suitable direct-reaction calculations leading to the excitation of high-lying final states. Developing reliable calculations for the wide variety of applicable direct reactions (stripping, pickup, inelastic scattering, and charge exchange) is a challenge for theory. Steps for developing a theoretical treatment of the Surrogate approach have been outlined in the present report. It is crucial that the theory developments be accompanied by suitable experiments that test their predictions.

- Yields of low-lying γ's following γ cascades de-exciting high-lying compound states can provide useful information on $J\pi$ distributions to supplement and test the results of direct-reaction calculations. This requires an increased focus on modeling γ cascades for selected test cases, preferably starting with non-fissioning nuclei in order to avoid uncertainties associated with the fission models needed otherwise. Efforts are presently underway to extract spin-parity information from measured γ yields of decaying even-even rare-earth nuclei. Additional experiments will be necessary to gain confidence for modeling the decay of odd and odd-odd compound systems.

- Signatures of the spin-parity distribution of a compound nucleus prior to decay by fission may possibly be found in measured fission-fragment anisotropies. The theoretical description of the anisotropy and its dependence on the $J\pi$ distribution needs to be further developed and experimentally tested.

- As shown in the present report, (n,γ) cross sections extracted from Surrogate experiments are very sensitive to the spin-parity distribution of the compound nucleus; Weisskopf-Ewing or Ratio analyses of the measurements do not provide sufficiently accurate cross section results. Further theory developments, in particular the prediction of $J\pi$ distributions following the Surrogate reaction, and proper modeling of the γ cascades involved, are needed, and should be accompanied by Surrogate measurements of (n, γ) reactions, for both spherical and deformed nuclei. Such measurements are important for understanding the limits of the surrogate-reaction technique, in particular for low incident neutron energies. Successful reproduction of known (n,γ) cross sections will also give confidence when extracting cross sections for other mechanisms of interest, such as (n,p) reactions.

- The assumption the the direct-reaction process in a given Surrogate experiment leads to a fully-equilibrated compound nucleus is not necessarily correct and needs to be checked by appropriate calculations. For example, a neutron deposited in the target nucleus at sufficiently high excitation energies by a (d,p) reaction may be emitted into the continuum before the compound nucleus is formed. This has not been properly accounted for in past applications of the method, but can have significant effects on the cross sections extracted from Surrogate measurements, as explained in the present report. New theory developments, which have recently been initiated at LLNL, have to be extended to properly address this issue. This is particularly important for (d,p) reactions, which are clearly affected by this "escape prior to equilibration". As inverse-kinematics (d,p) experiments with radioactive beams can provide access to isotopes a few units off the valley of stability, it becomes very relevant to develop a theoretical effort, accompanied by suitable test experiments, to properly describe this competition between "damping into the compound nucleus" and "escape prior to equilibration".

Acknowledgments

This work performed under the auspices of the U.S. Department of Energy by Lawrence Livermore National Laboratory under contract DE-AC52-07NA27344.

A Appendix

A.1 Hauser-Feshbach formalism

The formalism appropriate for describing compound-nucleus reactions is the statistical Hauser-Feshbach theory (see, *e.g.*, chapter 10 of Ref. [52]). The average cross section per unit energy in the outgoing channel for reactions proceeding to an energy region in the final nucleus described by a level density is given by:

$$\frac{d\sigma^{HF}_{\alpha\chi}(E_a)}{dE_\chi} = \pi\lambdabar^2_\alpha \sum_{J\Pi} \omega^J_\alpha \sum_{lsl's'I'} \frac{T^J_{\alpha ls} T^J_{\chi l's'} \rho_{I'}(U')}{\sum'_{\chi''l''s''} T^J_{\chi''l''s''} + \sum_{\chi''l''s''I''} \int T^J_{\chi''l''s''}(E_{\chi''})\rho_{I''}(U'')dE_{\chi''}}. \tag{30}$$

Here α denotes the entrance channel $a + A$ and χ represents the relevant exit channel $c + C$, E_a is the kinetic energy of the projectile, and $\lambdabar_\alpha$ is the reduced wavelength in the incident channel (the inverse of the wave number). The spin of the incident particle is i, the target spin is I, the channel spin is $\vec{s} = \vec{\imath} + \vec{I}$, and the compound-nucleus angular momentum and parity are $J\pi$. The statistical-weight factor ω^J_α is $(2J + 1)/[(2i + 1)(2I + 1)]$. Similarly, the spin of the outgoing particle is i', the spin of the residual nucleus is I', and the channel spin for χ' is $\vec{s}' = \vec{\imath}' + \vec{I}'$. The transmission coefficients are written as $T^J_{\alpha ls}$ and $\rho_{I'}(U')$ denotes the density of levels of spin I' at excitation energy U' in the residual nucleus. All energetically possible final channels χ'' have to be taken into account, thus the denominator includes contributions from decays to discrete levels in the residual nuclei (given by the first sum in the denominator, $\sum'$) as well as contributions from decays to regions of high level density in the residual nuclei (given by the second sum in the denominator which involves an energy integral of transmission coefficients and level densities in the residual nuclei). In writing Eq. 30, we have suppressed the parity quantum number except for that of the compound nucleus. In fact, the level density depends in principle on parity (even though this dependence is weak in practice), and all sums over quantum numbers must respect parity conservation.

The above Hauser-Feshbach formula neglects correlations between the incident and outgoing reaction channels. These correlations can be taken into account formally by including width fluctuation corrections $W_{\alpha\chi}$ in the Hauser-Feshbach formula. The primary effect of the correlations is an enhancement of the elastic scattering cross section. Due to the requirement of flux conservation the inelastic and reaction cross sections are reduced, although this depletion rarely exceeds 10-20%, even at relatively low energies (below approximately 2 MeV). As the excitation energy of the compound nucleus increases and many reaction channels become available, the effect of the width fluctuations becomes quickly negligible for the non-elastic channels.

In the remainder of this report we will neglect the width fluctuation correlations. This then allows us rewrite the Hauser-Feshbach formula as:

$$\frac{d\sigma^{HF}_{\alpha\chi}(E_a)}{dE_\chi} = \sum_{J\Pi} \sigma^{CN}_\alpha(E_{ex}, J, \pi) G^{CN}_\chi(E_{ex}, J, \pi), \tag{31}$$

where $\sigma^{CN}(E_{ex}, J, \pi) = \sigma(a + A \rightarrow B^*)$ denotes the cross section for forming the compound nucleus at excitation energy E_{ex} with angular-momentum and parity quantum numbers $J\pi$ and $G_{\chi}^{CN}(E_{ex}, J, \pi)$ is the branching ratio for the decay of this compound state into the desired exit channel χ.

Although the cross section expressed in Eq. 31 is differential in the outgoing-channel energy, this is not actually the quantity of interest. For the (n,f) reaction, we need the cross section integrated over all final-state energies, which for fission are the energies of the transition states built on top of the fission barriers. For radiative capture, we need the integral over the energy spectrum of primary gamma rays emitted from the compound nucleus. Therefore, we need to integrate the quantity $\mathcal{G}_{\chi}^{CN}$ appearing on the right side of Eq. 31 over the energy E_{χ} of the final-state channel. In the main body of this report, we have assumed this has been done, and have therefore removed the differentiation with respect to energy on the left side of Eq. 31 and in all equations derived from it.

A.2 Dependence of fission probabilities on spin cutoff parameters

One of the requirements for the reduction of the Hauser-Feshbach expression to the Weisskopf-Ewing form is that the level densities in the decay channels of the compound nucleus must be proportional to $2J_c + 1$, where J_c is the spin of the residual nucleus. Thus for sufficiently high spins in the compound nucleus, the presence of the spin-cutoff factor in the level densities in principle invalidates the Weisskopf-Ewing assumption that branching ratios are independent of compound-nuclear spin J. In favorable cases the branching ratios may still be only weakly dependent on spin, but this cannot be guaranteed and must be studied on a case-by-case basis. In this Appendix we use a simple model to study the effects of the spin cutoff parameters on the fission probability and will show that the very significant spin dependence of the fission probabilities as seen (for example) in Fig. 26 is explained by the differences in the spin-cutoff parameters in the neutron and fission decay channels.

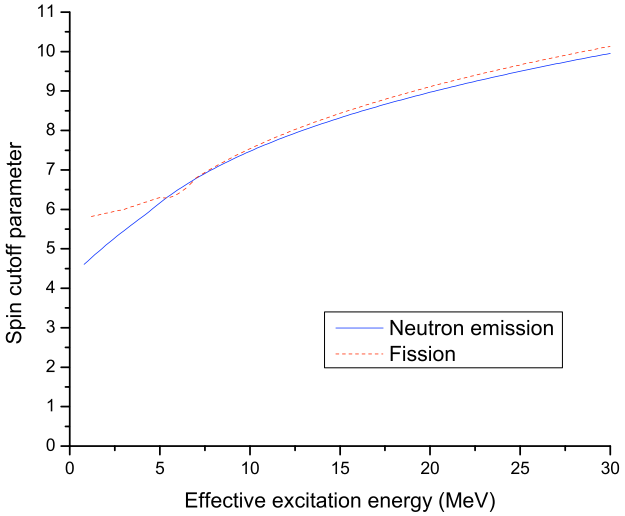

Figure 54: Spin cutoff parameters in the neutron and fission decays of the compound nucleus ^{236}U. The horizontal axis is either the excitation energy of the residual ^{235}U following neutron emission, or the energy above the fission barrier for the fission channel.

Fig. 54 shows the spin cutoff parameters in the neutron and fission channels that determine the fission probability of ^{236}U, and were used in the calculation of the first-chance portion of the “reference” fission cross section of ^{235}U(n,f) shown in Fig. 28. The effective excitation energy in Fig. 54 is the excitation energy of the residual ^{235}U following neutron emission, or the energy above the fission barrier for the fission channel. A double-humped barrier was used for the fission channel, and the energy dependence of the spin cutoff parameter was chosen to be the same for both barriers. The most significant difference between the two curves occurs below approximately 5 MeV, where the behavior of the spin cutoff parameter in the neutron channel was chosen to fit the average value of J^2 for the known discrete levels in the lower part of the ^{235}U level spectrum, whereas in the fission channel the values were chosen close to those used in the review article on the double-humped fission barrier of Bjørnholm and Lynn [17] (Table XXIX, page 875). The differences between the spin cutoff parameters in the competing neutron and fission channels in all other parts of the calculations in this report are very similar to those shown here for ^{236}U. The behavior of the spin cutoff parameters for gamma emission resembles that for neutron emission. However, for simplicity we will not include gamma emission in the following discussion.

We now make a rough model for the fission probability, assuming competition between fission and neutron emission from the compound nucleus. The numerator of the Hauser-Feshbach expression for this probability is an energy integral over the level density of the fission transition states; we neglect the discrete fission transition states near the barrier. Similarly, the neutron contribution to the Hauser-Feshbach denominator is represented by an integral over the level density in the residual nucleus. For neutron emission there are also sums over the orbital and spin angular momentum of the emitted neutron, but we make the simple (but crude) approximation that the average residual nuclear spin is the same as the compound spin J, and use this value in the spin factor in the level density. We then write an approximate value for the spin-dependent fission probability as

$$P_f(J) = \frac{c_f\ (2J+1)\exp\left[-\frac{(J+\frac{1}{2})^2}{2\sigma_f^2}\right]}{c_n\ (2J+1)\exp\left[-\frac{(J+\frac{1}{2})^2}{2\sigma_n^2}\right] + c_f\ (2J+1)\exp\left[-\frac{(J+\frac{1}{2})^2}{2\sigma_f^2}\right]}, \tag{32}$$

where c_f and c_n represent the energy integrals over the spin-independent parts of the level densities for fission and neutron emission, respectively, and the spin-dependent part has been evaluated at the compound-nuclear spin J. The fission and neutron spin cutoff parameters σ_f and σ_n, vary with energy much more slowly than the exponentially-increasing spin-independent part of the level density. To achieve the simple expression above, we have evaluated them at the most probable decay energy (which will be near the maximum effective decay energy for each of the channels) and removed the spin-cutoff factors from the energy integrals. We define r, the ratio of the two energy integrals, by $R = c_f/c_n$, and rewrite the expression for $P_f(J)$ as

$$P_f(J) = \frac{R\ \exp\left[-\frac{1}{2}\,(J+\frac{1}{2})^2\left(\frac{1}{\sigma_f^2} - \frac{1}{\sigma_n^2}\right)\right]}{1 + R\ \exp\left[-\frac{1}{2}\,(J+\frac{1}{2})^2\left(\frac{1}{\sigma_f^2} - \frac{1}{\sigma_n^2}\right)\right]}. \tag{33}$$

This expression gives the spin dependence of the level density in terms of the fission and neutron spin cutoff parameters and the single additional parameter R. From this last expression, we can see that to a high degree of accuracy, R is simply related to the fission probability at zero spin by $R = P_f(0)/(1 - P_f(0))$.

Fig. 55 shows the spin dependence of the fission probability calculated from Eq. 33 with parameters $\sigma_f = 6.0$, $\sigma_n = 5.0$, and $R = 0.538$. These values were chosen to model the behavior of the fission probability in the 2.5–3 MeV neutron energy region for ^{235}U(n,f), as shown in Fig. 26. The values of the neutron separation energy and fission barrier heights in ^{236}U are such that for a given energy of the ^{236}U compound nucleus, the effective excitation energy in Fig. 54 is about the same for both neutron emission and fission. The values chosen for σ_n and σ_f are similar to those shown in Fig. 54 near 2.5 MeV.

The results of the simple model as shown in Fig. 55 are in reasonable qualitative agreement with the full Hauser-Feshbach calculations of Fig. 26. We see that a very significant

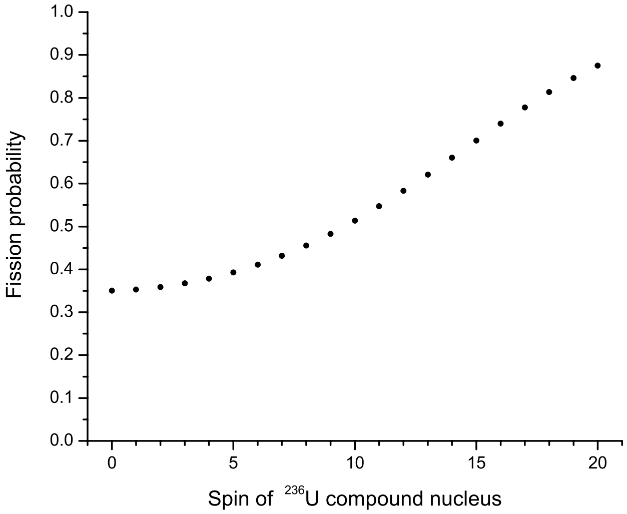

Figure 55: Spin dependence of the fission probability.

spin dependence of the fission probability results from a difference of only 1 unit between σ_f and σ_n. The much smaller spin dependence seen near 5 MeV in Fig. 26 may be associated with the closeness of σ_f and σ_n at that energy as seen in Fig. 54.

The use of a double-humped fission barrier in the full Hauser-Feshbach calculations is not mirrored explicitly in the simple model above. In the full calculation, the numerator N for the fission decay is actually calculated by calculating the appropriate sums and integrals to yield values N_1 and N_2 for the two barriers separately, and then combining them by the well-known relation $N = N_1 N_2/(N_1 + N_2)$. However, this relation shows that the form of N is similar to that for a single barrier if $N_1 = N_2$ or if one of the factors is much larger than the other.

From the above results we conclude that the spin dependence of the fission probability is highly sensitive to the spin cutoff parameters in the fission channel and the competing particle emission channels. A detailed understanding of the spin dependence of the fission transition states is difficult since it requires an accurate treatment of the barrier symmetries and an understanding of the inertial parameters. Additional complications not addressed here include a possible spin dependence in the barrier heights. The present results should be taken only as an indication of the sensitivity to the spin-dependent parameters in the fission calculation.

A.3 Optical-model parameterization

The choice of optical model parameters is important for the theoretical calculation of cross sections of interest. The optical model enters into several aspects of our calculations:

- It determines the cross section for formation of the compound nucleus in the initial neutron-target interaction;
- it is used to compute the transmission coefficients used in the Hauser-Feshbach calculations;
- it determines the cross sections for inelastic excitation of the coupled states in the ground-state rotational band.

The dependence of the direct reaction cross sections on the optical model parameters is detailed in the internal report [32]. In the work in Ref. [32] a preliminary version (Flap 1.5) of a regional potential tuned for actinides was employed. InRef. [42, 43] an improved potential (Flap 2.2) was used that was originally developed as part of the evaluation of the ^{239}Pu(n,2n) cross section by a subtraction technique [73]. The parameters of both optical potentials are shown in Tables 1 and 2, and their predictions for total and compound cross sections are compared with experimental data in Fig. 56. All calculations are carried out with the coupled-channel code ECIS [81].

The parameterization of the optical potential is a standard one (see, *e.g.*, Ref. [13]), employing Woods-Saxon volume form factors for the real and volume-imaginary potentials, a derivative Woods-Saxon for the surface-imaginary potential, and a Thomas form for the spin-orbit potential. The strength and geometry parameters are shown in Tables 1 and 2. The Flap 2.2 potential is a piecewise-linear potential that allows an energy-dependent geometry for the real potential that is in accord with expectations based on dispersive phenomenological and microscopic folding optical models [49, 62, 63]. This treatment allows an improved reproduction of total cross sections compared to the energy-independent geometry model of Flap 1.5, as shown in Fig. 56. The new potential was constrained to coincide with the older one at zero energy, so as to preserve the excellent reproduction of the low-energy resonance parameters (S_0, S_1, and R') that was attained with Flap 1.5.

The experimental total cross section data shown in Fig. 56 are from Ref. [80] below 5 MeV and from [2] above that energy. The Flap 2.2 results are indistinguishable from the experimental data in the upper region; the energy-dependent geometry was required to achieve this result. There is significant scatter in the available experimental data on the compound cross section. We have chosen to show one set which we judge to be reliable, that of Ref. [71]. The agreement with both calculations is good at the level of approximately 3%.

Transmission coefficients used in all stages in the present ^{235}U(n,2n) calculations were generated for neutrons incident on ^{234}U using a coupled-channel model (ECIS) in which the 0^+, 2^+, and 4^+ members of the ground-state band were coupled in a rotational model. The resulting compound-formation cross section is shown in Fig. 57. The calculation used experimental values for the deformation parameters ($\beta_2 = 0.198$ and $\beta_4 = 0.057$) that are typical in this region of the actinides. For ^{239}Pu(n,2n), similar calculations were performed

Real Volume	
V_R	$52.0 - 0.3E - (26.0 - 0.15E)\eta$
r_V	1.25
a_V	0.63
Imaginary Volume	
W_V	$\begin{cases} 0, & E \leq 10 \\ -3.8 + 0.38E - (-1.9 + 0.19E)\eta, & E > 10 \end{cases}$
r_W	1.27
a_W	0.62
Imaginary Surface	
W_S	$\begin{cases} 3.08 + 0.4E - (1.54 + 0.2E)\eta, & E \leq 10 \\ 8.496 - 0.142E - (4.248 - 0.071E)\eta, & E > 10 \end{cases}$
r_S	1.27
a_S	0.62
Real Spin Orbit	
V_{so}	6.2
r_{so}	1.15
a_{so}	0.75

Table 1: Parameters for Flap 1.5 n+U optical potential. The asymmetry parameter η is $(N-Z)/A$, where N, Z, A are the neutron, proton, and mass numbers of the target. Energies are in MeV, and lengths in fm.

on ^{238}Pu, changing only the energies of the coupled states. Calculations of the same type on ^{238}U were made for the cross section results shown in Fig. 56. The use of a common set of transmission coefficients for all nuclei in each reaction is reasonable, since the mass range is small.

Finally, we indicate the procedures used to obtain the transmission coefficients from the ECIS calculations. Each channel in the coupled system is identified by quantum numbers $c \equiv [(ls)jI]J^\pi$, where the order of the symbols indicates a particular coupling scheme leading to total angular momentum and parity J^π for the entire system. In this scheme the relative orbital angular momentum l is coupled to the projectile spin s to a resultant j, which is then coupled to the target spin I to yield the total angular momentum J. The transmission coefficients are obtained from the calculated S-matrix elements by the well-known expression

$$T_c = 1 - \sum_{c'} \left| S_{cc'} \right|^2 . \tag{34}$$

Whereas the transmission coefficients calculated from ECIS depend on the full set of quantum numbers $[(ls)jI]J^\pi$, those required by STAPRE depend only on the orbital angular momentum l. An averaging procedure is used to suppress the unwanted quantum numbers. This procedure is rather arbitrary, but is chosen so that the most important quantity, the reaction cross section for compound nucleus formation, is preserved in the averaging procedure.

Energy	0	1	5	10	20	50
Real Volume						
V_{R0}	52.000	52.000	51.661	49.856	46.810	38.351
V_{R1}	26.000	26.000	25.830	24.928	23.405	19.175
r_V	1.250	1.249	1.245	1.240	1.230	1.210
a_V	0.63	0.63	0.63	0.63	0.63	0.63
Imaginary Volume						
W_{V0}	0.000	0.000	0.000	0.338	2.143	7.557
W_{V1}	0.000	0.000	0.000	0.169	1.072	3.779
r_W	1.270	1.270	1.270	1.270	1.270	1.270
a_W	0.62	0.62	0.62	0.62	0.62	0.62
Imaginary Surface						
W_{S0}	3.080	3.480	4.737	6.768	6.768	1.354
W_{S1}	1.540	1.740	2.369	3.384	3.384	0.677
r_S	1.270	1.270	1.270	1.270	1.270	1.270
a_S	0.62	0.62	0.62	0.62	0.62	0.62

Table 2: Parameters for Flap 2.2 n+U optical potential. This is a piecewise-linear potential, so that parameters are to be interpolated linearly between the indicated energies. The strength parameters are given in an isospin representation (subscript 0 for isoscalar, 1 for isovector), which are to be combined as $U = U_0 - U_1\eta$, where η is the asymmetry parameter $(N-Z)/A$. Energies are in MeV, and lengths in fm. The spin-orbit potential is the same as for Flap 1.5 (see Table 1).

Following Ref. [?], the dependence on total angular momentum J is first removed,

$$T_{lsjI} = \sum_J \frac{2J+1}{(2I+1)(2j+1)} T^J_{lsjI}, \tag{35}$$

then the dependence on j is removed,

$$T_{lsI} = \sum_j \frac{2j+1}{(2l+1)(2s+1)} T^J_{lsjI}. \tag{36}$$

This is the desired expression in which the only variable is l, since s and I are fixed. The transmission coefficients depend on the spin of the target state, I. In practical calculations the target state is chosen as the lowest state of the ground-state rotational band. In the present case we have used even-even targets so that $I = 0$, and the above expressions simplify. To our knowledge the accuracy of the averaging procedure and the appropriateness of using transmission coefficients based only on the ground state of the target have never been tested. However, the preservation of the reaction cross section encourages the expectation that the errors incurred are not severe.

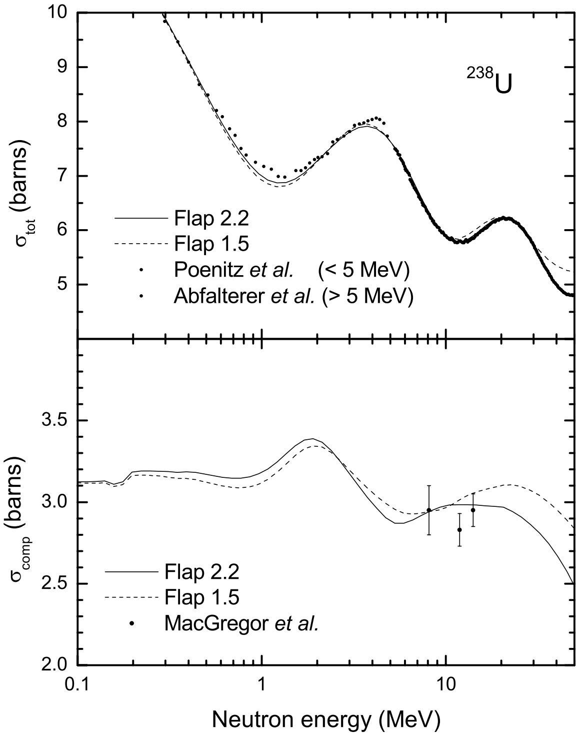

Figure 56: Comparison of optical-model total and compound cross sections with experiment for neutrons incident on ^{238}U. The calculated compound cross section is the complete reaction (nonelastic) cross section with the inelastic cross sections for the ground-state rotational band removed. The Flap 2.2 total cross section is indistinguishable from the experimental data above 5 MeV.

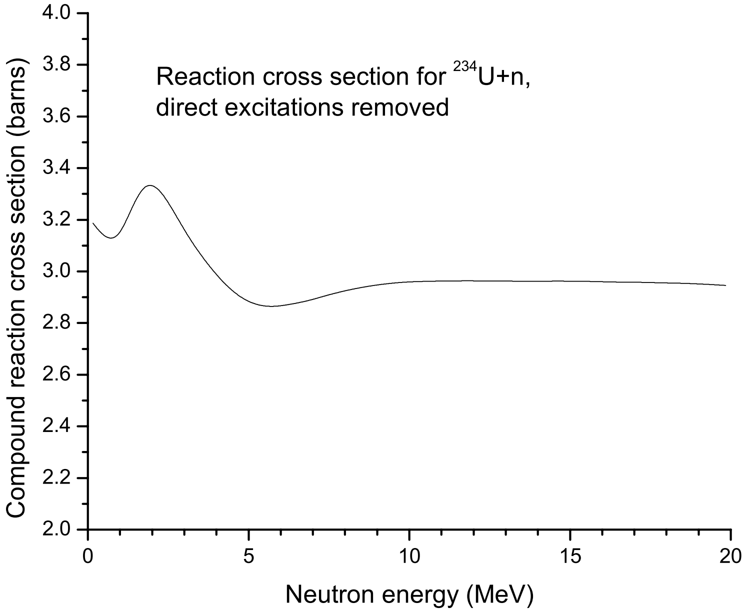

Figure 57: Compound-nuclear reaction cross section for n+^{234}U

A.4 The role of preequilibrium neutron emission

Preequilibrium neutron emission is important for neutron-induced reactions at incident energies above a few MeV, and was therefore included in the calculations of (n,f) and (n,γ) described above. However, the simplified model for Surrogate reactions that is being assessed in this report does not allow for preequilibrium processes. In this section we show the effects of preequilibrium emission on the (n,f) cross section.

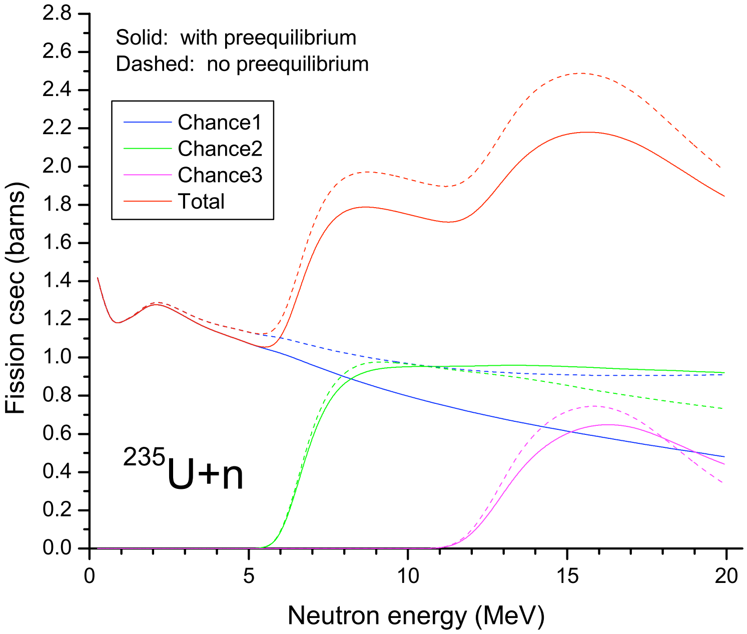

Figure 58: Hauser-Feshbach calculation illustrating the effect of preequilibrium neutron emission. The solid lines represent the fit to the known ^{235}U(n,f) cross section discussed in Section 3.5. The dashed lines are a calculation with identical parameters except that preequilibrium is turned off.

Fig. 58 shows the full calculation of the ^{235}U(n,f) cross section as described earlier (solid line), together with the same calculation without preequilibrium but identical parameters otherwise (dashed line). The main features of preequilibrium emission visible in the figure are:

- The principal effect of preequilibrium neutron emission is on first-chance fission; *i.e.* fission of the compound nucleus formed by fusion of the incident neutron with the target. Preequilibrium neutron emission corresponds to a fast (n,n') process that bypasses this stage. The sum of cross sections for all reaction processes induced by the incident neutron, both preequilibrium and compound, must be approximately the area of the nucleus. Consequently, the compound-nucleus formation cross section (which would correspond to the nuclear area in the absence of prequilibrium) must be reduced by the calculated preequilibrium emission cross section. This is reflected in a reduction of first-chance fission.

- In the region ($\lesssim$ 7 MeV) where first-chance fission dominates, the correction to the total fission is less than 10%. At the highest energies ($\approx$ 20 MeV), the depletion of first-chance fission is quite large, in the neighborhood of 40%. However, second- and third-chance fission are dominant in this region, so the net correction to the total fission is much less, not exceeding $\approx$15% over the entire energy range.

- The effects of preequilibrium on second- and third-chance fission are much smaller than for first-chance. Although the preequilibrium (n,n') process bypasses the first compound nucleus, for sufficiently low energies of the inelastically scattered neutrons the residual nucleus will be sufficiently excited to be able to fission. This component of the fission cross section originates from the same residual nucleus that is reached by neutron emission from the first compound nucleus, and thus must be added to the fission component (second-chance fission) arising from purely compound processes. The net result is that second- and higher-chance fission cross sections are much less sensitive to the inclusion of preequilibrium than the first-chance process.

Because the interplay between the preequilibrium and compound parts of the reaction is complicated, it is not possible to make a straightforward correction for preequilibrium emission in the simple Weisskopf-Ewing picture of the Surrogate reaction or in the Ratio method based on it. However, we have noted above that the total fission cross sections calculated with and without preequilibrium are within 15% of each other. Moreover, we expect that the corrections for preequilibrium should be very similar for targets differing only by two neutrons (^{233}U(n,f) *vs.* ^{235}U(n,f) as studied here, or ^{235}U(n,f) *vs.* ^{237}U(n,f) as presently being inferred from experiments using the Ratio method [79]). Therefore, the errors incurred by ignoring preequilibrium emission are likely to be much smaller than 15% when the Ratio method is used. We will not discuss this issue further in this report, but note that it deserves additional attention in a more complete treatment of Surrogate reactions.

A.5 Fission-fragment anisotropies

Neutron-induced reactions allow experimentalists to vary the incident neutron energy and study the decay mechanism of nuclei, whereas direct reactions allow us to vary the incident energy, excitation energy and momentum transfer imparted to a target nucleus.They also allow us to study fission below the neutron separation barrier. One particularly interesting indicator is the angular distribution of fission fragments following a direct reaction. The angular distribution of fission fragments along with a theoretical model provides some indications of the spin of the nucleus prior to fission, and hence contrains the fission probability of a nucleus as a function of spin of the initial states of the decay nucleus.

Direct reactions that induce fission can produce very anisotropic distributions of the fission fragments relative to the symmetry axis of the nucleus. This phenomena has been observed for more than 45 years. The first work on even-even nuclei using (d,p) and (α,α') was reported by Wilkins in 1964 [97] and Britt in 1965 [21]. Vandenbosch et al. were the first to study odd-A nuclei using fission fragment angular distributions [**?**]. The effect is evident at low equivalent neutron energies where there are discrete states. In general, the fission fragment anisotropy is most pronounced in the first 2 MeV above the fission barrier for most actinides. Above 2 MeV the number of states increases significantly and many different spin states are populated, which dilutes the strength of any one particular spin and the anisotropy disappears.

Nuclear fragments resulting from fission of a nucleus B* that has been excited in a direct reaction, such as a transfer reaction or an inelastic excitation, are in general not isotropically distributed. This is because the decaying compound nucleus in spin/parity J^π will have a probability distribution of magnetic substates M that is not uniform over the range $-J \leq M \leq J$.

Angular correlations between the outgoing direct-reaction particle and fission fragments were studied in the 1960s for (d,pf), (t,pf), (t,df), and (α, α') reactions [97, 21, 22, 93, 98, 23, 19]. For a given projectile-target combination, the distributions W(χ, β) were found to depend on:

- the energy E^* to which the nucleus B* was excited in the direct reaction;
- properties of the transition states populated in B*, such as the parity π of the relevant state, as well as the angular momentum J and its projection M on the laboratory-fixed axes;
- the intrinsic properties of those transition states in B*, such as their projections K on body-fixed axes;
- the angle θ_x of the outgoing direct-reaction particle with respect to the beam direction.

Both the stripping and the inelastic scattering studies found the anisotropies in the fission fragment distribution to be particularly large near the fission threshold. In fact, the dependence of W(χ, β) near the fission barrier on the J, K, M, and π quantum numbers of the transition states was exploited to study the structure of these states.

When the intrinsic state of the nucleus can be characterized by a projection K on some body-fixed frame, then all compound nuclear decays (whether fission, gamma decay, or particle evaporation) will then be anisotropic in that frame in proportion to the square modulus of the rotation function $|d^J_{MK}(\chi,\beta)|^2$. At and below the fission barrier there will be only a few rotational bands labeled by their band-head K, and large fragment anisotropies will be found. If the excitation energy E^* is much above the fission barrier, by contrast, the increasing level density at these higher energies will mean there must be a much wider distribution of rotational bands. There will then typically be a statistical distribution of K values, which, in the absence of further knowledge, we represent by a Gaussian probability distribution $p(K) \propto \exp(-K^2/K_0^2)$ for some width parameter K_0 fitted to the data.

The very fact of non-isotropic fission fragment distributions has the immediate and practical consequence that it is not straightforward to infer the total number of fission fragments from a realistic experiment in which the fission detectors cover only a portion of 4π. In a surrogate reaction, fission fragments are detected in coincidence with the outgoing particle from the direct reaction. The distributions of fission fragments is characterized by the angular distribution function $\mathrm{W}(\chi,\beta)$, which relates the differential fragment cross section $d\sigma_{\mathrm{ff}}/d\Omega$ to the total fission cross section σ_f:

$$\frac{d\sigma_{\mathrm{ff}}(\chi,\beta)}{d\Omega} = W(\chi,\beta)\ \sigma_f. \tag{37}$$

Distributions both within the reaction plane and perpendicular to the reaction plane have to be considered. The reaction plane is defined as the plane spanned by the velocity vectors of the projectile and the ejectile. The velocity vector of the recoiling compound nucleus B^* lies in this plane, at an angle β_R relative to the beam axis. We denote the in-plane projection of the angle of the fission fragment with respect to the direction of the recoiling compound nucleus by $\beta - \beta_R$. The azimuthal angle χ describes the out-of-plane fission-fragment direction. It is defined with respect to a vector that is perpendicular to the reaction plane; $\chi = 90^0$ when the fragment is emitted in the plane. The quantity $\mathrm{W}(\chi,\beta)$ is normalized so that integration $\int_{4\pi} W(\chi,\beta)d\Omega = 1$.

A measurement of the angular correlations of α particles with fission fragments resulting from inelastic α-particle scattering with $E_\alpha \approx 40$ MeV and $\theta_x = 75°$ illustrated that anisotropies are particularly large near the fission threshold [22]. The largest differential cross sections were found along the direction of the recoil axis: $W(\chi = 90°,\ \beta{-}\beta_R = 0$ or $180°)/\ W(\chi = 90°,\ \beta{-}\beta_R = 90°)$ can be as large as 5-6; it decreases for $\beta{-}\beta_R \rightarrow 90°$ and for increasing E^*. The azimuthal distribution was found to be uniform, in agreement with theoretical predictions based on a plane-wave approximation.

A study of angular correlations in the ^{239}Pu(d,pf) reaction found the anisotropies to be strongly dependent on the angle θ_x of the outgoing particle (the proton in that case) [98]. The anisotropies in the reaction plane were seen to significantly decrease as the angle θ_x was decreased from 140° to 50°. At the same time, significant out-of-plane angular correlations were observed in this reaction and were found to *increase* as θ_x was increased. Similar studies for (α,α') reactions have not been carried out.

These findings imply that for a proper application of the surrogate method, the angular correlations have to be known. A detailed description of the spatial anisotropies is required if one needs to determine the total number of fission fragments from a measurement at a particular location in space. Alternatively, it might be possible to carry out the fission fragment measurements in coincidence with detecting the outgoing direct-reaction particle at an angle that is associated with only minor anisotropies in the fission-fragment distribution.

The latter strategy was followed by Cramer and Britt [**?**], who detected outgoing protons from (t,pf) reactions on several actinide targets at back angles in order to minimize the effects of the angular correlations on their results. It is not obvious that such angles can be found for all cases of interest.

Similarly, knowledge of the angular correlations is important for a successful application of the Ratio method. The two strategies outlined above for surrogate applications, correcting the measured fission counts or restricting the coincidence measurements to selected angles for the direct-reaction particle, can be pursued here as well. However, the treatment of the anisoptropies greatly simplifies in the Ratio approach when the angular correlations for the two compound nuclei that are being compared are very similar. In this case, the ratio of the angular distribution functions for the two nuclei can be approximately set to 1.

To test whether the angular correlations for two given compound nuclei, excited by a specific direct reaction, are similar, a systematic study of the dependence of W(χ, β) on the reaction mechanism, angle θ_x and excitation energy E^* is necessary. In most cases this information is not readily available, but a few studies have been carried out. Comparing the angular correlations for $(\alpha, \alpha'$f) on two different nuclei (^{238}U and ^{240}Pu), Britt and Plasil found essentially the same dependence on the energy of the compound nucleus [i.e. they observed that the ratio $W(\chi = 90°, \beta - \beta_R = 0)/W(\chi = 90°, \beta - \beta_R = 90°)$ decreases with energy and that the rate of the decrease the same for both ^{238}U and ^{240}Pu], except for a shift in energy which is related to the different fission thresholds in these two nuclei. While this finding is very encouraging, it is still extremely important to study the issue of angular correlations in much greater detail. In particular, we recommend that each application of the Ratio method be accompanied by a sufficient study of the angular correlations, both in-plane and out-of-plane, for the two compound nuclei under consideration.

References

[1] *Energy Loss and Straggle Tool [adapted from the Computer program* ENELOSS*, written by H. Ernst (1981) with stopping power routines by K. Lesko (1984).].*

[2] W. P. Abfalterer, F. B. Bateman, F. S. Dietrich, R. W. Finlay, R. C. Haight, and G. L. Morgan, Phys. Rev. C, **63** (2001), p. 044608.

[3] J. M. Allmond, L. A. Bernstein, C. W. Beausang, L. Phair, D. L. Bleuel, J. T. Burke, J. E. Escher, K. E. Evans, B. L. Goldblum, R. Hatarik, H. B. Jeppesen, S. R. Lesher, M. A. McMahan, J. O. Rasmussen, N. D. Scielzo, and M. Wiedeking, *Relative* ^{235}*U(n,γ) and (n,f) cross sections from* ^{235}*U(d,p γ) and (d,pf)*, Physical Review C (Nuclear Physics), **79** (2009), p. 054610.

[4] B. L. Andersen, B. B. Back, and J. M. Bang, *One-particle transfer reactions to highly excited states in deformed nuclei*, Nucl. Phys. A, **147** (1970), pp. 33–44.

[5] B. B. Back, J. P. Bondorf, G. A. Otroschenko, J. Pedersen, and B. Rasmussen, *Fission of u, np, pu and am isotopes excited in the (d, p) reaction*, Nuclear Physics A, **165** (1971), pp. 449 – 474.

[6] B. B. Back, H. C. Britt, O. Hansen, B. Leroux, and J. D. Garrett, *Fission of odd-a and doubly odd actinide nuclei induced by direct reactions*, Phys. Rev. C, **10** (1974), pp. 1948–1965.

[7] B. B. Back, O. Hansen, H. C. Britt, and J. D. Garrett, *Fission of doubly even actinide nuclei induced by direct reactions*, Phys. Rev. C, **9** (1974), pp. 1924–1947.

[8] M. Basunia, R. Clark, B. Goldblum, L. Bernstein, L. Phair, J. Burke, C. Beausang, D. Bleuel, B. Darakchieva, F. Dietrich, M. Evtimova, P. Fallon, J. Gibelin, R. Hatarik, C. Jewett, S. Lesher, M. McMahan, E. Rodriguez-Vieitez, and M. Wiedeking, *The (3he,tf) as a surrogate reaction to determine (n,f) cross sections in the 10-20mev energy range*, Nuclear Instruments and Methods in Physics Research Section B: Beam Interactions with Materials and Atoms, **267** (2009), pp. 1899 – 1903.

[9] E. Bauge, J.-P. Delaroche, and M. Girod, Phys. Rev. C, **58** (1998), p. 1118.

[10] ——, Phys. Rev. C, **63** (2001), p. 024607.

[11] E. Bauge, J.-P. Delaroche, M. Girod, G. Haouat, J. Lachkar, Y. Patin, J. Sigaud, and J. Chardine, Phys. Rev. C, **61** (2000), p. 034306.

[12] G. Baur, F. Rösel, D. Trautmann, and R. Shyam, *Fragmentation processes in nuclear reactions*, Physics Reports, **111** (1984), pp. 333 – 371.

[13] F. D. Becchetti and G. W. Greenlees, Phys. Rev., **182** (1969), p. 1190.

[14] L. A. Bernstein. private communication.

[15] L. A. Bernstein, J. Burke, L. Ahle, J. A. Church, J. Escher, et al., *Deducing the* ^{237}*U(n,*γ*) and (n,2n) cross sections using a new Surrogate Ratio method*, tech. rep., Lawrence Livermore National Laboratory, Livermore, CA, 2006.

[16] L. A. Bernstein et al., *Surrogate nuclear reactions using STARS*, in Proceedings of the International Conference on Nuclear Data for Science and Technology (ND2004, Santa Fe, NM), vol. 769, American Institute of Physics, AIP Conference Proceedings, 2005, pp. 890–893.

[17] S. Bjornholm and J. E. Lynn, Rev. Mod. Phys., **52** (1980), p. 725.

[18] S. Boyer, D. Dassie, J. Wilson, M. Aiche, G. Barreau, S. Czajkowski, C. Grosjean, A. Guiral, B. Haas, B. Osmanov, G. Aerts, E. Berthoumieux, F. Gunsing, C. Theisen, N. Thiolliere, and L. Perrot, *Determination of the* ^{233}*Pa(n,*γ*) capture cross section up to neutron energies of 1 MeV using the transfer reaction* ^{232}*Th(*^{3}*He,p)*^{234}*Pa**, Nucl. Phys. A, **775** (2006), pp. 175–187.

[19] H. C. Britt and J. D. Cramer, Phys. Rev., **181** (1969), p. 1634.

[20] ——, *Fission of odd-a uranium and plutonium isotopes excited by (d,p), (t, d), and (t, p) reactions*, Phys. Rev. C, **2** (1970), pp. 1758–1768.

[21] H. C. Britt, W. R. Gibbs, J. J. Griffin, and R. H. Stokes, Phys. Rev., **139** (1965), p. B354.

[22] H. C. Britt and F. Plasil, Phys. Rev., **144** (1966), p. 1046.

[23] H. C. Britt, F. A. Rickey, and W. S. Hall, Phys. Rev., **175** (1968), p. 1525.

[24] H. C. Britt and J. B. Wilhelmy, *Progress report: Study of the feasibility of simulating (n,*α*) and (n,p) cross sections with charged particle direct reaction techniques*, tech. rep., Los Alamos National Laboratory, Los Alamos, NM, 1976.

[25] H. C. Britt and J. B. Wilhelmy, Nucl. Sci. and Eng., **72** (1979), p. 222.

[26] G. E. Brown and M. Rho, Nucl. Phys., **A372** (1981), p. 397.

[27] J. Burke.

[28] J. Burke, L. Bernstein, J. Escher, et al., *Deducing the* ^{237}*U(n,f) cross section using the Surrogate Ratio method*, Tech. Rep. UCRL-214631, Lawrence Livermore National Laboratory, Livermore, CA, 2005.

[29] ——, *Deducing the* ^{237}*U(n,f) cross section using the Surrogate Ratio method*, Phys. Rev. C, **73** (2006), p. 054604.

[30] J. T. Burke, L. A. Bernstein, J. Escher, L. Ahle, J. A. Church, F. S. Dietrich, K. Moody, E. B. norman, L. Phair, P. Fallon, R. M. C. adn M. A. Deleplanque, M. Descovich, M. Cromaz, I.-Y. Lee, A. O. Macchiavelli, M. A. McMahan, L. G. Moretto, E. Rodriguez-Vieitez, F. S. Stephens, H. Ai, C. Plettner, C. Beausang, and B. Crider, **73** (2006), p. 054604.

[31] M. B. Chadwick. private communication, 2001.

[32] H. Chen, W. E. Ormand, and F. S. Dietrich, *The $^{239}Pu(n,2n)$ cross section inferred from* IDA *calculations* GEANIE *measurements*, Tech. Rep. UCRL-ID-141663, Lawrence Livermore National Laboratory, Livermore, CA, 2001, 2001.

[33] J. D. Cramer and H. C. Britt, Nucl. Sci. and Eng., **41** (1970), p. 177.

[34] ——, Phys. Rev. C, **2** (1970), p. 2350.

[35] Cross Section Evaluation Working Group, edited by P. Oblozinsky and M. Herman, *ENDF/B-VII beta2 Summary Documentation*, National Nuclear Data Center, Brookhaven National Laboratory, Upton, NY, 2006.

[36] F. S. Dietrich, *Simple derivation of the Hauser-Feshbach and Weisskopf-Ewing formulae, with application to Surrogate reactions*, Tech. Rep. UCRL-TR-201718, Lawrence Livermore National Laboratory, Livermore, CA, 2004.

[37] F. S. Dietrich, *Compound-nucleus formation following direct interactions to highly-excited final states*, AIP Conference Proceedings, **1005** (2008), pp. 125–128.

[38] G. Duchêne, F. A. Beck, P. J. Twin, G. de Fance, D. Curien, L. Han, C. W. Beausand, M. A. Bentley, P. J. Nolan, and J. Simpson, **432** (1999), p. 90.

[39] Z. Elekes, T. Belgya, G. L. Molnár, A. Z. Kiss, M. Csatlós, J. Gulyás, A. Krasznahorkay, and Z. Máté, **503** (2003), p. 580.

[40] J. Escher, *Producing a compound nucleus via a inelastic scattering: The $^{90}Zr(\alpha,\alpha')^{90}Zr^{*}$ case*, Tech. Rep. UCRL-TR-xxx, Lawrence Livermore National Laboratory, Livermore, CA, 2007. In preparation.

[41] J. Escher, N. Scielzo, et al., *(n,γ) cross sections from surrogate experiments*. Work in progress, 2009.

[42] J. E. Escher and F. S. Dietrich, *Examination of the validity of the Surrogate Ratio Method for determining (n,f) and (n,γ) cross sections of actinides*, Tech. Rep. UCRL-TR-212509-Draft, Lawrence Livermore National Laboratory, Livermore, CA, 2005.

[43] ——, *Determining (n,f) cross sections for actinide nuclei indirectly: Examination of the Surrogate Ratio Method*, Phys. Rev. C, **74** (2006), p. 054601.

[44] B. I. F. et al., Conf. Nucl. Data for Sci. And Techn. Trieste, (1997), p. 488.

[45] F. T. et al., Phys. Rev. Lett., **88** (2002), p. 06502.

[46] J. D. et al., Nucl. Sci. Eng., **83** (1983).

[47] P. V. et al., Yadern. Fiz., **40** (1984).

[48] S. P. et al., Phys. Rev. Lett., **46** (1981), p. 633.

[49] R. W. Finlay, J. R. M. Annand, J. S. Petler, and F. S. Dietrich, Phys. Lett., **155B** (1985), p. 313.

[50] E. Fomushkin, At. Energ., **69** (1990), p. 258.

[51] C. Forssén, F. Dietrich, J. Escher, R. Hoffman, and K. Kelley, *Determining neutron capture cross sections via the surrogate reaction technique*, Phys. Rev. C, **75** (2007), p. 055807.

[52] P. Fröbrich and R. Lipperheide, *Theory of Nuclear Reactions*, Clarendon Press, Oxford, 1996.

[53] E. Gadioli and P. E. Hodgson, *Pre-Equilibrium Nuclear Reactions*, Clarendon Press, Oxford, 1992.

[54] A. Gavron, H. C. Britt, E. Konecny, J. Weber, and J. B. Wilhelmy, *Measurement and interpretation of* $\gamma n \gamma f$ *for actinide nuclei*, Phys. Rev. Lett., **34** (1975), pp. 827–830.

[55] ——, $\gamma n \gamma f$ *for actinide nuclei using* $(he3, df)$ *and* $(he3, tf)$ *reactions*, Phys. Rev. C, **13** (1976), pp. 2374–2384.

[56] B. L. Goldblum, S. G. Prussin, U. Agvaanluvsan, L. A. Bernstein, D. L. Bleuel, W. Younes, and M. Guttormsen, *Determination of (n,gamma) cross sections in the rare-earth region using the surrogate ratio method*, Physical Review C (Nuclear Physics), **78** (2008), p. 064606.

[57] F. S. Goulding, D. A. Landis, J. Cerny, and R. H. Pehl, Nucl. Instrum. Meth., **31** (1964), p. 1.

[58] C. J. Guess, R. G. T. Zegers, B. A. Brown, S. M. Austin, D. Bazin, C. Caesar, J. M. Deaven, G. F. Grinyer, C. Herlitzius, G. W. Hitt, S. Noji, R. Meharchand, G. Perdikakis, H. Sakai, Y. Shimbara, and C. Tur, *Spectroscopy of 13b via the 13c(t,3he) reaction at 115 amev*, Physical Review C, **80** (2009), p. 024305.

[59] R. Hatarik et al., AIP Conf. Proc., **1005** (2008), p. 105.

[60] W. Hauser and H. Feshbach, *The inelastic scattering of neutrons*, Phys. Rev., **87** (1952), pp. 366–373.

[61] M. Herman, R. Capote, B. V. Carlson, P. Oblozinsky, M. Sin, A. Trkov, H. Wienke, and V. Zerkin, *EMPIRE: Nuclear reaction model code system for data evaluation*, NUCLEAR DATA SHEETS, **108** (2007), pp. 2655–2715.

[62] J.-P. Jeukenne, A. Lejeune, and C. Mahaux, Phys. Rev. C, **15** (1977), p. 10.

[63] ——, Phys. Rev. C, **16** (1977), p. 80.

[64] J.H.McNally, J. Barnes, B. Dropesky, P. Seeger, and K. Wolfsberg.

[65] B. Jurado, G. Kessedjian, M. Aiche, G. Barreau, A. Bidaud, S. Czajkowski, D. Dassie, B. Haas, L. Mathieu, B. Osmanov, L. Audouin, N. Capellan, L. Tassan-Got, J. N. Wilson, E. Berthoumieux, F. Gunsing, C. Theisen, O. Serot, E. Bauge, I. Ahmad, J. P. Greene, and R. V. F. Janssens, *Fission cross sections and fission-fragment mass yields via the surrogate reaction method*, AIP Conference Proceedings, **1005** (2008), pp. 90–95.

[66] M. Kawai, A. K. Kerman, and K. W. McVoy, *Modification of hauser-feshbach calculations by direct-reaction channel coupling*, Annals of Physics, **75** (1973), pp. 156 – 170.

[67] A. K. Kerman and K. W. McVoy, Ann. Phys., **122** (1979), p. 197.

[68] I. Y. Lee, **A520** (1990), p. 641c.

[69] S. R. Lesher, J. T. Burke, L. A. Bernstein, H. Ai, C. W. Beausang, D. L. Bleuel, R. M. Clark, F. S. Dietrich, J. E. Escher, P. Fallon, J. Gibelin, B. L. Goldblum, I. Y. Lee, A. O. Macchiavelli, M. A. McMahan, K. J. Moody, E. B. Norman, L. Phair, E. Rodriguez-Vieitez, N. D. Scielzo, and M. Wiedeking, *Surrogate ratio method in the actinide region using the (alpha,alpha[sup ']f) reaction*, Physical Review C (Nuclear Physics), **79** (2009), p. 044609.

[70] B. F. Lyles, L. A. Bernstein, J. T. Burke, F. S. Dietrich, J. Escher, I. Thompson, D. L. Bleuel, R. M. Clark, P. Fallon, J. Gibelin, A. O. Macchiavelli, M. A. McMahan, L. Phair, E. Rodriguez-Vieitez, M. Wiedeking, C. W. Beausang, S. R. Lesher, B. Darakchieva, and M. Evtimova, *Absolute and relative surrogate measurements of the ^{236}U(n,f) cross section as a probe of angular momentum effects*, Physical Review C (Nuclear Physics), **76** (2007), p. 014606.

[71] M. H. MacGregor, R. Booth, and W. P. Ball, Phys. Rev., **130** (1963), p. 1471.

[72] J. H. McNally, J. W. Barnes, B. J. Dropesky, P. A. Seeger, and K. Wolfsberg, *Neutron-induced fission cross section of* u237, Phys. Rev. C, **9** (1974), pp. 717–722.

[73] P. Navratil and D. P. McNabb, *Calculation of 239pu(n,2n) cross section by the subtraction and the ratio methods*, Tech. Rep. UCRL-ID-140697, Lawrence Livermore National Laboratory, Livermore, CA, 2000, 2000.

[74] B. K. Nayak, A. Saxena, D. C. Biswas, E. T. Mirgule, B. V. John, S. Santra, R. P. Vind, R. K. Choudhury, and S. Ganesan, *Determination of the [sup 233]pa(n,f) reaction cross section from 11.5 to 16.5 mev neutron energy by the hybrid surrogate ratio approach*, Physical Review C (Nuclear Physics), **78** (2008), p. 061602.

[75] J. A. Northrop, R. H. Stokes, and K. Boyer, *Measurement of the fission thresholds of pu*239*, u*233*, u*235*, and u*238 *using the (d,p) reaction*, Phys. Rev., **115** (1959), pp. 1277–1286.

[76] F. Osterfeld, *Nuclear spin and isospin excitations*, Rev. Mod. Phys., **64** (1992), pp. 491–557.

[77] W. E. Parker, M. B. Chadwick, F. S. Dietrich, J. E. Kammeraad, S. J. Luke, K. E. Sale, R. M. Chasteler, M. A. Godwin, L. H. Kramer, G. J. Schmid, H. R. Weller, and A. K. Kerman, Phys. Rev. C, **52** (1995), p. 252.

[78] M. Petit, M. Aiche, G. Barreau, et al., *Determination of the* ^{233}*Pa(n, f) reaction cross section from 0.5 to 10 MeV neutron energy using the transfer reaction* ^{232}*Th(*^{3}*He, p)*^{234}*Pa*, Nucl. Phys. A, **735** (2004), pp. 347–371.

[79] C. Plettner et al., *Estimation of (n,f) cross sections by measuring reaction probability ratios*, Phys. Rev. C, **71** (2005), p. 051602(R).

[80] W. P. Poenitz, J. F. Whalen, and A. B. Smith, Nucl. Sci. Eng., **81** (1981), p. 333.

[81] J. Raynal, Tech. Rep. CEA-N-2772, Commissariat à l'Energie Atomique, Paris, 1994, 1994.

[82] Y. Sakuragi, M. Yahiro, and M. Kamimura, Prog. Theor. Phys. Suppl., **89** (1986), p. 211.

[83] N. D. Scielzo et al. to be published.

[84] H. J. Specht, J. S. Fraser, and J. C. D. Milton, *Fission-fragment angular anisotropy in the reactions* $u235(d, pf)$ *and* $pu239(d, pf)$, Phys. Rev. Lett., **17** (1966), pp. 1187–1190.

[85] N. C. Summers, F. M. Nunes, and I. J. Thompson, *Core transitions in the breakup of exotic nuclei*, Physical Review C (Nuclear Physics), **73** (2006), p. 031603.

[86] ——, *Extended continuum discretized coupled channels method: Core excitation in the breakup of exotic nuclei*, Physical Review C (Nuclear Physics), **74** (2006), p. 014606.

[87] J. Terasaki, J. Engel, M. Bender, J. Dobaczewski, W. Nazarewicz, and M. Stoitsov, *Self-consistent description of multipole strength in exotic nuclei: Method*, Phys. Rev. C, **71** (2005), p. 034310.

[88] I. Thompson and J. E. Escher, *Theory of (*^{3}*He,*α*) surrogate reactions for deformed uranium nuclei*, Tech. Rep. UCRL-TR-225984, Lawrence Livermore National Laboratory, Livermore, CA, 2006.

[89] I. J. Thompson and A. Diaz-Torres, *Modelling effects of halo breakup on fusion*, Progress of Theoretical Physics Supplement, **154** (2004), pp. 69–76.

[90] F. Tovesson and T. S. Hill, *Neutron induced fission cross section of [sup 237]np from 100 kev to 200 mev*, Physical Review C (Nuclear Physics), **75** (2007), p. 034610.

[91] T. Udagawa and T. Tamura, *Breakup-fusion description of massive transfer reactions with emission of fast light particles*, Phys. Rev. Lett., **45** (1980), pp. 1311–1314.

[92] ——, *Derivation of breakup-fusion cross sections from the optical theorem*, Phys. Rev. C, **24** (1981), pp. 1348–1349.

[93] R. Vandenbosch, K. L. Wolf, J. Unik, C. Stephan, and J. R. Huizenga, Phys. Rev. Lett., **19** (1967), p. 1138.

[94] C. M. Vincent and H. T. Fortune, *New method for distorted-wave analysis of stripping to unbound states*, Phys. Rev. C, **2** (1970), pp. 782–792.

[95] Weston, L. W. and Young, P. G. and Poenitz, W. P. and Lubitz, C.R., *ENDF/B-VI Evaluation, Revision 5*, National Nuclear Data Center, Brookhaven National Laboratory, Upton, NY, 1977.

[96] M. Wiedeking, P. Fallon, A. O. Macchiavelli, L. A. Bernstein, J. Gibelin, L. Phair, J. T. Burke, D. L. Bleuel, R. M. Clark, M.-A. Deleplanque, S. Gros, R. Hatarik, H. B. Jeppesen, I.-Y. Lee, B. F. Lyles, M. A. McMahan, L. Moretto, J. Pavan, E. Rodriguez-Vieitez, and A. Volya, **77** (2008), p. 054305.

[97] B. D. Wilkins, J. P. Unik, and J. R. Huizenga, Phys. Lett., **12** (1964), p. 243.

[98] K. L. Wolf, R. Vandenbosch, and W. D. Loveland, Phys. Rev., **170** (1968), p. 1059.

[99] W. Younes and H. C. Britt, Phys. Rev. C, **67** (2003), p. 024610.

[100] ——, Phys. Rev. C, **68** (2003), p. 034610.

[101] ——, *Simulated (n,f) cross sections on various th, u, np, pu, and am targets*, Tech. Rep. UCRL-PROC-206823 (unpublished), Lawrence Livermore National Laboratory, Livermore, CA, 2004.

[102] ——, *Estimates of the* $^{237,239}U(n,f)$ *cross sections for* $0.1 < e_n(mev) \leq 20$, Tech. Rep. UCRL-TR-212600, Lawrence Livermore National Laboratory, Livermore, CA, 2005.

[103] W. Younes, H. C. Britt, and Becker, *Estimated (n,f) cross sections for* $^{236,236m,237,238}np$, $^{237,237m}pu$, *and* $^{240,241,242,242m,243,244,244m}am$ *isotopes*, Tech. Rep. UCRL-TR-201913 (unpublished), Lawrence Livermore National Laboratory, Livermore, CA, 2004.

[104] W. Younes, H. C. Britt, J. A. Becker, and J. B. Wilhelmy, *Initial estimate for the* $^{237}U(n,f)$ *cross section for* $0.1 \leq E_n$ *(MeV)* ≤ 20, Tech. Rep. UCRL-ID-154194, Lawrence Livermore National Laboratory, Livermore, CA, 2003.

[105] W. Younes, H. C. Britt, and J. B. Wilhelmy, *The* $^{237}U(n,f)$ *cross section*, Tech. Rep. UCRL-ID-152621, Lawrence Livermore National Laboratory, Livermore, CA, 2003.

[106] J. F. Ziegler, **219-220** (2004), p. 1027.